I. THE USE OF DEUTERATED PHOSPHOLIPIDS TO ELUCIDATE LIPID-LIPID INTERACTIONS IN BILAYER VESICLES

II. THE EFFECT OF CHAIN LENGTH ON THE SECONDARY STRUCTURE OF OLIGOADENYLATES

Thesis by

PAULUS ARIE KROON

In Partial Fulfillment of the Requirements
for the Degree of
Doctor of Philosophy

California Institute of Technology
Pasadena, California 91125
1974

(submitted December 19, 1974)

To Lois, with love

ACKNOWLEDGMENTS

I want to thank Karen Gleason for typing this thesis.

I thank Sunney Chan for his support, both academic and financial, during the course of this work.

I owe special thanks to Masatsune Kainosho, whose friendship and collaboration with much of this work have been most enjoyable to me.

I want to thank Michael Raftery for his friendship and advice during my stay at Caltech.

The Chan group as a whole has provided a stimulating environment. I have enjoyed the sharing of ideas and views over cups of coffee.

I am grateful to my wife Lois who has worked very hard for the past six years.

ABSTRACTS

PART I: The Use of Deuterated Phospholipids to Elucidate Lipid-Lipid Interactions in Bilayer Vesicles

The motional state of lecithin molecules in single walled bilayer vesicles has been studied by nuclear magnetic resonance spectroscopy. Inter- and intramolecular relaxation rates have been determined for the hydrocarbon chain methylene protons. The intermolecular contribution is much smaller than previously estimated. The data suggest a model in which hydrocarbon chain motion is described by rapid kink formation and diffusion along the chains in addition to slower C-C trans-gauche rotations. A lateral diffusion coefficient of $2.5 - 5.5 \times 10^{-8}$ cm^2 sec^{-1} is estimated. Both linewidths and spin-lattice relaxation rates have been measured for lecithins with different hydrocarbon chain lengths. Above the crystal to liquid crystal phase transition temperature, the linewidths are independent of chain length. This is taken to indicate that the hydrocarbon chain mobility and order are also independent of chain length.

The motional state of cholesterol in bilayer vesicles has been studied. Cholesterol dispersed in bilayers consisting of dipalmitoyl lecithin with perdeuterated hydrocarbon chains has an NMR spectrum with well defined features. Two of the five methyl resonances are sharp and clearly resolved. These are assigned to the isopropyl methyls of the hydrocarbon tail. The

other methyl resonances are much broader. This is taken to indicate that the hydrocarbon tail is much more mobile and disordered than the steroid nucleus. These conclusions are in agreement with and provide experimental support for the model proposed by Rothman and Engelman, but contrast with recent NMR studies which conclude that both the steroid nucleus and hydrocarbon tail are highly immobilized.

PART II: The Effect of Chain Length on the Secondary Structure of Oligoadenylates

The oligoadenylates $(Ap)_{2-4}A$ have been studied by proton magnetic resonance (pmr) spectroscopy. All the exterior base protons and a number of the interior base proton resonances have been assigned. The results of this work showed that the adenine bases in these oligoadenylates are intramolecularly stacked at 20°C with their bases oriented preferentially in the anti conformation about their respective glycosidic bonds. The oligomers were found to associate extensively even at concentrations of 0.02 M, primarily via "end to end" stacking. With increasing temperature the oligomer bases destack, but it is argued that this unfolding process cannot be described in terms of a two-state stacked versus unstacked model. Instead, the temperature dependences of the base proton chemical shifts support a base-oscillation model. The relationship between this model and the "two-state" model is discussed. Finally, on the basis of the chain-length dependence of the proton chemical shifts

of the various adenine bases, it was concluded that subtle variations in the secondary structure of these oligomers exist with increasing chain length. Evidence is presented to show that the effects of distant base shielding are considerably smaller than what was previously estimated. The observed departures from the "extended dimer" model are attributed to differences in the relative orientations of the bases with respect to their neighbors in the oligomer.

TABLE OF CONTENTS

	Title	Page
PART I.	The Use of Deuterated Phospholipids to Elucidate Lipid-Lipid Interactions in Bilayer Vesicles	1
Chapter I	General Introduction	
	1. Development of Membrane Models	2
	2. Model Membranes	6
	3. NMR and Molecular Motion	11
	4. NMR Studies of Model Membranes	18
Chapter II	Molecular Motion: Its Effects on Inter- and Intramolecular Relaxation in Lecithin Bilayers	
	1. Introduction	25
	2. Experimental	27
	3. Results	29
	4. Discussion	53
Chapter III	The Motional State of Cholesterol in Phospholipid Bilayers	
	1. Introduction	74
	2. Experimental	77
	3. Results and Discussion	78
	4. Conclusions	88
Chapter IV	Synthesis of Deuterated Lecithins	
	1. Introduction	95
	2. General Methods	99
	3. Synthesis of Perdeuterated Fatty Acids	100
	4. Synthesis of Fatty Acid Anhydrides	113
	5. Purification of Egg Lecithin	114
	6. Preparation of GPC from Egg Yolk Lecithin	115
	7. Preparation of Lysolecithin from Dipalmitoyl Lecithin	116
	8. Acylation of GPC	117
	9. Acylation of Lysolecithin	122

	Title	Page
PART II	The Effect of Chain Length on the Secondary Structure of Oligoadenylates, P. A. Kroon, G. P. Kreishman, J. H. Nelson and S. I. Chan, Biopolymers, 13, 0000 (1974)	131
PROPOSITIONS		185

PART I

THE USE OF DEUTERATED PHOSPHOLIPIDS TO ELUCIDATE LIPID-LIPID INTERACTIONS IN BILAYER VESICLES

I. General Introduction

Our primary concern in this introduction will be to place the chapters which follow in their proper context. After a brief summary of current membrane models we shall examine the use and value of model membrane systems. We shall follow this by a discussion of nuclear magnetic resonance spectroscopy, its value and limitations in membrane problems, and how some of the limitations can be overcome by methods discussed in subsequent chapters.

1. DEVELOPMENT OF MEMBRANE MODELS

In 1925 Gorter and Grendel proposed[1] that every red blood cell "... is surrounded by a layer of lipoids, of which the polar groups are directed to the inside and the outside, in much the same way as Bragg supposes the molecules to be oriented in a crystal of fatty acid and as the molecules of a soap bubble are according to Perrin". They based their proposal on the observation that red blood cells contained enough lipid to form a monolayer with twice the area of the red blood cell. Subsequent studies of unicellular marine organisms indicated a very low membrane surface tension.[2] Since it was known that the adsorption of denatured protein to oil droplets markedly lowered their interfacial tension, Davson and Danielli postulated that the basic structure of plasma membranes consists of a bilayer with globular protein absorbed to it on either side.[3] Robertson extended and modified the Davson-Danielli

concept[4] to account for the differential staining of the two sides of the membrane which he observed in electron microscopy studies. The resulting "unit membrane" structure consisted of a bilayer covered on one side with mucoprotein or mucopolysaccharide and on the other side with extended polypeptide chains. The Gorter and Grendel, Davson and Danielli, and Robertson models are illustrated in Fig. 1a, b, and c.

During the mid-1960's the bilayer and unit membrane concepts were vigorously questioned. This led to a series of alternative models,[5-7] most of which are less general in that they picture more intimate lipid-protein interactions, possibly to the complete exclusion of the lipid bilayer. The Benson model is an example.[5] Its fundamental structural feature is hydrophobic lipid-protein association. This is also the basic feature of the Green model[7] in which the membrane is viewed as a network of lipoprotein subunits. Other models combine features of both the bilayer and Benson models.

There is now however much direct evidence for the presence of bilayers in biological membranes. Differential scanning calorimetry studies have shown that a cooperative phase change corresponding to the crystal → liquid crystal transition occurs both in mycoplasma laidlawii membranes and in their extracted lipids in the bilayer form.[8] This transition can also be detected in a variety of mammalian membranes.[9] The presence of lipid bilayers in cell membranes may be considered established, and current models focus their attention more on the details of protein organization and protein mobility in the membranes.

FIGURE 1

Evolution of membrane models: (a) Gorter and Grendel model; (b) Davson-Danielli model; (c) Robertson unit-membrane model.

a.

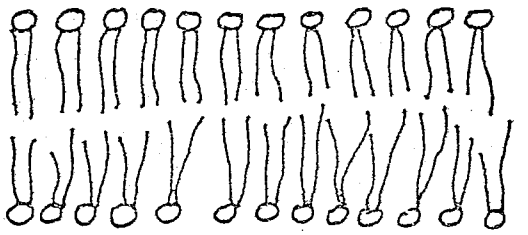

Lipid

b.

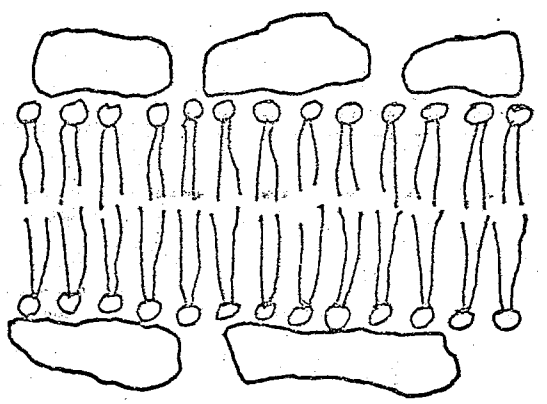

Globular Protein

Lipid

Globular Protein

c.

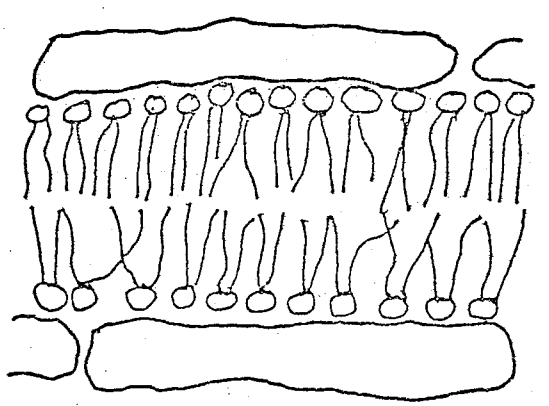

Extended Mucoprotein

Lipid

Extended Polypeptide

There is now much evidence that membranes should be viewed as a dynamic rather than a static structure. Singer[10] concludes for example that membranes are best described in terms of a fluid mosaic model. In this model the proteins that are integral to the membrane (i.e., those that cannot be removed under mild conditions) are globular molecules, arranged with their highly polar groups protruding from the membrane into the aqueous phase and with their nonpolar groups buried in the hydrophobic interior of the membrane. The phospholipids are therefore organized as a discontinuous fluid bilayer. The fluid mosaic structure is considered to be analogous to a two-dimensional oriented solution of integral proteins embedded in a viscous phospholipid bilayer solvent.

2. MODEL MEMBRANES

The ultimate goal in the study of biological membranes is a detailed understanding of the composition, organization and function of unaltered biological membranes. This goal can be pursued on various levels. One very fruitful approach has been to study model systems, that is systems which embody features common to all membranes and which provide a conceptual framework from which specific models for individual membranes can be constructed.

Since the bilayer appears to be the basic structural feature associated with membranes, multiple and single walled phospholipid bilayers (liposomes and vesicles respectively, see Fig. 2) have been studied extensively as models of biological membranes.

FIGURE 2

Model membranes. Amphiphatic lipid dispersed in aqueous solution forms multilamellar liposomes. Sonication of liposomes converts them to small single walled bilayer vesicles.

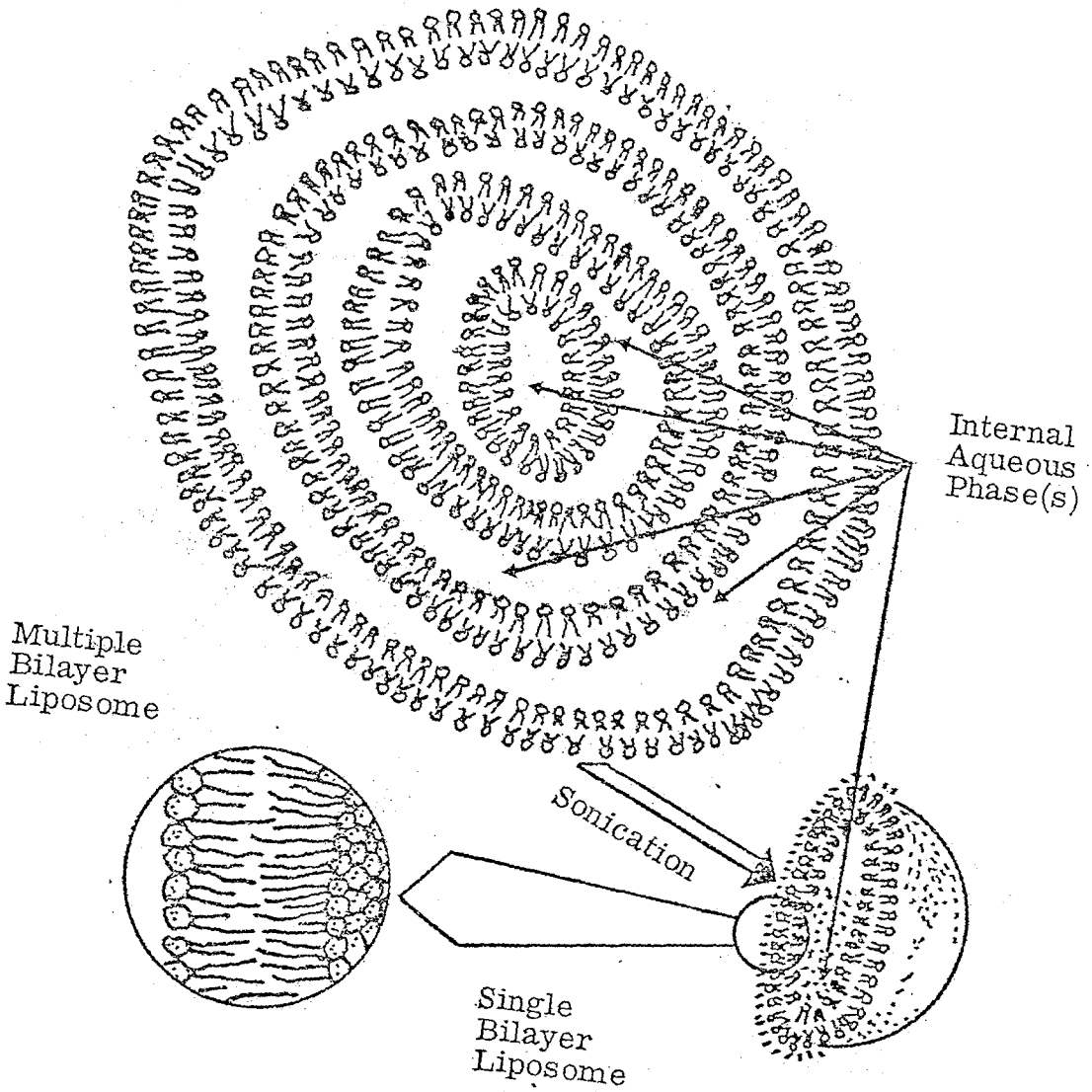
Internal
Aqueous
Phase(s)
Multiple
Bilayer
Liposome
Sonication
Single
Bilayer
Liposome

The study of liposomes has been extremely fruitful.[11-14] There are however certain problems associated with liposomes such as the unknown surface area, the extremely complicated kinetics associated with exchange across the concentric bilayers, and the fact that it is difficult to study incorporated enzymes which exhibit vectorial behavior since the inside of one bilayer is the outside of the next. Vesicles on the other hand have a measurable surface area and thickness,[15] they are suitable for permeability studies and can be used to study the vectorial behavior of incorporated enzymes.[16] The only apparent problem associated with vesicles is their small diameter (~300 Å) which results in a highly curved surface.[17] Recent experimental and theoretical nuclear magnetic resonance (NMR) studies have demonstrated that the phospholipid chain packing is disturbed as a result of this curvature.[18,19] This may of course have an important effect on ion permeabilities and the activity of incorporated proteins. Racker has found that the efficiency of oxidative phosphorylation in reconstituted mitochondrial vesicles depends on the kinds of lipids used,[16] and has speculated that different lipids produce different sized vesicles which in turn affect the enzyme activity. It is easy to see how a change in vesicle size, and therefore in curvature and packing, might alter the binding and activity of enzymes as well as the permeability of ions, all of which are crucial factors in oxidative phosphorylation. It should be pointed out that vesicles which contain incorporated enzymes are generally somewhat larger than vesicles without enzyme.[16] Recently it has

become possible to prepare such larger sized vesicles without enzyme.[20] This clearly extends the usefulness of vesicles as a model system since it allows one to study membrane phenomena as a function of curvature, which may clarify questions surrounding lipid order, enzyme activity and ion permeability.

Many investigators have turned to spectroscopic methods such as fluorescence,[21] electron spin resonance[13, 22-26] and nuclear magnetic resonance[14, 18, 19, 27-34] to study these model systems, in the hope of resolving questions of order and mobility of the bilayer components. Fluorescence probe studies have indicated that the lecithin polar head groups are more mobile and are further apart above the phase transition than below it. ESR studies have been used to investigate the order and mobility of lipid hydrocarbon chains,[22-24] rates of lateral diffusion,[26] and the binding of lipids to enzymes incorporated in bilayers.[25] Results have been interpreted to mean that above the thermal phase transition temperature there is rapid motion about the lipid hydrocarbon chain axis, together with trans-gauche interconversions, giving rise to off axis motions. It has been pointed out however that the ESR probe has a profound perturbing effect.[30] At the position of the spin label the diameter of the chain is almost twice that of a normal hydrocarbon chain. The spin label therefore distorts the parallel packing of the chains and thus creates free space for a more disordered molecular motion. Finally, many investigators have used NMR to determine structure and mobility of membrane components. In the next section

we shall briefly review some of the concepts involved in NMR studies. We shall follow this by a discussion of the advantages and problems associated with NMR studies. We shall show how some of these problems can be overcome to make NMR an extremely powerful tool to study not only bilayers, but also reconstituted bilayer systems which contain functional enzymes.

3. NMR AND MOLECULAR MOTION

Nuclear magnetic resonance studies can give information about molecular structure and about molecular motion. Structural information is derived from chemical shifts and spin-spin coupling constants, with which we shall not be concerned. We shall be concerned primarily with molecular motion and what NMR can tell us about motion. We shall assume for our discussion that we are dealing with systems in which the static dipolar coupling is effectively averaged out. While this is true for small bilayer vesicles, with which we shall be concerned, it is not true for multilayer liposomes.

The motional characteristics of a set of protons on a molecule can be ascertained from their linewidth, spin-spin (T_2) and spin-lattice (T_1) relaxation times. The linewidth and T_2 are of course related; for a lorentzian line the full width at half height $\Delta\nu$ is related to T_2 by $T_2 = 1/\pi\Delta\nu$. Relaxation times for a particular nucleus are determined by the fluctuating magnetic fields which it experiences. These fields may have a number of different origins. For protons, fields from fluctuating magnetic dipole moments of

nearby protons often dominate. These may be located on the same molecule, in which case we have an intramolecular contribution, or they may be located on other molecules, resulting in an intermolecular contribution. Fluctuating fields arise if the distance between two protons or their relative orientation with respect to the magnetic field is modulated by random molecular motion. For rigid molecules, intramolecular relaxation is only affected by rotational motions. Intermolecular relaxation on the other hand is affected by both rotational and translational motion, since both of these can modulate the distance between nuclei and their relative orientation with respect to the magnetic field. Of course if the molecule is not rigid, internal motions complicate the situation since they further contribute to inter- and intramolecular relaxation.

T_1 and T_2 depend on the details and rates of molecular motion in a different manner. Both can be described in terms of the spectral density function $J(\omega)$ of the molecular motion. T_1 depends on $J(\omega_0)$ and $J(2\omega_0)$, whereas T_2 depends on $J(0)$, $J(\omega_0)$ and $J(2\omega_0)$, where ω_0 is the NMR spectrometer frequency.

By considering the dependence of these spectral density functions on the frequency for several values of τ_c (the correlation time for the motion) we can gain some insight into the relation between T_1, T_2 and τ_c. In Fig. 3 we have illustrated how $J(\omega)$ varies with ω, for short ($\omega_0 \tau_c \ll 1$), intermediate ($\omega_0 \tau_c \sim 1$) and long ($\omega_0 \tau_c \gg 1$) values for τ_c. For short correlation times, the molecular motions are distributed over a wide frequency range ($0\text{-}\tau_c^{-1}$) and result in

FIGURE 3

Spectral density functions $J(\omega)$, for random isotropic molecular motion described by a single long correlation time ($\omega_0 \tau_c \sim 10^3$), intermediate correlation time ($\omega_0 \tau_c \sim 1$) and short correlation time ($\omega_0 \tau_c \sim 10^{-3}$).

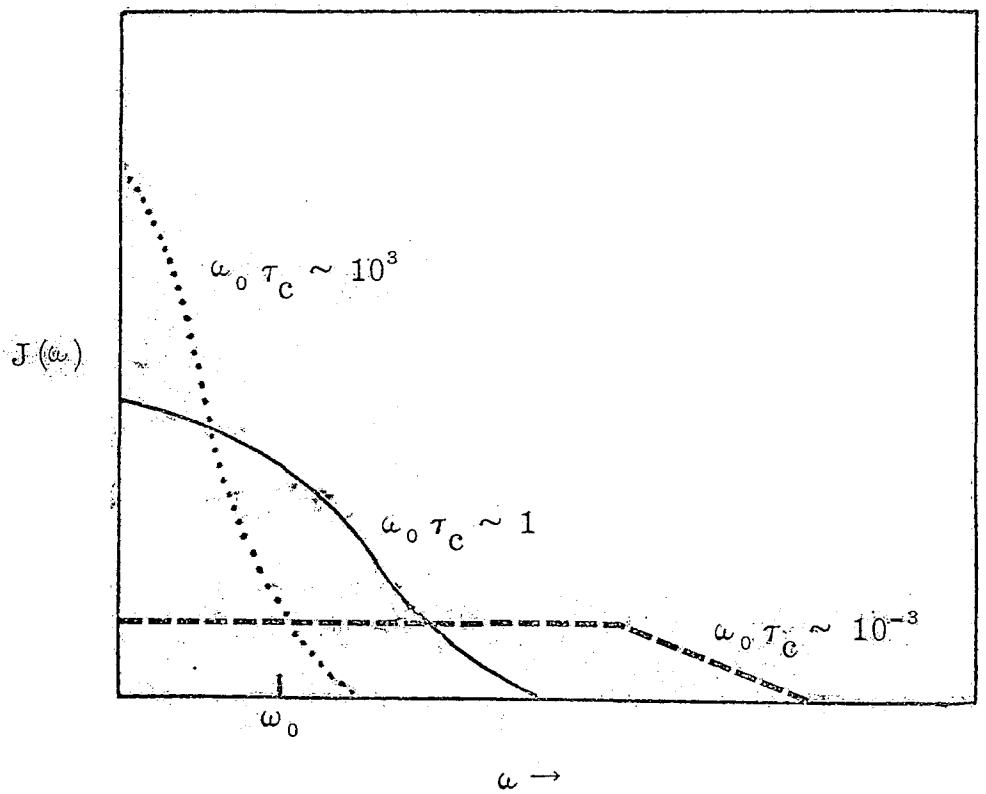
$\omega_0 \tau_c \sim 10^3$
$J(\omega)$
$\omega_0 \tau_c \sim 1$
$\omega_0 \tau_c \sim 10^{-3}$
ω_0
$\omega \rightarrow$

a small spectral density at any of these frequencies. As τ_c increases however, $J(\omega)$ increases until it reaches a maximum at $\tau_c \sim 1/\omega_0$). At this point it begins to decrease with increasing τ_c. The T_1 relaxation rate mimics the behavior of $J(\omega)$, reaching a maximum at $\tau_c \sim 1/\omega_0$. The behavior of T_2 is more complicated because it depends on components at zero frequency $J(0)$, which becomes more important as the motion becomes slower. As a consequence the T_2 relaxation rate shows no maximum, but increases continually with increasing τ_c until the rigid lattice limit is reached. The T_1 and T_2 curves for isotropic rotational motion with a single correlation time are shown in Fig. 4.

A description of anisotropic motion is much more complicated. Consider for example a cigar-shaped molecule which undergoes rapid motion about its long axis and tumbles much more slowly about its short axis. These motions can be described by correlation times τ_a and τ_b respectively. The dependence of the relaxation rates on the inverse temperature is rather complicated.[35] T_1 exhibits two minima. However, as long as $\omega_0 \tau_a \sim 1$, T_1 will be determined primarily by the faster motion. T_2 on the other hand is dominated by the slower component of the motion in this situation.

The motion of hydrocarbon chains in bilayer vesicles is both restricted and anisotropic. Recently Seiter and Chan have presented a theoretical treatment to deal with this problem.[18] Using their formulism, it is possible to interpret NMR data in terms of motional details of the hydrocarbon chains.

FIGURE 4

The variation of the nuclear magnetic relaxation times, T_1 and T_2, as a function of the motional correlation time.

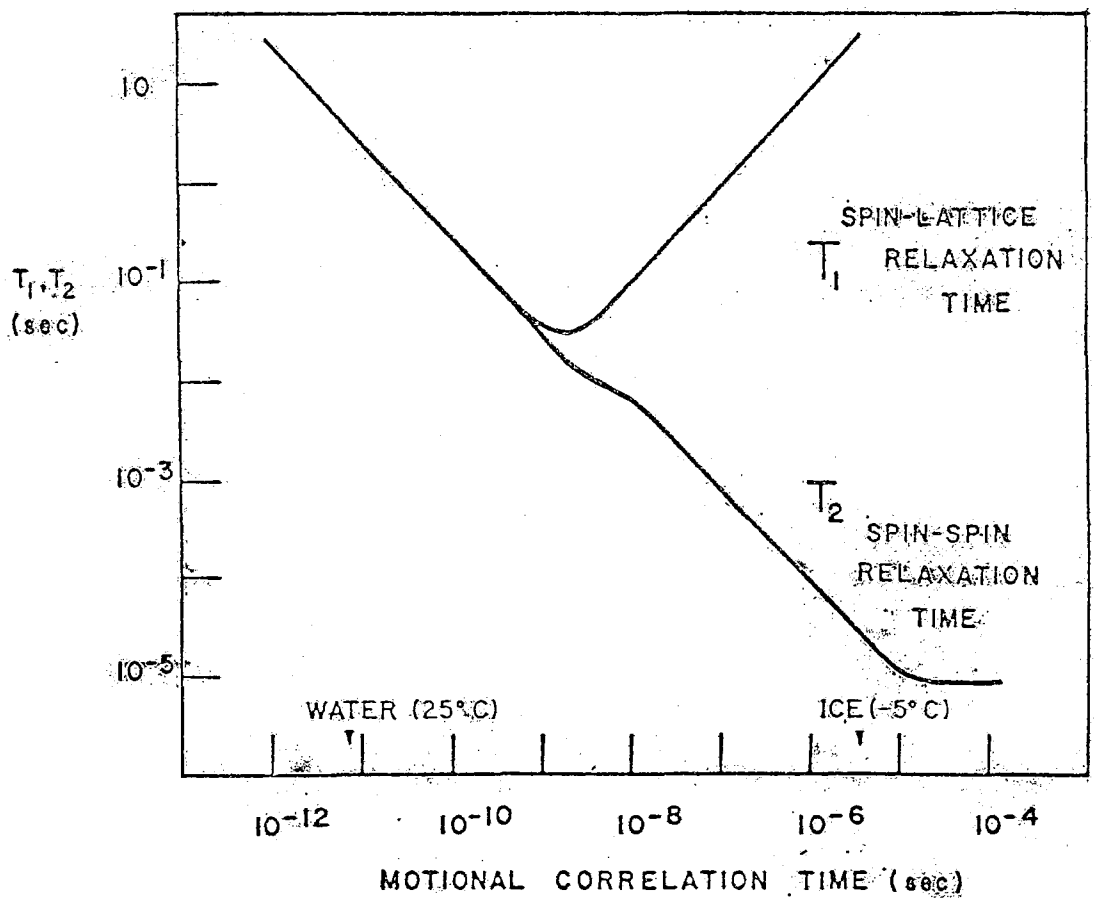
10
10⁻¹
10⁻³
10⁻⁵
T₁, T₂ (sec)
SPIN-LATTICE
T₁ RELAXATION
TIME
T₂
SPIN-SPIN
RELAXATION
TIME
WATER (25°C)
ICE (-5° C)
10⁻¹²
10⁻¹⁰
10⁻⁸
10⁻⁶
10⁻⁴
MOTIONAL CORRELATION TIME (sec)

4. NMR STUDIES OF MODEL MEMBRANES

The sensitivity of NMR parameters such as T_1, T_2 and linewidth to the details of molecular motion makes NMR an extremely powerful method to probe the motional state of membrane components. It provides a method to study internal motions, such as lipid chain motions, as well as motions involving the molecule as a whole, such as rotational and translational diffusion. It has definite advantages over ESR spin label and fluorescence probe studies in that the system is not perturbed in any way.

There are disadvantages however. The separation of inter- and intramolecular effects is usually difficult. This separation is much easier for spin label studies. The major disadvantage arises however when we try to study anything but simple bilayers. Our real interest is not simply to study bilayers for their own sake, but to extend the bilayer studies to systems resembling biological membranes. On the simplest level we may want to study the interaction of cholesterol with lecithin bilayers. This system serves as a useful model for myelin membranes. In principle NMR can give us a detailed picture of what happens to the cholesterol molecule once it is inside the bilayer. In practice of course the cholesterol resonances overlap with the chain methylene and methyl resonances and all we see is a broadened hydrocarbon chain spectrum (see Chapter III). On a more sophisticated level we may want to study reconstituted membrane systems. One such system under study in Dr. S. I. Chan's laboratory is site III of the oxidative phosphorylation system

of the inner mitochondrial membrane. Purified cytochrome oxidase can be incorporated into phospholipid vesicles.[16] When reduced cytochrome c is added to the outside solution, the enzyme system functions. Cytochrome c shuttles electrons to the cytochrome oxidase complex which in turn reduces molecular oxygen. In the presence of coupling factors ATP can be generated. This system provides a fascinating challenge and has raised many questions. Why is the cytochrome oxidase activity so sensitive to the presence of phosphatidyl ethanolamine and cardiolipin?[16] Are head group interactions important, do the phospholipids perhaps bind selectively to the enzyme? Again NMR is a potentially useful tool to study these problems, and again there is the problem that we cannot distinguish one phospholipid from the other, and that any enzyme resonances of interest are completely obliterated by the lipid chain resonances. The ESR method, with all its limitations, has provided more information about these phenomena than NMR studies.[25] The spin label has a clearly identifiable spectrum. One can attach it to a specific phospholipid and therefore study the behavior of each phospholipid selectively.

There are solutions for NMR however. Instead of electron spin labels we can use nuclear labels such as ^{13}C, ^{19}F, or D, the first as a replacement for ^{12}C and the last two for protons. The immediate advantage is that these labels are much smaller than spin labels and, with the possible exception of ^{19}F, provide essentially no perturbing influence on the molecule itself or its surroundings.

The high sensitivity of ^{19}F makes it a favorable choice from the NMR point of view. One worrisome feature is the rather weak interaction between perfluorinated hydrocarbon chains[36] compared to proton containing hydrocarbon chains. Since the bilayer owes a large part of its stability to interactions between lipid hydrocarbon chains, the substitution of protons by ^{19}F may severely disturb the bilayer stability. ^{13}C and D labels do not share this problem and are therefore much more promising. A number of workers are now using these labels to study membranes.[30, 32] It is a very time consuming approach however. The sensitivity of ^{13}C and D are only 1.59 and 0.965% of the corresponding proton sensitivity. To illustrate the result of this, consider equal concentrations of deuterium and proton-containing molecules. Assume the linewidths to be the same. In order to get an equivalent signal to noise ratio, 10^4 deuterium spectra must be averaged for every proton spectrum!

We have approached the problem from a somewhat different angle. Since proton NMR is so sensitive we feel it is more sensible to label anything we don't want to see and thus to look only at protons of direct interest. This method has obvious applicability to the problems we mentioned before. If we want to study the binding of a particular phospholipid to cytochrome oxidase for example, we can simply deuterate all phospholipids except the one of interest. If we are interested in the protein resonances we could simply deuterate all of the phospholipids. By observing protonated lipids in a matrix of deuterated lipids we can also sort out the inter- and

intramolecular contributions to relaxation times. This can shed further light on the motional states of phospholipid molecules in a bilayer.

The work presented here is the beginning of a rather broad study of lipid-lipid and lipid-protein interactions currently in progress in Dr. S. I. Chan's laboratory, and should be viewed as such. A detailed description of the synthesis of lecithins with one or both hydrocarbon chains perdeuterated is given in Chapter IV. In Chapter II we examine in some detail the inter- and intramolecular relaxation times of lecithin hydrocarbon chain protons to elucidate motional characteristics of the lecithin molecules. Chapter III describes the use of deuterated lecithin to study the motional state of cholesterol molecules dispersed in a lecithin bilayer.

References

1. E. Gorter and F. Grendel, J. Exp. Medicine 41, 439 (1925).
2. J. F. Danielli and E.N. Harvey, J. Cell. Comp. Physiol. 5, 483 (1935).
3. H. Davson and J. F. Danielli, "The Permeability of Natural Membranes" (2nd ed.), London, Cambridge University Press, 1952.
4. J. D. Robertson, J. Biophys. Biochem. Cytol. 3, 1043 (1957).
5. A. A. Benson, in "Membrane Models and the Formation of Biological Membranes", L. Bolis and B. A. Pethics, North-Holland, 1968.
6. E. D. Korn, Science 153, 1491 (1966).
7. D. E. Green and J. F. Perdue, Proc. Nat. Acad. Sci. 55, 1295 (1966).
8. J. M. Steim, M. E. Tourtelotte, J. C. Reinert, R. N. McElhaney and R. L. Rader, Proc. Nat. Acad. Sci. 63, 104 (1969).
9. J. F. Blazykt and J. M. Steim, Biochim. Biophys. Acta 266, 737 (1972).
10. S. J. Singer and G. L. Nicolson, Science 175, 720 (1972).
11. A. D. Bangham, M. M. Standish and J. C. Watkins, J. Mol. Biol. 13, 238 (1965).
12. V. Luzzati and F. Husson, J. Cell. Biol. 12, 207 (1962).
13. R. D. Kornberg and H. M. McConnell, Biochemistry 10, 1111 (1971).

14. G. W. Feigenson and S. I. Chan, J. Amer. Chem. Soc. 96, 1312 (1974).

15. C. Huang, Biochemistry 8, 344 (1969).

16. E. Racker and A. Kandrach, J. Biol. Chem. 248, 5841 (1973).

17. M. P. Sheetz and S. I. Chan, Biochemistry 11, 4573 (1972).

18. C. H. A. Seiter and S. I. Chan, J. Amer. Chem. Soc. 95, 7541 (1973).

19. D. Lichtenberg, N. O. Petersen, J.-L. Girardet, M. Kainosho, P. A. Kroon, C. H. A. Seiter, G. W. Feigenson and S. I. Chan, Biochim. Biophys. Acta, in press.

20. R. Lawaczeck, M. Kainosho and S. I. Chan, manuscript in preparation.

21. E. Sackman and H. Trauble, J. Amer. Chem. Soc. 94, 4482 (1972).

22. W. L. Hubbell and H. M. McConnell, J. Amer. Chem. Soc. 93, 314 (1971).

23. E. Oldfield and D. Chapman, Biochem. Biophys. Res. Commun. 43, 610 (1971).

24. B. G. McFarland and H. M. McConnell, Proc. Nat. Acad. Sci. 68, 1274 (1971).

25. P. Jost, O. H. Griffith, R. A. Capaldi and G. Vanderkooi, Biochim. Biophys. Acta 311, 141 (1973).

26. C. J. Scandells, P. Devaux and H. M. McConnell, Proc. Nat. Acad. Sci. 69, 2056 (1972).

27. D. Chapman, D. J. Flack, S. A. Penkett and G. G. Shipley,

Biochim. Biophys. Acta 163, 255 (1968).

28. Y. K. Levine, Prog. Biophys. Mol. Bio. 24, 1 (1972).
29. E. G. Finer, A. G. Flook and H. Hauser, Biochim. Biophys. Acta 260, 59 (1972).
30. A. Seelig and J. Seelig, Biochemistry 13, 4839 (1974).
31. A. F. Horwitz, M. P. Klein, D. M. Michaelson and S. J. Kohler, Ann. N. Y. Acad. Sci. 222, 468 (1973).
32. Y. K. Levine, N. J. M. Birdsall, A. G. Lee and J. C. Metcalfe, Biochemistry 11, 1416 (1972).
33. A. G. Lee, N. J. M. Birdsall and J. C. Metcalfe, Biochemistry 12, 1650 (1973).
34. A. C. McLaughlin, F. Podo and J. K. Blasie, Biochim. Biophys. Acta, 330, 109 (1973).
35. D. E. Woessner, J. Chem. Phys. 37, 647 (1962).
36. T. J. Brice, in "Fluorine Chemistry," J.H. Simons, Ed., Academic Press, New York, 1950, Vol. 1, p. 436.

II. Molecular Motion: Its Effects on Inter- and Intramolecular Relaxation in Lecithin Bilayers

1. INTRODUCTION

The motion of hydrocarbon chains in phospholipid bilayer vesicles has been studied extensively by NMR[1-15] methods. Unlike multilayer spectra, which consist of very broad (4000 Hz) proton resonances,[16] vesicle spectra are characterized by rather sharp (10-50 Hz) methylene resonances. Finer has concluded that the narrower resonances are simply a consequence of overall tumbling of the vesicle,[14] and that the basic bilayer structure is unchanged. However we have recently shown that Finer's conclusion is based on incorrect theoretical arguments and that the narrower resonances actually reflect a more disordered bilayer strucutre.[15] Lee et al.[10] go even further. On the basis of an extensive NMR study, they conclude that the methylene linewidths tell us little of the order or disorder of the hydrocarbon chains since the chain motion is extremely fast and almost isotropic, with the possible exception of a few methylenes near the polar end of the chain. They argue that the linewidths are actually determined by intermolecular effects which they attribute to translational diffusion. This enables them to calculate self-diffusion coefficients for phospholipids in bilayer vesicles. They extend this to give estimates of self-diffusion coefficients for intact biological membranes, such as the sarcoplasmic reticulum, rabbit sciatic nerve, and electroplax membranes. It is clear that

in order to resolve the origin of the methylene linewidth, the various contributions (i. e. intrachain, interchain and intermolecular) to the linewidth must be determined experimentally.

Spin lattice relaxation times have also been used to study hydrocarbon chain motion. Again there is the objection that without a detailed knowledge of all the different contributions it is difficult to interpret the observed temperature and frequency dependence.[9,10]

In the first part of this chapter we shall focus on the problems mentioned above. The various relaxation contributions can be effectively sorted out by isotopic "dilution" experiments with deuterated hydrocarbon chains. If we recall that the dipole-dipole interaction between two nuclei A and B is proportional to $\gamma_A^2 \gamma_B^2$, and that the gyromagnetic ratio for deuterons γ_D is approximately 1/6 that for protons, it is obvious that by substituting deuterons for protons we can effectively remove their dipole relaxation contribution. For example, if we take a DPL molecule and surround it by DPL molecules with deuterated hydrocarbon chains, we have removed most of the intermolecular relaxation. If we now replace one of the hydrocarbon chains of our DPL molecule by a deuterated chain, we have effectively removed interchain relaxation. Using this approach, we come to the conclusion that interchain effects are small, and although intermolecular contributions do exist they do not dominate the linewidth or T_1.

In the second part of this chapter we turn our attention to the effect of chain length on the methylene linewidth and T_1 and what

this tells us about the motional state of the hydrocarbon chains. It is well established that the order and mobility of the hydrocarbon chains depend on whether the temperature is above the thermal phase transition. It is generally assumed that the order and mobility also depend on how far the temperature is above the thermal phase transition temperature. We show that this assumption is incorrect for lecithins with saturated hydrocarbon chains.

2. EXPERIMENTAL

Materials. Dipalmitoyl lecithin with one chain deuterated (1, palmitoyl-2-palmitoyl (d_{31})-phosphatidylcholine, which we shall refer to as DPL (H, D)), and with both chains deuterated (1, 2-dipalmitoyl (d_{62})-phosphatidylcholine, which we shall refer to as DPL (D)) were synthesized and purified as described in Chapter IV. Distearoyl lecithin (DSL), dipalmitoyl lecithin (DPL), dimyristoyl lecithin (DML) and dilauroyl lecithin (DLL) were obtained from General Biochemicals. For experiments involved in the evaluation of inter- and intramolecular relaxation, purified DPL was used. The purification procedure was the same as that used for deuterated DPL (Chapter IV). Otherwise the lecithins were used without further purification. Deuterium oxide (99.8% D) was obtained from Stohler Isotope Chemicals.

Sample preparation. Samples containing deuterated DPL and protonated DPL were prepared by dissolving weighed amounts of the lipids in chloroform in a 3 ml centrifuge tube. Most of the

chloroform was removed by placing the centrifuge tube in a sand bath at ~50°C and directing a stream of dry nitrogen into the tube. The remaining viscous solution was frozen in liquid nitrogen and dried overnight under high vacuum. D_2O (1 ml) was added to the sample, which was then sonicated for 20 minutes using a MSE 150 Watt ultrasonic disintegrator at high power. During sonication the sample was partially immersed in a glycerol cooling bath to avoid overheating. Samples containing one lipid component only were prepared in the same way, except that the chloroform step was omitted. All samples contained 5% (weight/volume) of lipids.

Instrumentation. NMR measurements were made at 220 MHz with a Varian HR-220 spectrometer modified for Fourier transform operation. The system is interfaced with a Varian 16 K 620/i computer and Sykes compucorder 120. The probe temperature was regulated (± 1°C) by a Varian 4540 variable temperature unit. Measurements at 100 MHz were made using a Varian XL-100 system equipped with a 12-inch magnet. This system is equipped with a Varian 16 K 620/i computer and a Sykes compucorder 100. The probe temperature on both spectrometers was monitored by measuring the ethylene glycol splitting. Temperature calibration charts were provided by Varian Associates.

Fourier transform measurements were made using programs provided by Dr. S. Smallcombe (Varian Associates). These programs (SSFT-1-D/X for the XL-100 and SSFT-1-D/S for the HR-220) made it possible to time average and store up to 10 inversion recovery

spectra automatically on a cassette tape.

T_1 measurements were made using the ($\frac{\pi}{2}$-free induction decay-π-homospoil-τ) inversion recovery sequence. Typically 200 transients were collected for samples containing deuterated DPL. T_1's were calculated from the amplitude of each line in the partially relaxed spectrum[17] by plotting ln (M_Z (∞) - $M_Z(\tau)$ versus τ. The slope of this plot is $-1/T_1$. The T_1's are accurate to within 5%.

3. RESULTS

The 220 MHz NMR spectrum of the choline methyl, hydrocarbon chain methylene and terminal methyl protons for DPL vesicles in D_2O is shown in Fig. 1. The high resolution features observed are characteristic for small (300 Å) vesicles and contrast sharply with the 4000 Hz wide lines found for multilayers.[16] We shall mainly be concerned with the choline methyl and hydrocarbon chain methylene protons.

Linewidth studies. In order to estimate inter- and intramolecular contributions to the methylene linewidth, spectra of DPL in a protonated matrix were compared with spectra of DPL in a deuterated matrix.

Figure 2 shows the results at 100 and 220 MHz and over a temperature range of 50-90°C. We must point out that the linewidths are sensitive to the choice of a baseline. For vesicle spectra this choice is somewhat ambiguous. As long as a baseline is chosen using the same spectral width, however, linewidths are very

FIGURE 1

NMR spectrum at 220 MHz, of dipalmitoyl lecithin vesicles (5% w/v) in D_2O at 77°C. Only resonances upfield from and including the choline methyl resonance are shown.

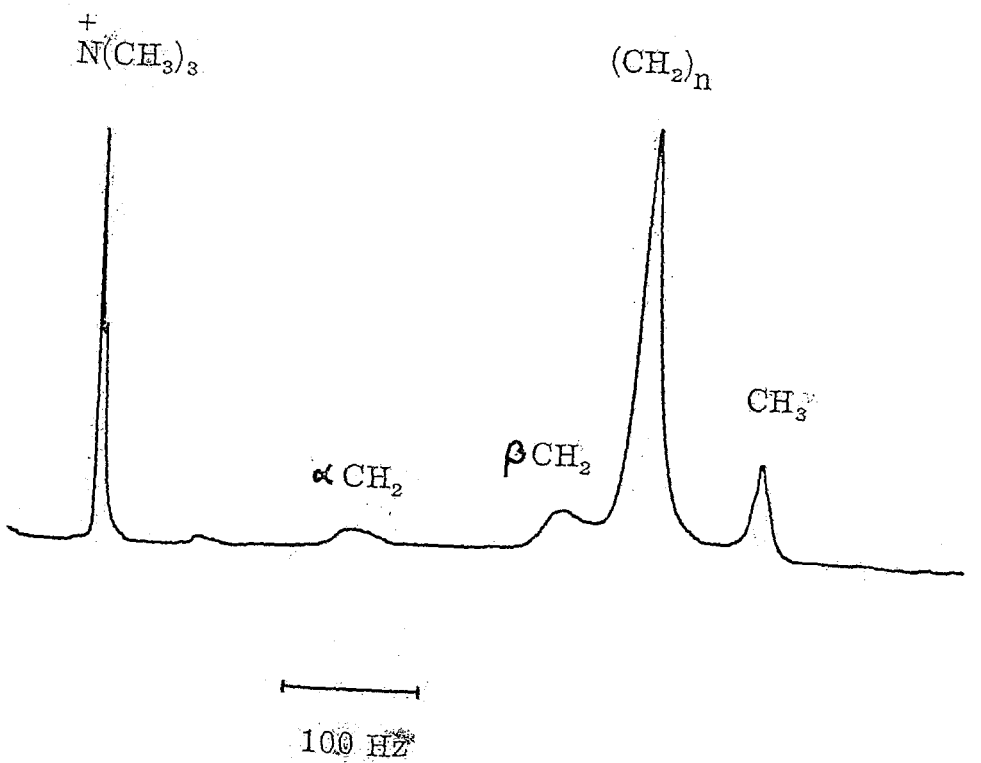
$\overset{+}{N}(CH_3)_3$
$(CH_2)_n$
CH_3
αCH_2
βCH_2
100 Hz

FIGURE 2

Methylene linewidths for 100% DPL and 10% DPL, 90% DPL (D) vesicles as a function of temperature. At 220 MHz a spectral width of 500 Hz was used, and at 100 MHz a spectral width of 200 Hz was used to measure the linewidths.

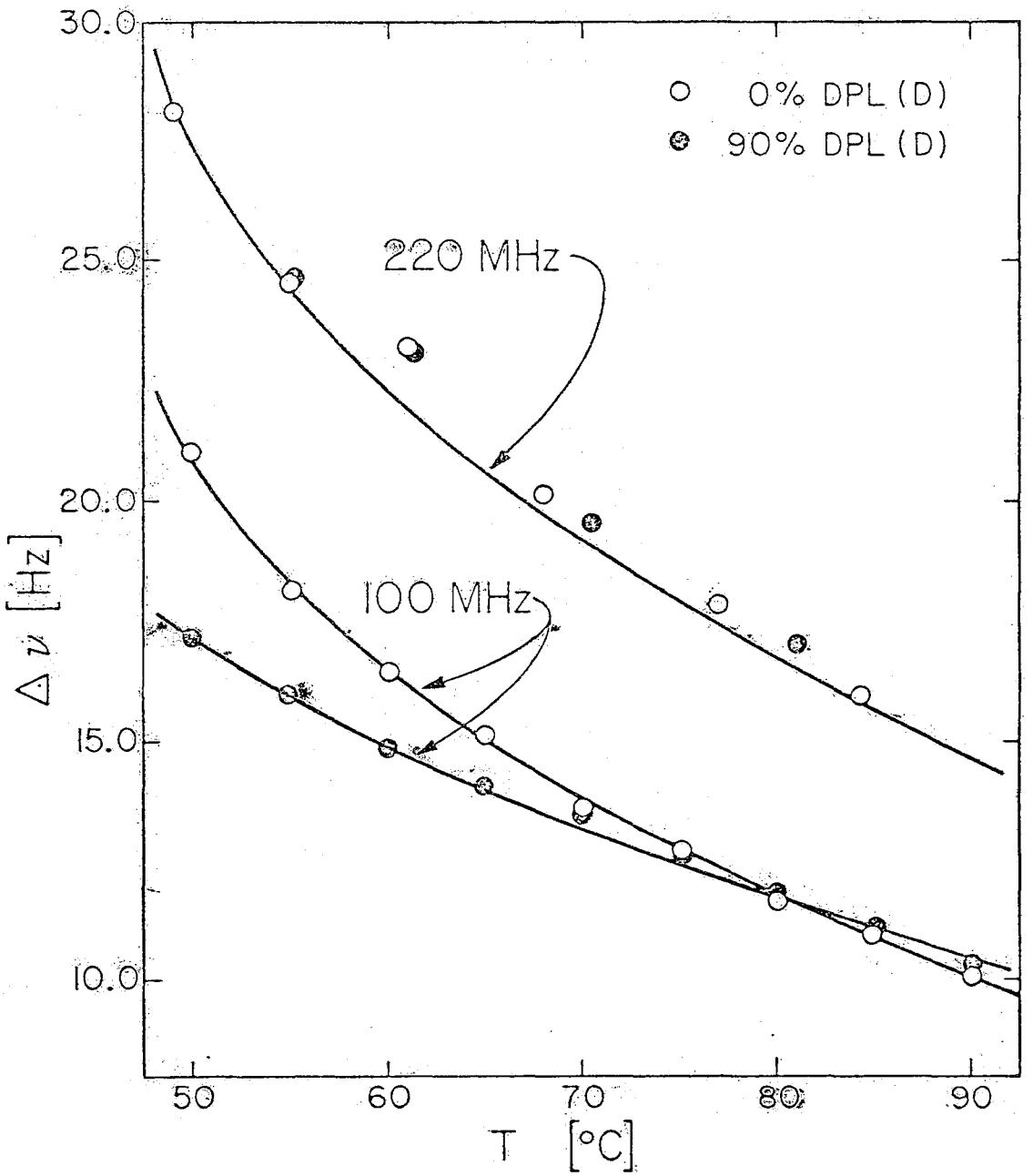
30.0
25.0
20.0
15.0
10.0
Δ ν [Hz]
50
60
70
80
90
T [°C]
0% DPL (D)
90% DPL (D)
220 MHz
100 MHz

reproducible.

Returning to Fig. 2, we note that the 100 MHz linewidths are smaller in a DPL (D) than in a DPL matrix, especially at low temperatures. In light of this observation the 220 MHz data are somewhat surprising in that the linewidths are the same in a DPL (D) and DPL matrix. It must be remembered however that the hydrocarbon chain deuteron content in DPL (D) is not 100%, but 98.8%. The residual protons (approximately three for every four phospholipid molecules))exist as CHD and CH_2 groups. From the $CDCl_3$ spectrum (see Chapter IV) one finds these two resonances separated by 13 Hz at 220 MHz. The difference between the CH_2 and CHD proton T_1's has enabled us to eliminate the CH_2 resonance and to measure the CHD linewidth. At 55°C this linewidth is ~14 Hz. Spectral simulation has shown that the presence of a resonance ~14 Hz wide results in a broadening of the 220 MHz resonance, which effectively overshadows narrowing effects. At 100 MHz this effect is much smaller.

A meaningful comparison of methylene linewidths of DPL in a protonated and deuterated matrix is valid only under the condition that the presence of DPL (D) does not change the nature of the matrix and that ideal mixing occurs. The first question is of concern since the bilayer owes part of its stability to the van der Waals interaction between the hydrocarbon chains, which may be different for DPL (D). Actually the phase transition temperature of DPL (D) is about 4°C lower than that of DPL,[18] which indicates a slightly weaker

interaction between deuterated chains than between protonated chains. This difference is too small to cause any changes in the vesicle structure. The fact that the choline methyl T_1's for DPL (D) and DPL vesicles are the same within experimental error (see Fig. 3) supports this contention. Finally, differential thermal analysis studies[18] have shown that DPL (D) and DPL exhibit ideal mixing. Therefore no segregation occurs.

It is interesting to note that the T_1's of the inside and outside choline resonances are different. The difference between the T_1's is probably a manifestation of the different packing of the head groups on the inside and outside. The outside cholines are expected to be more loosely packed than the inside cholines as a result of surface curvature.[1] They should therefore have a greater mobility and disorder and a longer T_1 than the inside cholines. This is observed.

An interesting feature of the data in Fig. 2 is the frequency dependence of the intramolecular linewidth contribution. Since all indications are that the linewidth is controlled by dipolar interactions, this observation is somewhat surprising. Sheard[19] made a similar observation for egg lecithin and has attributed it to differences in the diamagnetic susceptibility along the hydrocarbon chain.

Factors which determine the motional state of the hydrocarbon chains are largely unknown, except for the fact that double bonds and increasing temperature increases the disorder and the mobility. In order to determine the effect of chain length on the motional state, we have measured spectra of saturated lecithins as a function of

FIGURE 3

Inside and outside choline methyl spin-lattice relaxation rates (T_1^{-1}) as a function of 1/T for 100% DPL and 10% DPL, 90% DPL(D) vesicles.

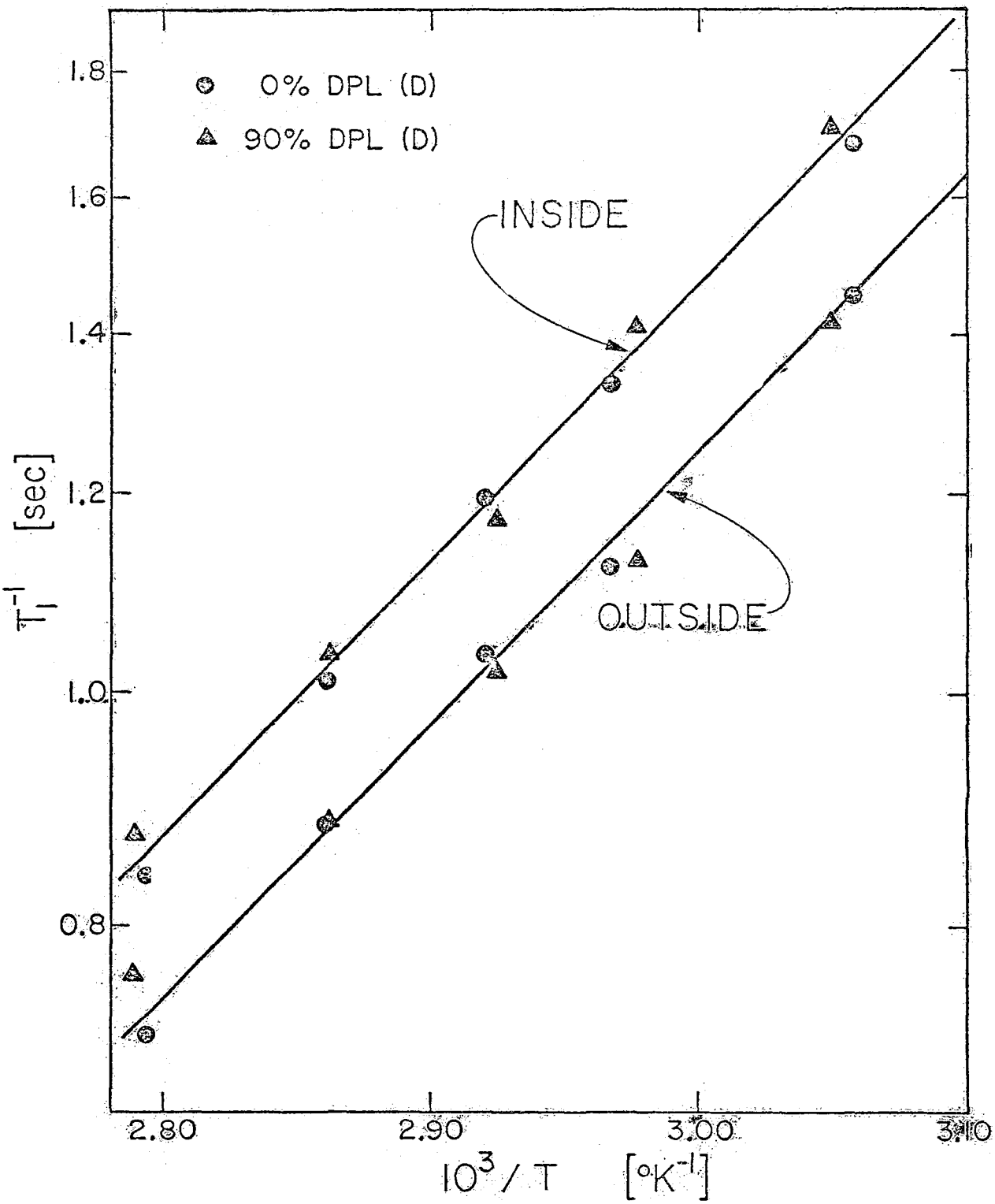
0% DPL (D)
90% DPL (D)
INSIDE
OUTSIDE
1.8
1.6
1.4
1.2
1.0
0.8
T_1^{-1} [sec]
2.80
2.90
3.00
3.10
$10^3 / T$ [°K^{-1}]

chain length and temperature. The linewidth results are shown in Fig. 4. Since the linewidth increases very rapidly around the phase transition temperature, these points are off scale and are not shown. The somewhat surprising conclusion we must draw from these data is that the linewidth is essentially independent of the chain length, except in the region close to the phase transition temperatures where the linewidth rapidly increases with decreasing temperature.

In light of this observation we briefly return to the questions relating to methylene linewidths measured in a DPL (D) and DPL matrix. Since the DLL and DSL linewidths are the same above their thermal phase transition temperatures of 0°C and 58°C respectively, we feel safe to conclude that the 4°C difference between the DPL and DPL (D) phase transition temperatures will be insignificant to the linewidths measured above the phase transition temperatures.

T_1 studies. Intermolecular methylene T_1's were determined by isotopic dilution with DPL (D). In each case the CH_2's were characterized by a single T_1. This does not exclude a distribution of T_1's, but rather tells us that the distribution is not very large. One manifestation of a small T_1 distribution is the fact that the so-called null point T_1 is different from the T_1 determined graphically (see Experimental section). The null point is the point at which the magnetization in the Z direction has relaxed to zero after a π pulse. The time interval between the pulse and the null point, τ_{null}, is related to T_1 by $\tau_{null} = T_1 \ln 2$. This is only true however if a particular resonance is described by a single T_1, otherwise the

FIGURE 4

Methylene linewidth for DLL, DML, DPL and DSL vesicles at 100 MHz, as a function of temperature. A spectral width of 500 Hz was used to measure the linewidth.

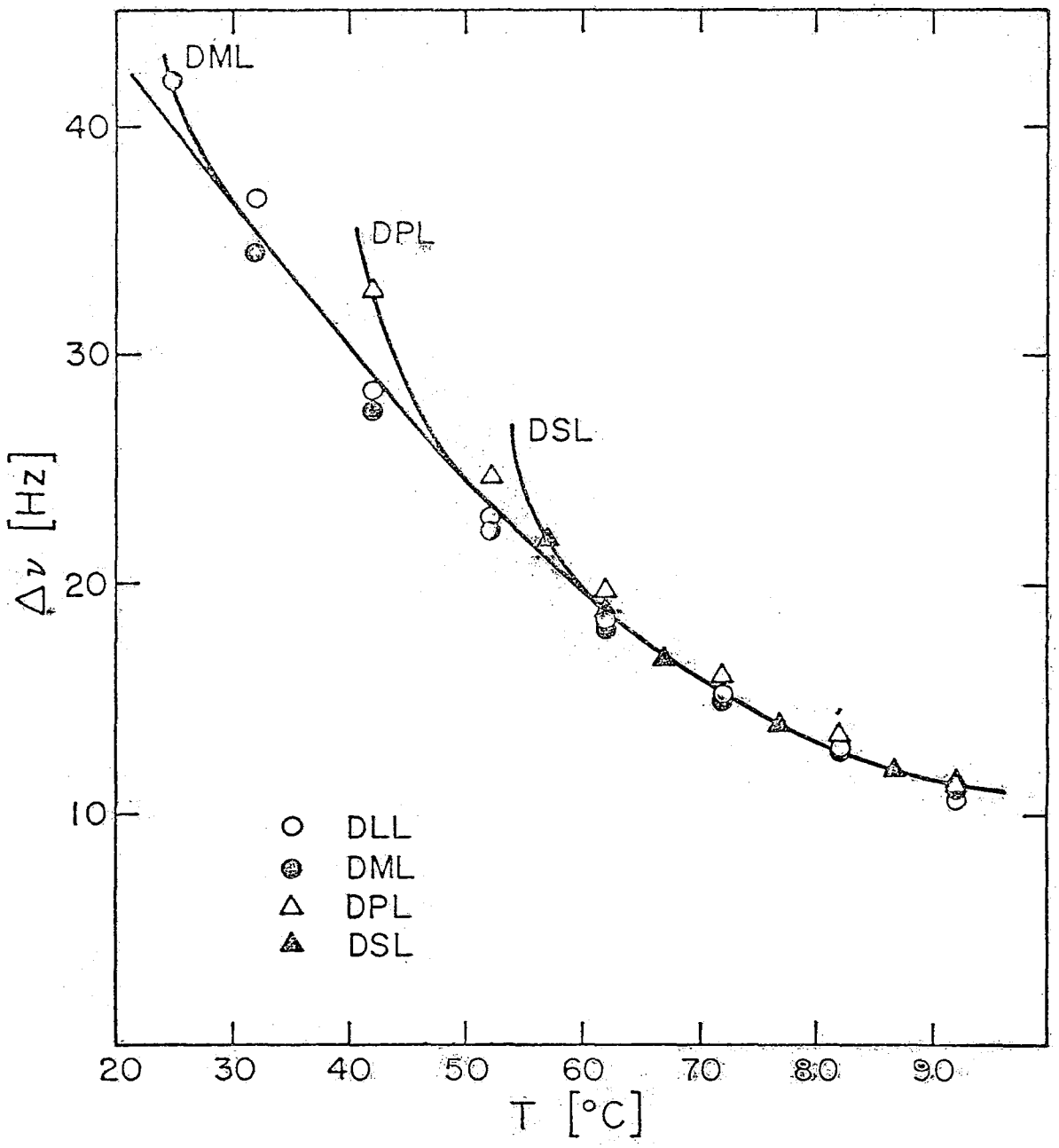
DML
DPL
DSL
40
30
20
10
Δν [Hz]
20
30
40
50
60
70
80
90
T [°C]
DLL
DML
DPL
DSL

null point occurs when the faster relaxing positive components exactly cancel the slower relaxing negative components; an average T_1 is then obtained. Of course if the T_1's are close enough, the graphical method also gives an average T_1, but this average is generally different from the null point average. The results of T_1 experiments at 100 and 220 MHz and between 50° and 85°C are shown in Fig. 5. Both the inter- and intramolecular T_1's are frequency dependent. Furthermore $(T_1^{-1})_{inter}$ decreases with increasing temperature, except at temperatures above 80°C.

The possible existence of interchain T_1 contributions (i.e. contributions from the hydrocarbon chain belonging to the same lecithin molecule) was examined by comparing the methylene T_1's of DPL (H, D) and DPL, both in a DPL (D) matrix. The percentage of DPL (H, D) used was twice that of DPL to keep the ratio of protonated to deuterated chains the same. The results are shown in Fig. 5. At 220 MHz no effect is observed within experimental error. At 100 MHz however there is a definite interchain contribution at low temperatures.

We should mention that although the DPL (H, D) was chromatographically pure, there was a small amount of yellow contaminating material present (see Chapter IV). We have found that T_1's are quite insensitive to small impurities. Linewidths, on the other hand, are much more sensitive to small perturbations. For this reason we have not discussed the DPL (H, D) linewidth data. We find experimentally that at 100 MHz these linewidths are actually

FIGURE 5

Methylene spin-lattice relaxation rates at 100 and 220 MHz, as a function of 1/T, for 100% DPL; 10% DPL, 90% DPL (D); and for 20% DPL (H, D), 80% DPL (D) vesicles.

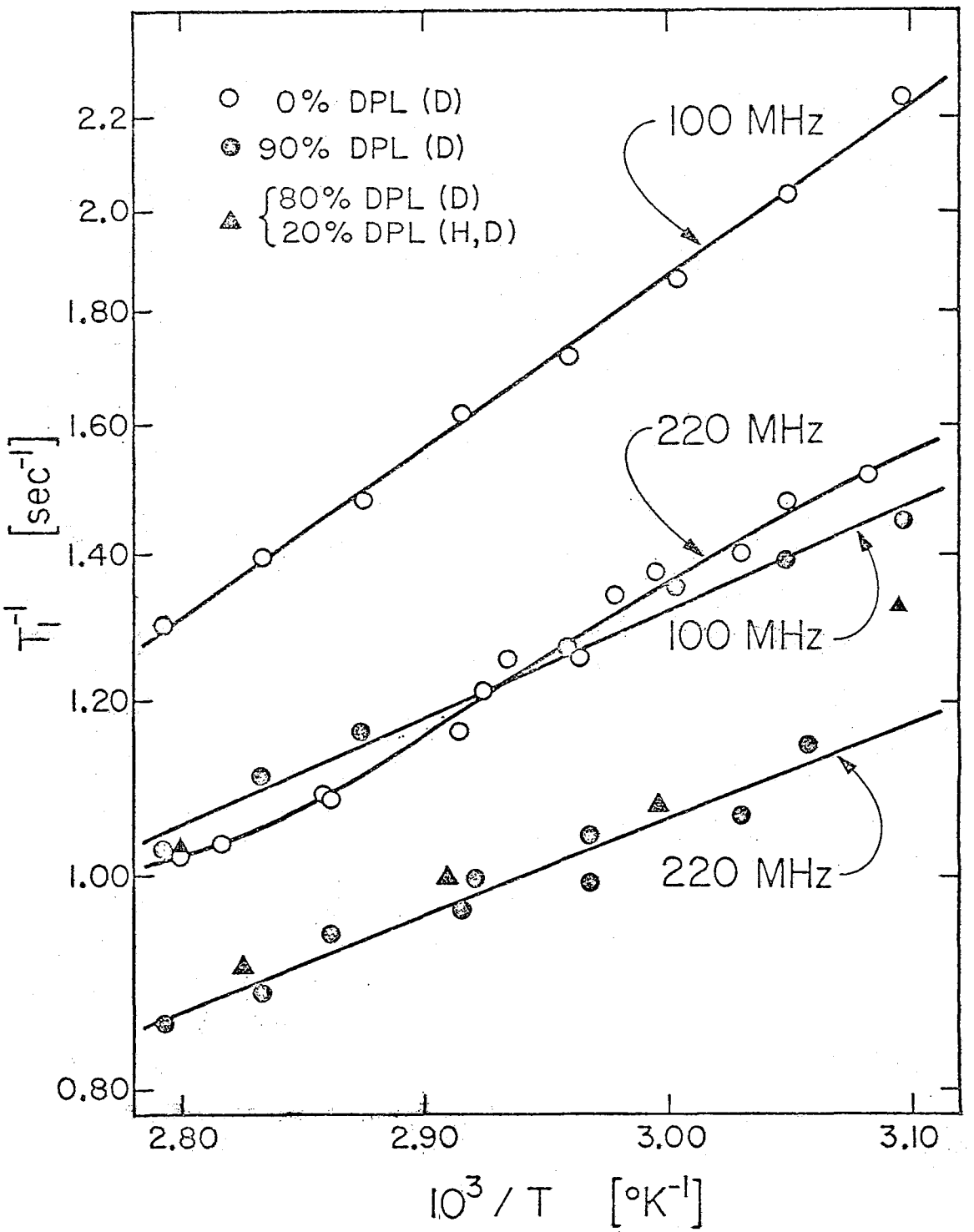
0% DPL (D)
90% DPL (D)
80% DPL (D)
20% DPL (H,D)
100 MHz
220 MHz
100 MHz
220 MHz
2.2
2.0
1.80
1.60
1.40
1.20
1.00
0.80
T_1^{-1} [sec^{-1}]
2.80
2.90
3.00
3.10
$10^3 / T$ [°K^{-1}]

somewhat larger (by approximately 1 Hz) than those for DPL in DPL (D).

T_1 relaxation rates were also studied as a function of chain length to complement the linewidth studies reported previously. The results are shown in Fig. 6. Although there is a chain length dependence the effect is rather small. This may be compared with the absence of any effect on the linewidths except near the phase transition temperature.

Corrections to relaxation times for finite concentration of DPL and DPL (H, D). The differences between the linewidths and the T_1 relaxation rates in a DPL and DPL (D) matrix only give an approximate value for the intermolecular relaxation contributions. Obviously the finite concentration of protonated molecules, whether it be DPL or DPL (H, D), gives a finite contribution to the methylene T_1 and linewidth. This contribution can be estimated if we assume a definite model for the arrangement of phospholipid molecules.

The first model we shall consider is one in which the hydrocarbon chains are packed in a hexagonal lattice, as they are below the phase transition temperature in a multilayer. The phospholipid orientation may be random or regular. This is illustrated in Fig. 7a and 7b. What we want to know is the average number of protonated chains which surround a particular chain if a certain percentage of the chains are deuterated. The problem is rather complicated if we try to calculate all possible configurations since the hydrocarbon

FIGURE 6

Methylene spin-lattice relaxation rates as a function of 1/T, for DLL, DML, DPL and DSL vesicles.

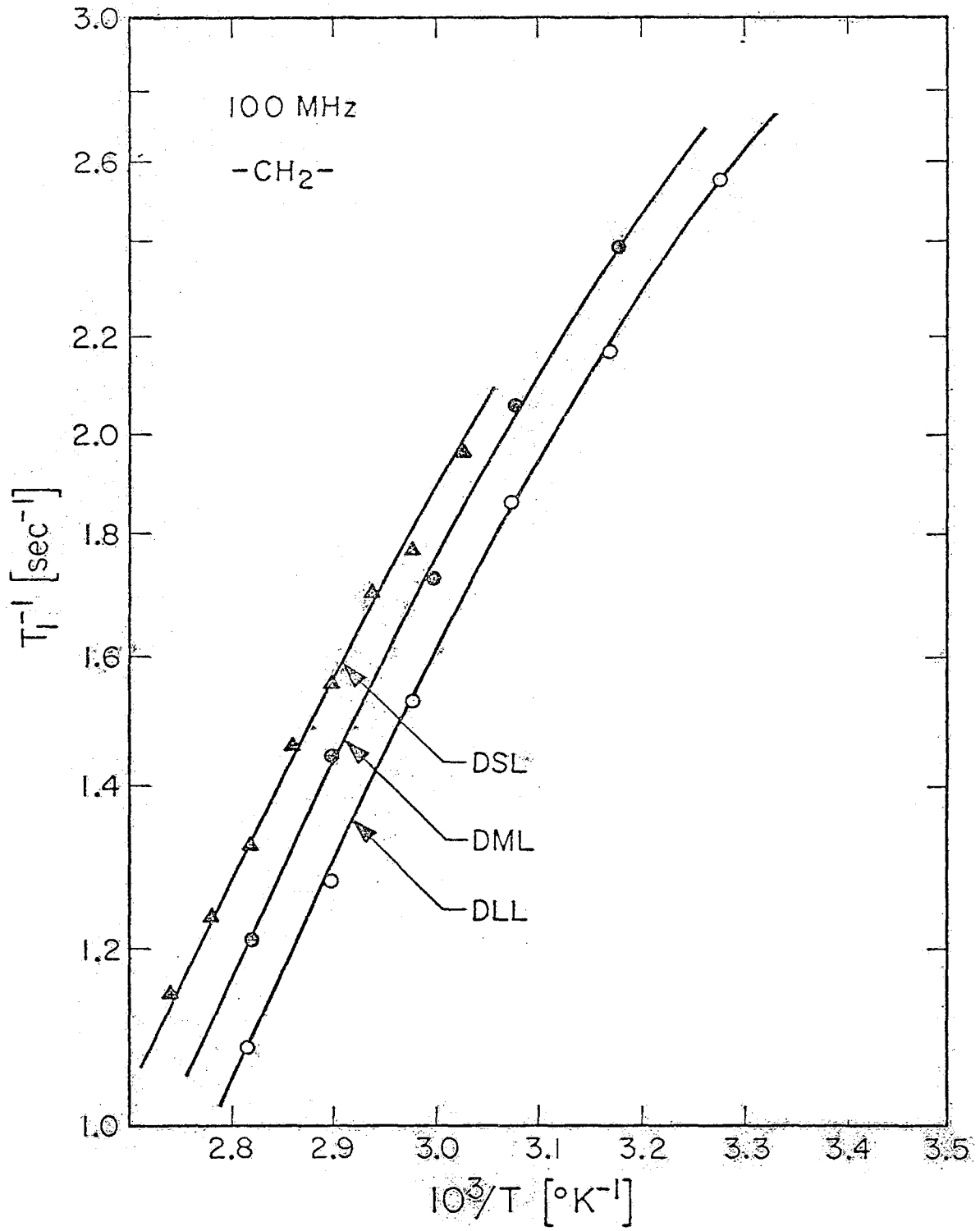
100 MHz
-CH2-
DSL
DML
DLL
T1-1 [sec-1]
10³/T [°K-1]
3.0
2.6
2.2
2.0
1.8
1.6
1.4
1.2
1.0
2.8
2.9
3.0
3.1
3.2
3.3
3.4
3.5

FIGURE 7

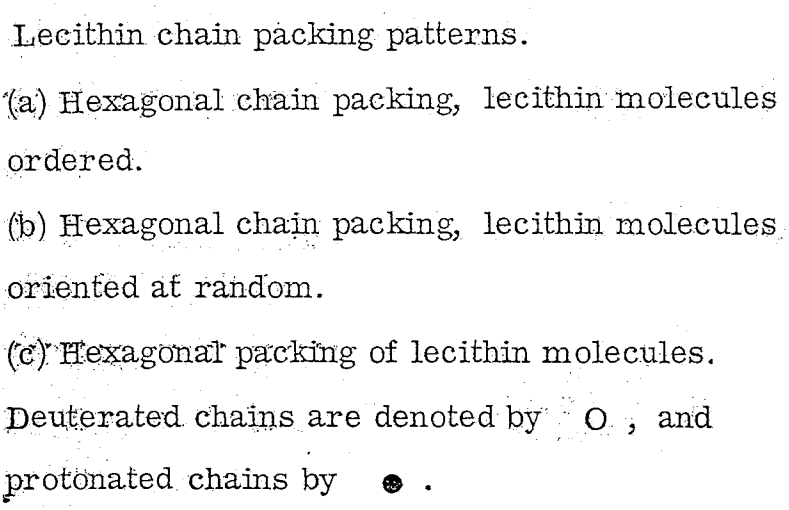

Lecithin chain packing patterns.

(a) Hexagonal chain packing, lecithin molecules ordered.

(b) Hexagonal chain packing, lecithin molecules oriented at random.

(c) Hexagonal packing of lecithin molecules. Deuterated chains are denoted by O , and protonated chains by ● .

a.

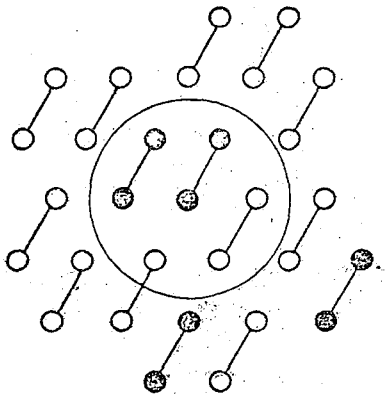

b.

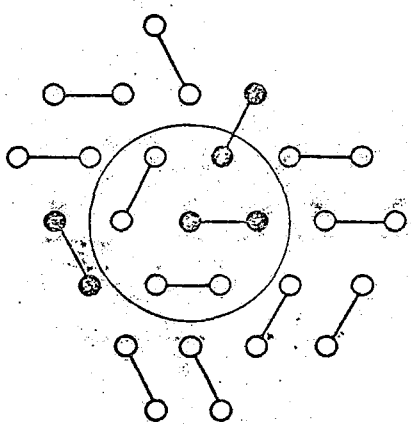

c.

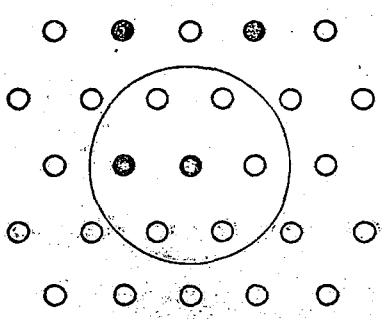

chains are not independent but exist as connected pairs. We are not interested in the exact details, however, but only in an average number. The problem is greatly simplified if we recall that the expectation value of a sum of random variables (not necessarily independent) is equal to the sum of the respective expectation values. If we now consider each lattice site as a random variable (i. e. it can be protonated or deuterated), the expectation value of the number of protonated or deuterated species for all six lattice sites is equal to the sum of the expectation values for each site, which may or may not be equal.* For our model (Fig. 7a, b) five sites can be occupied by either protonated or deuterated chains, whereas the sixth site is always occupied by a protonated chain in the case of DPL or a deuterated chain in the case of DPL (H, D). For a vesicle sample containing a fraction f of protonated chains, the expectation value of having a protonated chain at any position is simply f. The expectation value for five lattice sites is therefore 5f.

We have neglected the sixth position since there is little interchain relaxation for DPL or DPL (H, D). The observed relaxation rate $(1/T_1)_{obs,\,f}$ can therefore be written as

$$\left(\frac{1}{T_1}\right)_{obs,\,f} = \left(\frac{1}{T_1}\right)_{intra} + 5f\left(\frac{1}{T_1}\right)_{inter/chain}$$

where $(1/T_1)_{inter/chain}$ is the intermolecular relaxation contribution

---

* I thank Dr. G. Lorden of the Mathematics Department for pointing this out to me.

per chain. The difference $\Delta(1/T_1)$, between $(1/T_1)_H$, the relaxation time in a protonated matrix, and $(1/T_1)_{obs}$, the relaxation time in a deuterated matrix is therefore

$$\Delta\left(\frac{1}{T_1}\right) = 5\,(1 - f)\left(\frac{1}{T_1}\right)_{\text{inter/chain}}$$

It follows that total intermolecular effect is

$$\left(\frac{1}{T_1}\right)_{\text{inter}} = \frac{1}{1 - f}\,\Delta\left(\frac{1}{T_1}\right) \qquad (1)$$

All of the above arguments obviously also hold for T_2.

A second model which can be considered is one in which phospholipid molecules are packed in a hexagonal manner (Fig. 7c). This is the model used by McConnell for ESR spin exchange studies.[25] If we use the approach presented above we find the same expression for $(1/T_1)_{inter}$ as for the first model (see Eq. 1).

With the use of Eq. 1 we have corrected the apparent intermolecular T_1 contributions obtained from Fig. 5 to obtain more realistic values of $(1/T_1)_{inter}$. These data are shown in Fig. 8. We have not corrected the relaxation rates for dipole-dipole interactions with deuterated hydrocarbon chains. This correction is of the order of $\dfrac{\gamma_D^2 I_D (I_D + 1)}{\gamma_H^2 I_H (I_H + 1)} \approx 0.06$.

FIGURE 8

Methylene intermolecular spin-lattice relaxation rates for DPL vesicles, at 100 and 220 MHz, as a function of 1/T.

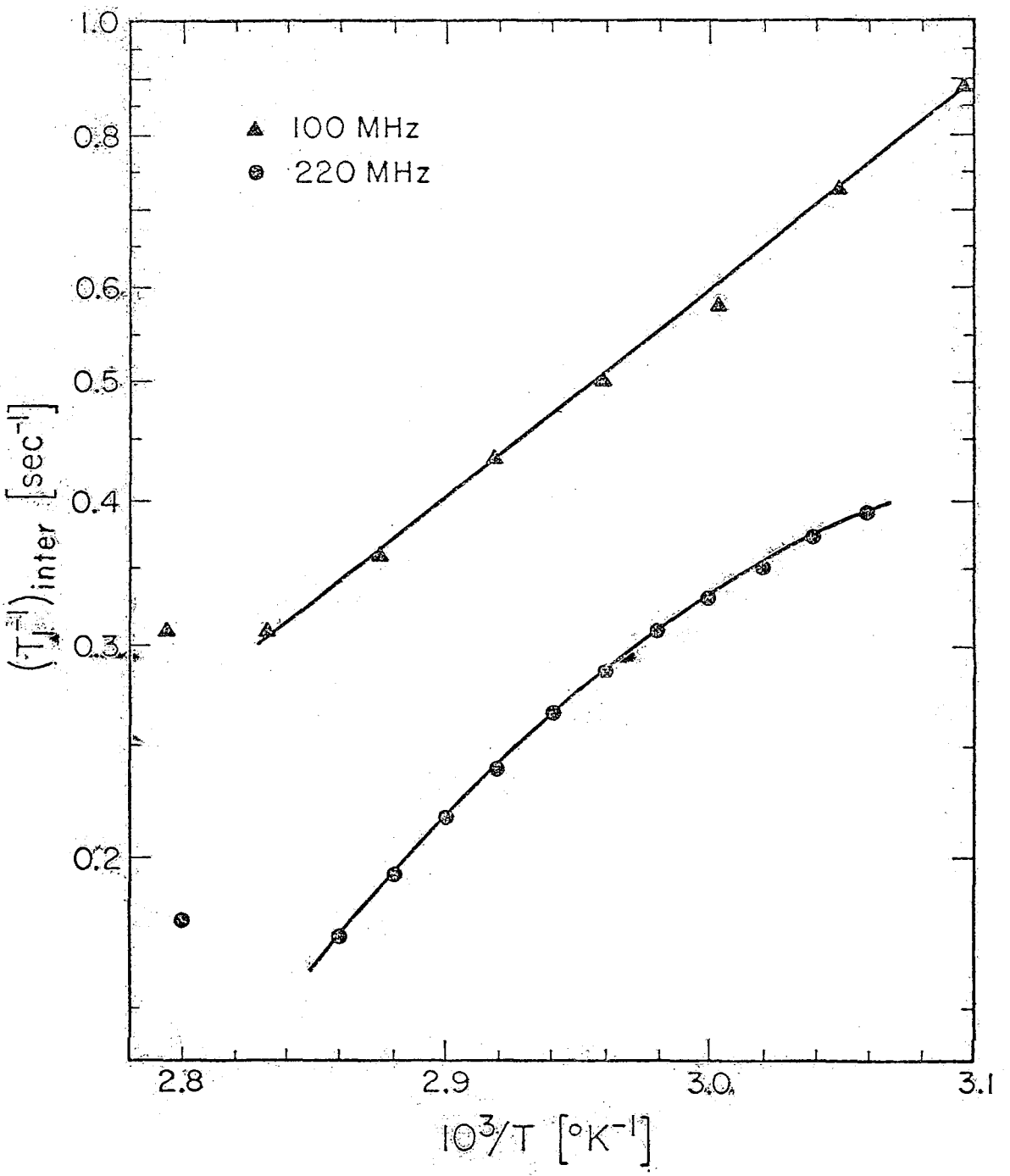
1.0
0.8
0.6
0.5
0.4
0.3
0.2
100 MHz
220 MHz
$(T_1^{-1})_{inter}$ [sec^{-1}]
2.8
2.9
3.0
3.1
$10^3/T$ [°K^{-1}]

4. DISCUSSION

The data presented clearly show that the relaxation rates of phospholipid hydrocarbon chain protons contain both inter- and intramolecular contributions. We shall discuss the origin of both contributions in some detail. Following this we shall discuss the effect of chain length on the motional state and the degree of order of the hydrocarbon chains.

Although the intermolecular contributions to T_1 and T_2 are significant, they do in no way dominate the intramolecular relaxation times. This is contrary to the conclusions of Lee et al.,[10] who argue that the methylene linewidth is largely intermolecular in nature. Their reasoning is based on the notion that the chain methylenes undergo fast ($\omega_0 \tau_c \ll 1$) and almost isotropic motion, with the possible exception of a few methylenes at the polar end of the chain. This assertion is based on an analysis of ^{13}C T_1 data assuming isotropic motion.[5] In any case, this motion effectively averages out intramolecular dipole-dipole interactions and therefore, they argue, the linewidth will be dominated by much slower intermolecular effects, such as translational diffusion. There is of course a basic flaw in this argument. If the intramolecular motion is actually as fast and isotropic as these authors claim, intermolecular dipole-dipole interactions will be averaged out rather effectively by the same motion!

The CH_2 linewidth and T_1 for DPL in a matrix of DPL (D) (see Figs. 2 and 5) are a good measure of the intramolecular

contributions. Since intramolecular effects dominate relaxation, the behavior of $(T_1)_{intra}$ and $(T_2^*)_{intra}$ $(T_2^* = \frac{1}{\pi \Delta \nu})$ closely resembles that of the total relaxation rates. The only difference is that the frequency and temperature dependence are considerably smaller than those estimated from the total relaxation rates. This is clearly important if one wants to estimate activation energies for particular relaxation processes.[6]

The intramolecular relaxation times reflect the motional state of the hydrocarbon chain. This motion may be nearly isotropic[10] or it may be anisotropic.[6, 9, 15] In the first case, the relaxation times will exhibit a rather simple dependence on the motional correlation time (see Fig. 4, Chapter I) and therefore of course on the absolute temperature, since $\tau_c = \tau_0 e^{-E_a/RT}$, where E_a is the activation energy associated with the motion. However the hydrocarbon chain $(T_1)_{intra}$ and $(T_2^*)_{intra}$ do not behave in such a simple manner. For example, since the T_1 relaxation rate decreases with increasing temperature, the "one isotropic correlation time model", tells us that for this motion $\omega_0 \tau_c < 1$, and then predicts that $T_1 \approx T_2$ and that T_1 will be independent of frequency. However $T_1 \neq T_2$ and T_1 is frequency dependent. This leads us to conclude that the hydrocarbon chain motion is anisotropic and that for every methylene group there are at least two correlation times, one short dominating the T_1 behavior, and another long dominating T_2 behavior. Theoretical considerations[20] tell us that if the correlation time for each distinct motion is sufficiently different from the others, the relaxation rates

can be expressed as

$$1/T_{1,2} = \Sigma A_i f(\omega, \tau_i)$$

where $f(\omega, \tau_i)$ behaves as if the relaxation is determined by a single correlation time τ_i, and where the amplitude factors A_i are determined by the degree of anisotropy for each motion. The τ_i's in this expression do not necessarily correspond to actual correlation times, but are combinations of them. At any temperature the relaxation times can therefore be approximated by the sum of at least two $f(\tau_i, \omega)$ curves. The most important consequences of such a model are that the slower motions can dominate T_2 whereas the faster motions can dominate T_1. Furthermore, depending on the ratio of the correlation times, one can observe an increase in T_1 with increasing temperature and a frequency dependence in the region between the points where $\omega \tau_1 \sim 1$ and $\omega \tau_2 \sim 1$.

In systems as complex as bilayer vesicles it is difficult to give a precise physical interpretation of the different correlation times in terms of specific motions. For one thing we cannot be too sure that the usual assumption, which regards the environment of individual molecules as stationary on the time scale of their motions, is valid for liquid crystals. It may be more realistic to consider an environment which fluctuates with time in such a way that the probability of molecular motions changes with these fluctuations.[21] Then if the fluctuations are very rapid on the time scale of molecular motions, each molecule does in fact see a stationary

environment, but if the fluctuations occur on a slower time scale, different molecules will have different motional probabilities and thus different correlation times for the same motions. With these limitations in mind, however, we can consider several motions which may be important for intramolecular T_1 and T_2 relaxation.

T_1 is determined primarily by fast motions. These may be divided into two classes: (1) motions of the phospholipid molecule as a whole, and (2) internal motions which involve only the hydrocarbon chain. Motions involving the whole molecule are generally expected to be quite slow (e. g. lateral diffusion),[22] with the possible exception of overall rotation. There are several possible high frequency motions involving the hydrocarbon chain. The first example involves torsional oscillations about the chain C-C bonds. This concept has been used to explain the T_1 relaxation behavior of anhydrous fatty acid salts,[23] and of phospholipid multilayers in the liquid crystalline form.[16] Feigenson et al.[16] have considered a model in which a long series of weakly coupled high frequency ($\sim 10^{+14}$ sec^{-1}) torsional oscillators give rise to larger amplitude motions of lower frequency, as a result of statistical, in phase fluctuations of the oscillators. These motions are bounded at the high frequency, low amplitude end by the single bond oscillation frequency of $\sim 10^{+14}$ sec^{-1}. Since the chains are essentially anchored at the glycerol portion of the molecule, the first CH_2 group would have a correlation time of the order of 10^{-14} sec. This frequency is clearly too high to be an effective source of T_1 relaxation. However a higher amplitude, lower

frequency motion occurs when all oscillators are rotating in the same direction. The frequency of this occurrence is approximately $(1/2)^{16} \times 10^{14} \approx 10^{9}$ (for a chain of 16 methylene groups). Of course this frequency only applies to the terminal end of the chain. In the case of multilayers it was proposed that the terminal end (including the methyl group) essentially acts as a heat sink for the rest of the chain.[16] The spin energy of the chain methylenes therefore diffuses to the terminal end by a spin exchange mechanism, giving a single T_1 for the entire chain. The situation is different for lecithin vesicles however. Although experimentally the bulk methylenes are characterized by a single T_1, this does not exclude a distribution of T_1's, but rather tells us that the distribution is not very large. Actually there is a definite but small distribution of T_1's. The α,β and bulk methylene T_1's for example are 0.56, 0.70 and 0.80 sec respectively for DPL vesicles at 78°C. We also noted previously that the difference between the null point T_1, and the T_1 determined graphically is indicative of a distribution of T_1's. Spin diffusion can therefore not be important for vesicles.[6] This brings us back to small angle torsional oscillators. The model proposed for multilayers is clearly not applicable to vesicles, since without spin diffusion methylenes close to the polar end of the chain would have a very much longer T_1 (remember $\tau_c \sim 10^{-14}$ sec for the first methylene) than methylenes near the end of the chain. Actually the reverse seems to be true. A more plausible relaxation path we feel is one which involves large angle, and hence much slower torsional oscillations.

Trans-gauche rotations about C-C bonds may also provide important high frequency contributions. Rather than single trans-gauche rotations, however, we envisage coupled rotations in which pairs of gauche configurations of opposite polarities occur on sites separated by one (β-coupled) or more carbon atoms. These conformations, which are usually referred to as kinks, result in a roughly straight hydrocarbon chain and avoid the encounters with neighboring chains that result from single gauche conformations.[24] The probability of kink formation can be considered to increase slowly along the chain, which could give rise to a small T_1 gradient. Träuble[24] has proposed a molecular model of bilayer permeability, in which kinks are considered as intrinsic carriers which diffuse along the hydrocarbon chain, and has estimated a kink diffusion coefficient of $\sim 10^{-5}$ cm^2/sec. This corresponds to a correlation time for diffusion of $\tau_D \sim 10^{-10}$ sec, which is certainly fast enough for T_1 relaxation.

The next question is what motions determine T_2. Recently we have presented a theoretical analysis of methylene linewidths for bilayer vesicles,[15] and concluded that the motion is such that the methylene proton-proton vectors undergo large angular excursions with a correlation time of $\sim 10^{-8}$ seconds. We surmise that single trans-gauche rotations, which are expected to be much slower than kink formation, may be responsible for this motion. Since these rotations are expected to become more favorable near the terminal methyl end of the chain, it is clear that a distribution of T_2's may exist along the chain. Horwitz et al.[6] have in fact shown this to be

so. We stress however that we are dealing with bilayer vesicles and not with multilayers. For the latter case single trans-gauche rotations were considered to be an unlikely occurrence.[16]

Intermolecular relaxation. Since there are definite intermolecular contributions to the relaxation rates (see Figs. 2, 5 and 8), it is pertinent to ask what their origin is. The hydrocarbon chains in phospholipid vesicles constitute a rather complex system. There are a number of different motions which can modulate intermolecular dipole-dipole interactions, the most obvious candidates being lateral and rotational diffusion. Overall vesicle tumbling is also a possibility. Finally there are intrachain motions, such as kink formation and diffusion and trans-gauche rotations which can also modulate intermolecular dipole interactions.

An exact theoretical analysis of this problem involves an evaluation of the time dependence of the intermolecular dipolar Hamiltonian as a function of the microscopic details of each of these motions. This is a formidable theoretical problem for which no adequate treatment is currently available. We shall use a much simpler approach in that we shall consider each of the contributions separately. The correlation time for overall vesicle tumbling is about 5×10^{-6} sec for a 300 Å vesicle. This is much too slow to affect T_1. In principle however T_2 and therefore the linewidth can be affected by such low frequency motions. The Stokes-Einstein relationship $\tau_c = \frac{4\pi\eta a^3}{3kT}$, where τ_c is the rotational correlation time, tells us that an increase in viscosity results in an increase in τ_c,

which will be reflected in the observed T_2 or linewidth if vesicle tumbling is important. Actually there is no discernable change in linewidth when the viscosity of a vesicle solution is changed.[1,15] Overall vesicle tumbling therefore does not contribute to intermolecular relaxation.

The formation of a kink effectively results in the shortening of the hydrocarbon chain by 1.25 Å. If we let this kink diffuse along the chain, the methylene protons involved in the kink are displaced along and around the bilayer normal. This process therefore modulates the intermolecular dipole-dipole interactions. As we noted previously, this motion is very rapid ($D \sim 10^{-5}$ cm^2/sec). Lateral diffusion, on the other hand, is much slower. ESR measurements have estimated $D \sim 10^{-8}$-10^{-7} cm^2/sec.[25] The net "diffusive" motion of chain protons is therefore highly anisotropic, and it is therefore not surprising that the intermolecular relaxation behavior cannot be described in terms of a single correlation time. The observed behavior, $T_1 \neq T_2$, a T_1 which increases with increasing temperature, and which is frequency dependent suggests that the motion is in fact anisotropic, and that it must be described by at least two correlation times, one short which controls T_1, and one long which controls T_2.

Kink diffusion, we feel, provides one important intermolecular T_1 relaxation path. If this is so, of course, it should also provide an interchain relaxation path. Since there is only one interchain neighbor for every five intermolecular neighbors (assuming that the chains are

packed in a hexagonal lattice), the effect will be smaller by a factor of five. At 100 MHz we do actually see an effect at low temperature, where the total intermolecular contribution is large. At higher temperatures the intermolecular T_1 contribution is much smaller and no interchain effect is observed. This is true at 220 MHz over the whole temperature range.

T_2 is dominated by slower motions, such as translational diffusion, and possibly hydrocarbon chain trans-gauche rotations. The latter should contribute to both intermolecular and interchain relaxation. Unfortunately we have no reliable linewidth data for DPL (H, D), so that it is impossible to estimate the relative contributions from trans-gauche rotations. Let us assume for the moment that translational diffusion provides the main intermolecular T_2 contribution. Torrey[26] has developed a model for diffusion and its effects on relaxation times. In the Torrey model a molecule can exist in two states: (a) bound in a potential well, or (b) in a thermally excited state in which the molecule may move about rapidly in a random diffusive manner. It is assumed that the mean lifetime in the excited state is small compared with the lifetime of the trapped state, and that the motion in the excited state is so rapid that its details contribute only to very high frequencies and have therefore no effect on relaxation.

The correlation time τ_c for this diffusive motion can be expressed in terms of an effective molecular diameter d,[28] the mean-square jump distance $\langle r^2 \rangle$, and the translational diffusion constant D,[27]

$$\tau_c = (d^2/5 + \langle r^2 \rangle/12)/D$$

T_2 for intermolecular dipolar relaxation can now be written as

$$T_2^{-1} = \frac{2\pi \gamma_H^4 \hbar^2 N}{5 d^3 \omega_H} \chi \{ 3/2 + 5/2\, f(\alpha, \chi) + f(\alpha, 2\chi) \}$$

where $\alpha = \langle r^2 \rangle / 12\, d^2$, $\chi = \omega_H \tau_c$ and

$$f(\alpha, \chi) = 3/\chi^2 (1/5 + \alpha) \{ v (1 - 1/(u^2 + v^2)) +$$

$$[v (1 + 1/(u^2 + v^2)) + 2]\, e^{-2v} \cos 2u +$$

$$u (1 - 1/(u^2 + v^2))\, e^{-2v} \sin 2u \}$$

with $\left(\begin{matrix} u \\ v \end{matrix}\right) = \frac{1}{2} \left[\frac{q (1 \mp q)}{\alpha} \right]^{\frac{1}{2}}$

and $q = [1 + (1 + 1/5\, d)^2/\chi^2]^{-\frac{1}{2}}$

The spin density N can be evaluated from the area per molecule and the thickness of the hydrocarbon region of the bilayer. For egg lecithin the area per molecule has been estimated as ~ 62.7 Å^2[29]. The thickness of the hydrocarbon region can be estimated as ~ 33.9 Å.[29] This gives a proton spin density of $N \approx 6 \times 10^{22}$ spins/cm^3. With the use of molecular models the value of the parameter d can be estimated to be approximately 5 Å. This is the same value used by Lee et al.[10] in their calculations. The parameter α depends on the ratio of the mean-square jump distance and the molecular radius. T_2 however is essentially independent of α.[27] In Fig. 9 we

FIGURE 9

Intermolecular linewidth as a function of the translational diffusion coefficient, calculated using the Torrey model for molecular diameters d = 3, 4, 5 and 6 Å with $\alpha = 0.0086$.

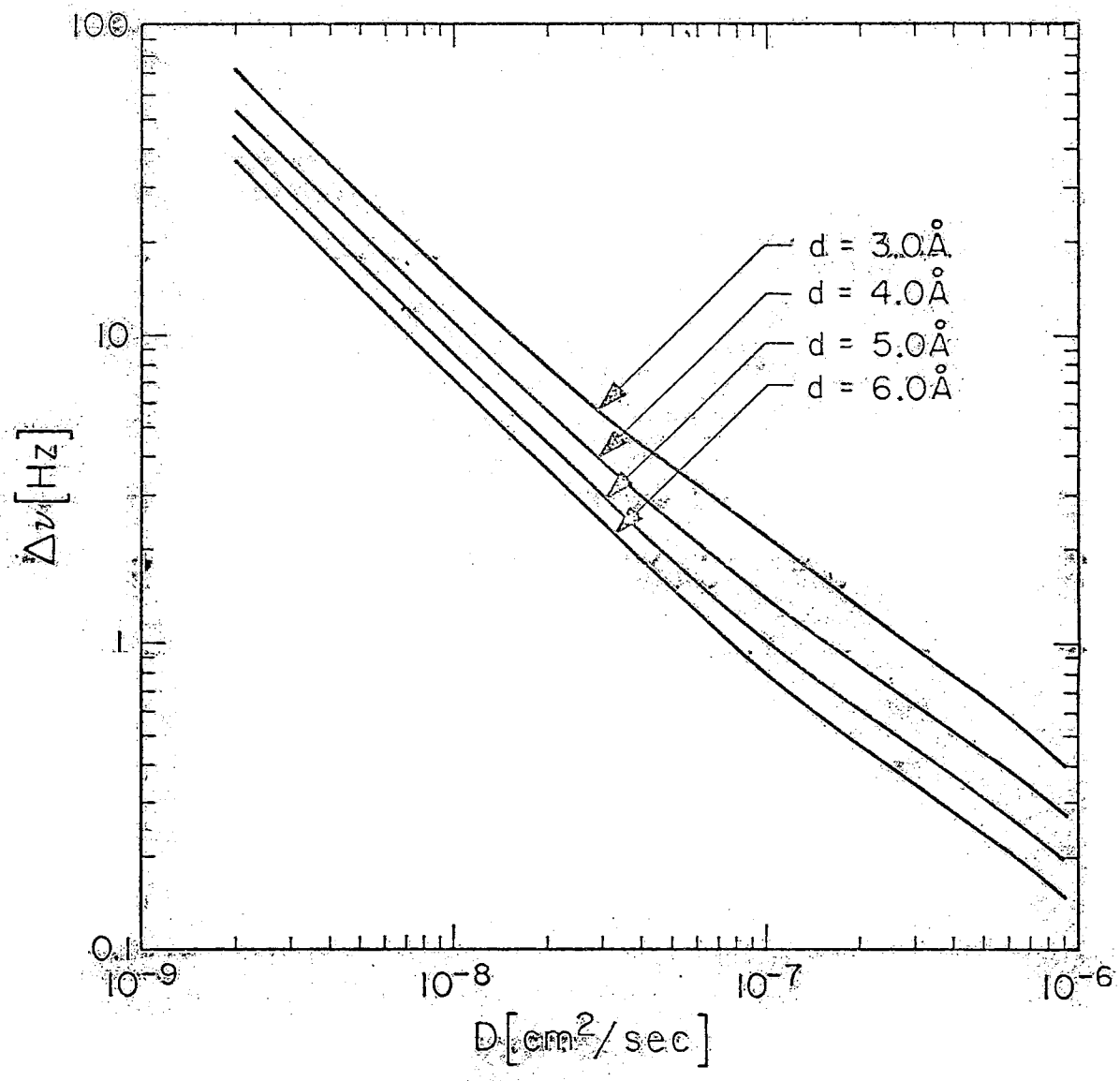
100
10
1
0.1
$\Delta\nu_{\frac{1}{2}}$[Hz]
d = 3.0Å
d = 4.0Å
d = 5.0Å
d = 6.0Å
10^{-9}
10^{-8}
10^{-7}
10^{-6}
D[cm²/sec]

have plotted the intermolecular linewidth contribution as a function of the diffusion coefficient. We have plotted these curves for a range of d's, since as Hubbard[30] has pointed out, when the spins are not at the center of the molecule, d will be something less than the molecular diameter. This is however partially compensated for by the neglect of rotational diffusion. In any case, if we consider a range of d, from 3 to 5 Å, we find $D = 2.5 - 5.5 \times 10^{-8}$ cm^2/sec. This value agrees well with ESR spin label and fluorescence measurements, which give values ranging from 10^{-8} to 10^{-7} cm^2/sec.[22] In view of the inherent theoretical assumptions (such as three-dimensional isotropic diffusion in the case of NMR), and unique practical difficulties for each of these methods, the agreement is surprisingly good.

To summarize, intermolecular relaxation is determined by anisotropic motion which is characterized by at least two correlation times, one fast, dominating the T_1 behavior, and one slow, dominating the T_2 behavior. Kink diffusion provides a probable T_1 relaxation path, whereas lateral diffusion and possibly hydrocarbon chain trans-gauche rotations, can be effective T_2 mechanisms. Assuming lateral diffusion dominates the intermolecular T_2, a diffusion coefficient of $2.5 - 5.5 \times 10^{-8}$ cm^2/sec can be estimated.

The effect of chain length on the mobility and order of the hydrocarbon chains. The linewidth of the hydrocarbon methylene resonance depends on the order and mobility of the hydrocarbon chain.[15] The order reflects restrictions which are placed on the chain. It may, for example, be confined to a cylinder of a certain diameter. Mobility, on the other hand, refers to the rate of motion. It is

generally accepted[31, 32] that the degree of order (or disorder) of the lipid chains depends upon whether the lipid is above or below its phase transition temperature (T_c) and how high the temperature of the lipid is above T_c. The first point has been well established.[31] The second point is mere conjecture. It is an important point however. Are dilauroyl lecithin chains (T_c = 0°C) for example more disordered than distearoyl lecithin chains (T_c = 58°C) at 65°C.

Recently we have demonstrated that the intramolecular CH_2 linewidth is governed primarily by the motional state of the hydrocarbon chain.[15] Furthermore we have shown that the linewidth is extremely sensitive to changes in the details of the motional state. Thus if the chain motion of two lecithins, differing in their hydrocarbon chain length, is not the same, this should be reflected in the CH_2 linewidths.

The temperature dependence of the CH_2 linewidths for the C_{12}, C_{14}, C_{16} and C_{18} lecithins, dilauroyl, dimyristoyl, dipalmitoyl and distearoyl lecithin, is shown in Fig. 4. Only DPL and DSL undergo a phase transition in the temperature range studied (see Table I). Near their phase transition temperatures, the DPL and DSL linewidths increase extremely rapidly with decreasing temperature, for the obvious reason that the motion of the hydrocarbon chains becomes slower and more restricted. Otherwise, however, the linewidths appear to be essentially independent of chain length. This leads us to conclude that the average chain motion, in terms of its amplitude and correlation times, is independent of chain length.

Table I. Chain length dependence of thermodynamic parameters for the crystal to liquid crystal phase transitions

	Lecithin		
	Distearoyl C_{18}	Dipalmitoyl C_{16}	Dimyristoyl C_{14}
Transition temperature (°C)	58	41	23
ΔH (Kcal mole^{-1})	10.67	8.66	6.64
ΔS (cal mole^{-1} deg^{-1})	32.4	27.6	22.4

Since chain motion occurs primarily through the formation of kinks, and through trans-gauche rotations, it follows that the number of kinks and trans-gauche rotations associated with a lipid chain is proportional to its chain length (at least for the chains we have studied here).

It is interesting to compare this observation with rough predictions from thermodynamic data. The phase transition temperature, enthalpy and entropy for DML, DPL and DSL are shown in Table I. Let us assume for simplicity that most of the entropy change associated with the crystal to liquid crystal phase transition can be attributed to an increase in the conformational disorder as a result of trans-gauche rotations. Boltzmann's theorem states that the entropy change accompanying a phase change equals $R \ln (W_L/W_S)$, where W_L and W_S are the number of ways in which the structure can be arranged in the liquid and solid respectively. In our case W refers to the number of configurations associated with trans-gauche rotamers. We shall assume that $W_S \sim 1$, i.e. the chains are in the all-trans configuration below the phase transition temperature. We can now estimate $W_L = \exp(\Delta S/R)$. The values are 7.3×10^4 for DML, 9.9×10^5 for DPL and 1.1×10^7 for DSL. From these we can estimate the number of gauche rotamers per molecule, assuming that the rotamers are located randomly along the chain. We find that at least 8 gauche rotamers per molecule are needed for DSL, 7 for DPL and 5-6 for DML. These numbers are of course underestimations, since we have neglected steric interactions. Seelig

has estimated that DPL at 50°C contains 6-12 gauche isomers per molecule, which agrees with the value given above. The essential feature is that as the chain length increases the number of gauche rotamers also increases. In fact the percentage of gauche rotamers estimated in this way is essentially independent of chain length. This simple calculation shows that the observed entropy changes are consistent with the notion that the chain order at any temperature is essentially independent of the chain length as long as $T > T_c$.

We have tacitly neglected the effects of chain length on the rate of lateral diffusion, that is on the intermolecular contribution to the linewidth. In light of the fact that there is no difference between the linewidths as long as we are above T_c, it seems reasonable to assume that the intermolecular contribution to the linewidths is also independent of chain length, and therefore that the rate of lateral diffusion is the same.

The chain length dependence of the T_1 relaxation rates (see Fig. 6) appears to present a somewhat different picture. The CH_2 relaxation rate for DSL is definitely faster than that for DLL, and since the rates decrease with increasing temperature, the correlation time for the DLL methylene protons appears to be shorter than that for the DSL methylene protons.

We must remember however that the linewidth and T_1 are determined by very different motions. A change in the correlation time for the fast motion, which will affect T_1, will have little effect on T_2. It may be, for example, that the kink diffusion coefficient has

a slight chain length dependence. This would have little effect on the linewidth. The order and mobility of saturated lecithin chains above the thermal phase transition temperature is therefore essentially independent of chain length, the only exception being a slight chain length dependence of the high frequency component of the chain motion.

We have only considered saturated chains. There is reason to believe that the situation is essentially different if the lipids are highly unsaturated. For example lecithin from R·pilimanae, a yeast, contains a large percentage of unsaturated fatty acids.[33] Multilayers from this lecithin exhibit far narrower lines than multilayers from more saturated lecithins,[33] indicating a greater degree of disorder and a shorter correlation time for chain motion.

References

1. M. P. Sheetz and S. I. Chan, Biochemistry 11, 4573 (1972).
2. S. I. Chan, M. P. Sheetz, C. H. A. Seiter, G. W. Feigenson, M.-C. Hsu, A. Lau and A. Yau, Ann. N. Y. Acad. Sci. 222, 499 (1973).
3. E. G. Finer, A. G. Flook and H. Hauser, Biochim. Biophys. Acta 260, 49 (1972).
4. E. G. Finer, A. G. Flook and H. Hauser, Biochim. Biophys. Acta 260, 59 (1972).
5. Y. K. Levine, P. Partington, G. C. K. Roberts, N. J. M. Birdsall, A. G. Lee and J. C. Metcalfe, FEBS Lett. 23, 203 (1972).
6. A. F. Horwitz, W. J. Horsley and M. P. Klein, Proc. Nat. Acad. Sci. 69, 590 (1972).
7. A. G. Lee, N. J. M. Birdsall, Y. K. Levine and J. C. Metcalfe, Biochim Biophys. Acta 255, 43 (1972).
8. Y. K. Levine, N. J. M. Birdsall, A. G. Lee and J. C. Metcalfe, Biochemistry 11, 1416 (1972).
9. A. C. McLaughlin, F. Podo and J. K. Blasie, Biochim. Biophys. Acta 330, 109 (1973).
10. A. G. Lee, N. J. M. Birdsall and J. C. Metcalfe, Biochemistry 12, 1650 (1973).
11. P. E. Godici and F. R. Landsberger, Biochemistry 13, 362 (1974).
12. B. Sears, W. C. Hutton and T. E. Thompson, Biochem. Biophys. Res. Commun. 60, 1141 (1971).

13. M. P. N. Gent and J. H. Prestegard, Biochem. Biophys. Res. Commun. 58, 549 (1974).

14. E. G. Finer, J. Magn. Resonance 13, 76 (1974).

15. D. Lichtenberg, N. O. Petersen, J.-L. Girardet, M. Kainosho, P. A. Kroon, C. H. A. Seiter, G. W. Feigenson and S. I. Chan, Biochim. Biophys. Acta, in press.

16. G. W. Feigenson and S. I. Chan, J. Amer. Chem. Soc. 96, 1312 (1974).

17. T. C. Farrar and E. D. Becker, Pulse and Fourier Transform NMR, New York, Academic Press, 1971.

18. M. Kainosho, P. A. Kroon, N. O. Petersen and S. I. Chan, manuscript in preparation.

19. B. Sheard, Nature 223, 1057 (1969).

20. D. E. Woessner, J. Chem. Phys. 37, 647 (1962).

21. J. E. Anderson and R. Ullman, J. Chem. Phys. 47, 2178 (1967).

22. M. Edidin, Ann. Rev. Biophys. Bioengineer 3, 179 (1974).

23. K. van Putte, J. Magn. Resonance 2, 216 (1970).

24. H. Träuble, J. Membrane Biol. 4, 193 (1971).

25. C. J. Scandella, P. Devaux and H. M. McConnell, Proc. Nat. Acad. Sci. 69, 2056 (1972).

26. H. C. Torrey, Phys. Rev. 92, 962 (1953).

27. G. J. Kruger, Z. Naturforsch. 24A, 560 (1969).

28. J. F. Harmon and B. H. Muller, Phys. Rev. 182, 400 (1969).

29. Y. K. Levine and M. H. F. Wilkins, Nature New Biology 230, 69 (1971).

30. P. S. Hubbard, Phys. Rev. 131, 275 (1963).

31. D. Chapman, in Biological Membranes, D. Chapman and D. F. H. Wallach, Eds., Academic Press, New York, 1973.

32. M. C. Phillips, R. M. Williams and D. Chapman, Chem. Phys. Lipids 3, 234 (1969).

33. S. Kohler, A. F. Horwitz and M. P. Klein, Biochem. Biophys. Res. Commun. 49, 1414 (1972).

III. The Motional State of Cholesterol in Phospholipid Bilayers

1. INTRODUCTION

Cholesterol is a major constituent of many biological membranes. The amount of cholesterol present is characteristic for a given type of membrane. Liver cell, erythrocyte and myelin membranes contain high proportions of cholesterol (molar ratio phospholipid:cholesterol, 1:1), whereas subcellular membranes such as those of mitochondria are low in cholesterol. Although its exact function is not completely understood, a large number of studies have indicated that cholesterol can affect the packing of lipid hydrocarbon chains, both in model and in biological membranes. The interaction is envisaged to be such, that above the thermal phase transition temperature (T_c), cholesterol prevents flexing of the hydrocarbon chains, whereas below T_c it prevents the chains from crystallizing into the rigid α-gel. This has been described as an "intermediate fluid" condition.[1] Evidence for this view has come from monolayer,[2, 3] thermal analysis,[4-6] x-ray,[7-9] ESR[10-12] and NMR[13-16] studies.

Rothman and Engelman have proposed a general model to explain NMR, ESR, calorimetric and x-ray data on a molecular basis.[17] The dominant feature of this model is a nonspecific, steric interaction of the phospholipid hydrocarbon chains with cholesterol. We shall discuss this model in some detail.

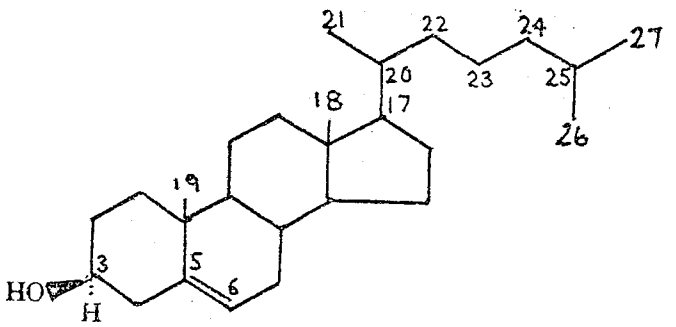

CHOLESTEROL

The cholesterol molecule consists of a ring system (the nucleus) and an isopropyl tail. The cross sectional area of the ring system is approximately twice that of the tail, and the border between the two sterically distinct regions of the molecule falls about 11 Å from the midpoint of the 3βC-OH bond. Now consider a phospholipid hydrocarbon chain next to the cholesterol molecule. The upper part of the chain parallels the rather bulky ring system, whereas the lower part of the chain parallels the much narrower cholesterol tail. The net effect will be to limit the number of accessible chain conformations along the upper part of the chain and to increase the number of accessible conformations of the lower part of the chain. X-ray diffraction measurements show that the lecithin and cholesterol molecules are rather tightly packed,[17] which indicates that the upper part of the hydrocarbon chain, in contact with and parallel to the cholesterol nucleus, must be very nearly in the all-trans configuration. The lower region of the hydrocarbon chain however is not tightly packed. Unlike the upper part of the chain, it lies next to the

cholesterol isopropyl tail, which according to Rothman and Engelman is highly mobile. Furthermore there is a greater effective volume for chain motion below the rigid ring system. This results in an enhanced number of configurations accessible to the lower part of the chain. Chapman has described the cholesterol-phospholipid state as an "intermediate fluid condition". Rothman and Engelman conclude that "this is an average statement about phospholipid hydrocarbons, which are half solid and half liquid like in their conformational character."

Phillips and Finer disagree with this model.[16] On the basis of NMR results they claim that the cholesterol molecules as a whole, including the tail, are highly immobile, as a consequence of the formation of a specific 1:1 phospholipid-cholesterol complex. This study, as well as several others which reach the same conclusion,[14,15] are based on linewidth and area measurements of the hydrocarbon chain resonances.

The question of the cholesterol mobility is intriguing and important. The model of Rothman and Engelman, while it appears reasonable, is based primarily on model building. Although spin label studies have provided some insight into the problem,[10-12] it is very clear from a number of recent studies that spin labels simply reflect an environment perturbed by the spin label.[18]

NMR studies have the clear advantage that no perturbations are introduced into the system. Unfortunately proton NMR spectra of cholesterol containing bilayer vesicles are not easy to analyze. There are not only broad hydrocarbon methyl and methylene

resonances, but also cholesterol resonances, none of which are resolved. We have avoided these problems by using lecithins with perdeuterated hydrocarbon chains.

We have observed well defined cholesterol spectra from vesicles containing cholesterol and deuterated DPL or DSL, and have studied these spectra as a function of temperature. Our data generally support the Rothman Engelman model.

2. EXPERIMENTAL

Deuterated dipalmitoyl and distearoyl lecithin were synthesized and purified as described in Chapter IV. Cholesterol was provided by Matheson Coleman and Bell (MP 148-149°C) and was used without further purification. Deuterium oxide (99.8% D) was obtained from Stohler Isotope Chemicals. Deuterochloroform (99.8% D) was obtained from Merck, Sharp and Dohme.

Weighed amounts of lecithin and cholesterol were dissolved in chloroform in a 3 ml centrifuge tube. Most of the chloroform was removed by placing the centrifuge tube in a sand bath at ~50°C and directing a stream of dry nitrogen into the tube. The remaining viscous solution was frozen in liquid nitrogen and dried overnight under high vacuum. D_2O (1 ml) was added to the sample, which was then sonicated for 20 minutes using a MSE 150 Watt ultrasonic disintegrator at high power. During sonication the centrifuge tube was partially immersed in a glycerol cooling bath to avoid overheating.

NMR measurements were performed at 220 MHz. A

description of the spectrometer is given in Chapter II. Methods of measurements and analysis of relaxation data were similar to those described in Chapter II.

3. RESULTS AND DISCUSSION

Figure 1 shows a spectrum of cholesterol in DPL vesicles. The broad chain methylene and methyl resonances completely dominate the spectrum, and although cholesterol protons account for 30% of the total intensity, none of its resonances can be resolved. This has led to the conclusion that the cholesterol molecule is highly immobilized and that its resonances are too broad to see.[14-16] Figure 2a shows the corresponding spectrum of cholesterol in deuterated DPL (molar ratio DPL (D) : cholesterol, 2:1). Removal of the broad and intense hydrocarbon chain resonances has uncovered a cholesterol spectrum with rather well defined features. It is pertinent to ask of course how much of the total cholesterol intensity we observe. Accurate intensity measurements of resonances with a broad background is difficult. The choice of baseline is always open to debate, and usually the measured intensity is smaller than the actual intensity. With these reservations in mind, we have compared the area of the DPL (D) choline resonance with that of the cholesterol resonances and conclude that at 82°C at least 70% of the cholesterol resonances are observable. Since the isopropyl tail protons correspond to only 40% of the total number of protons, at least part of the cholesterol ring protons are observed. This clearly shows that the cholesterol

FIGURE 1

High resolution 220 MHz spectrum of the hydrocarbon region of DPL vesicles containing cholesterol, molar ratio ~2:1, at 50°C.

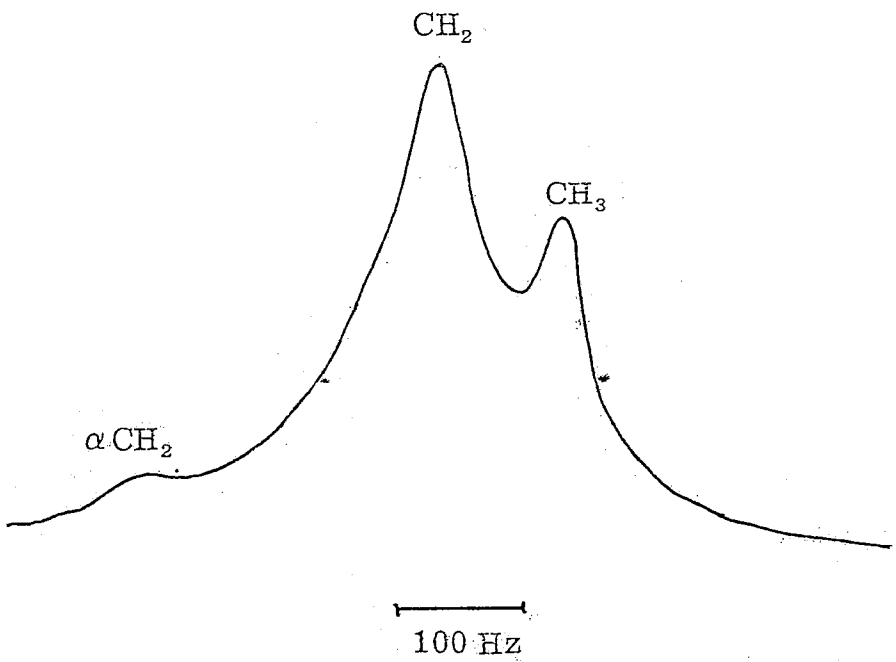
CH2
CH3
α CH2
100 Hz

FIGURE 2

High resolution 220 MHz spectra: (a) DPL (D) vesicles containing cholesterol, molar ratio 2:1, at 82°C; (b) same sample, freeze dried, and dissolved in $CDCl_3$ with TMS, at 20°C. Assignments are discussed in the text.

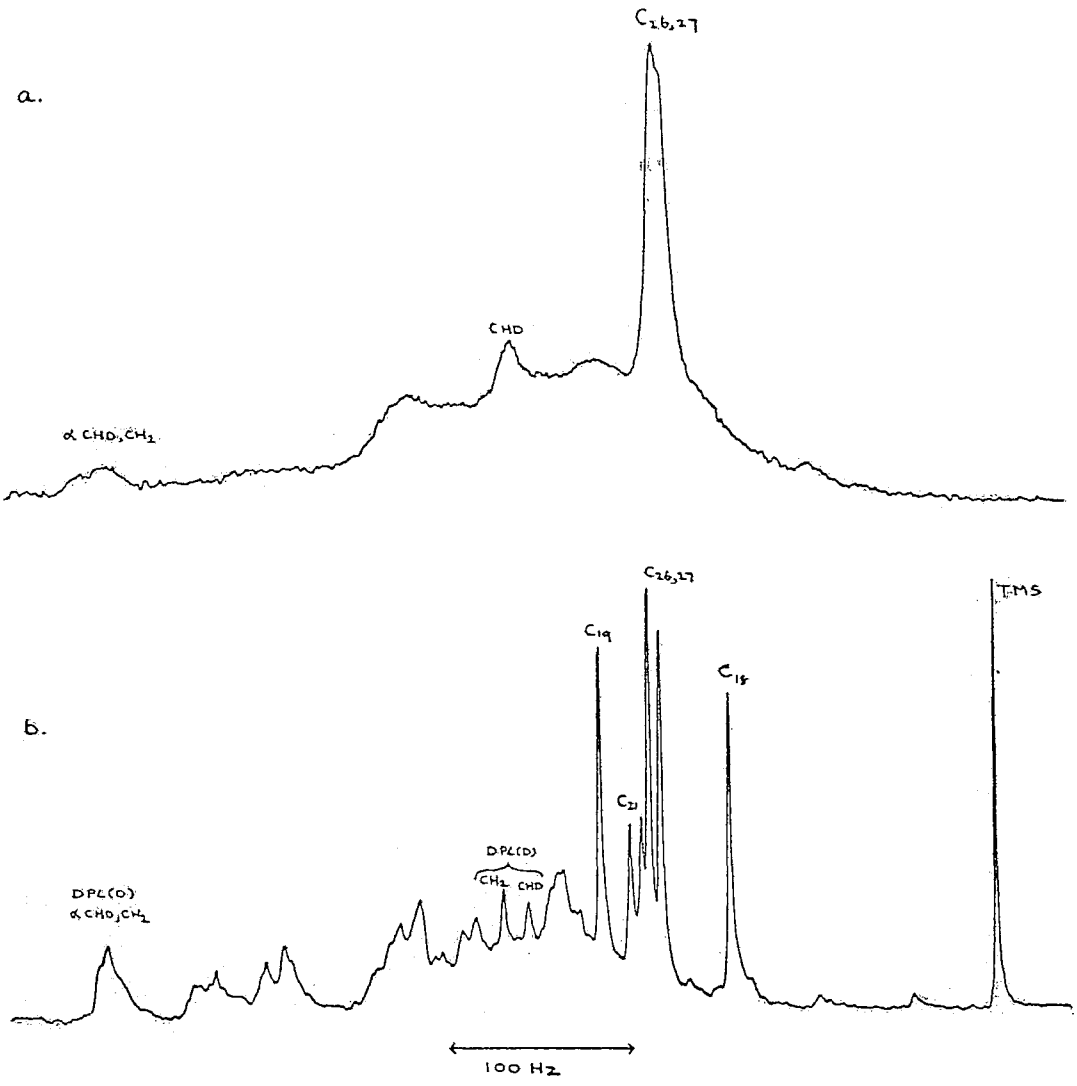
a.
$C_{26,27}$
CHD
α CHD_2CH_2
b.
$C_{26,27}$
TMS
C_{19}
C_{15}
C_{21}
DPL(D)
CH_2
CHD
DPL(O)
α CHD_2CH_2
100 Hz

molecule is not completely immobilized. It also casts serious doubts on the validity of a series of NMR studies of lecithin cholesterol interactions which are based on area measurements of the hydrocarbon resonances, assuming that no observable cholesterol resonances are present.

The most notable feature of the cholesterol spectrum is the rather sharp, intense resonance which is superimposed on a broad background. We assign this resonance by comparison with a spectrum of the same sample dissolved in $CDCl_3$ (see Fig. 2b). Cholesterol has five methyl groups and each one shows up clearly in the chloroform spectrum. Their chemical shifts and assignments are listed in Table I.[19] A simple comparison of the two spectra shows that the sharp cholesterol resonance observed in the vesicle spectrum can be assigned to the terminal methyl groups of the isopropyl tail, i. e. the C_{26} and C_{27} methyl groups. We rule out any appreciable contribution from a sharp C_{21} methyl resonance, since this would show up as a definite "hump" on the downfield side of the $C_{26,27}$ methyl resonance. If the assignment is correct, at least 80% of the $C_{26,27}$ methyl groups contribute to the signal. The three other methyl resonances are apparently much broader, which indicates that their motion is much more restricted than that of the tail methyl groups. This fits in nicely with the hypothesis of Rothman and Engelman and is the first experimental evidence for a differential mobility of the cholesterol ring system and its isopropyl tail. Still, the ring system is not completely immobilized. The fact that we do see a large part of the ring proton intensity implies that the cholesterol molecule is

TABLE I. Chemical Shifts and Assignments of Cholesterol Methyl Resonances for a Cholesterol DPL (D) Mixture (1:2) in $CDCl_3$. Chemical Shifts are Referenced to TMS. Temperature 20°C.

Chemical Shift (ppm)	Methyl Group
0.68	C_{18}
0.85 0.88	$C_{26,27}$
0.90 0.93	C_{21}
1.00	C_{19}

moving as a whole. The most likely candidate for this motion is rapid rotation about the long axis. A similar conclusion has been drawn from ESR studies,[12] which also estimated the correlation time for this motion as $\tau_c \sim 4 \times 10^{-10}$ seconds.

Some further insight can be gained from a study of partially relaxed spectra (see Experimental section of Chapter II for a description). A series of such spectra is shown in Fig. 3. The slowest relaxing component is a weak band downfield from the intense methyl resonance. It has a null point at about 1.5 sec, and therefore a T_1 of 2.2 seconds. The chemical shift of this resonance corresponds very closely to that of the residual CHD protons of DPL (D) (see Fig. 2a, b). Furthermore a similar study using deuterated DSL, with a lower percentage deuterium content, gave a similar spectrum but with a much more intense resonance in this position. We therefore assign this resonance to the residual CHD protons of the deuterated hydrocarbon chains. Of course the long T_1 for this resonance provides further support for this assignment. The residual CH_2 resonance which appears 13 Hz downfield from the CHD resonance in chloroform (Fig. 2b) is probably too broad to be observed (compare Fig. 1). The $C_{26,27}$ methyl resonance has a null point at $\tau = 0.5$ seconds. With this methyl absorption eliminated the broad "background" resonance is clearly visible. It consists of different types of protons (i.e. methylene and methene), chemically shifted from each other and with different mobilities (e.g. chain methylenes versus ring methylenes). All we can really say about it is that it has a null point between 0.2 and 0.3 seconds which gives

FIGURE 3

Partially relaxed 220 MHz Fourier transform spectra of DPL (D) vesicles containing cholesterol, molar ratio 2:1, at 82°C. The time between π and $\pi/2$ pulses is denoted by τ. The amplitude is increased by a factor of two for spectra at τ = 0.4, 0.5 and 0.7.

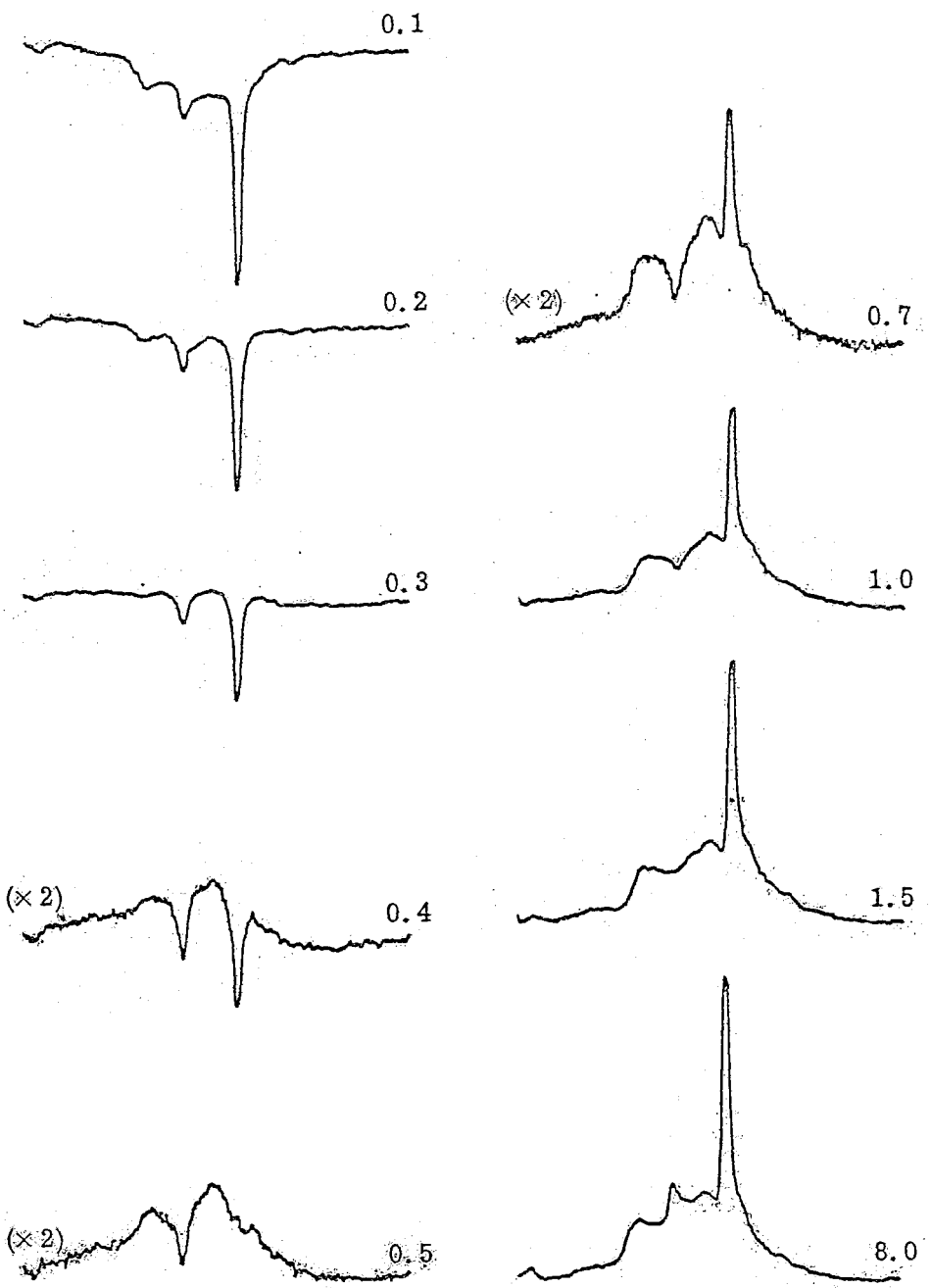
τ, [sec]
0.1
0.2
0.3
(×2)
0.4
(×2)
0.5
(×2)
0.7
1.0
1.5
8.0

an "average" T_1 of about 0.4 seconds.

So far we have only considered the system at 82°C. What happens when the temperature is lowered? Figure 4 shows spectra taken at 82°C, 60°C and 40°C. As the temperature is lowered the methyl, CHD and background resonances all show a gradual broadening. The methyl resonance linewidth for example goes from 12 Hz at 82°C to 26 Hz at 40°C. This reflects a gradual increase in order and a decrease in mobility as the temperature is lowered. This trend is also reflected by the methyl, CHD and "background" T_1's, which are summarized in Table II. We have also made some measurements at 20°C. At this temperature the cholesterol resonances are much broader but are still clearly observable. The methyl resonance for example has a width of approximately 50 Hz. This indicates that the terminal end of the isopropyl chain still undergoes a considerable amount of motion even at temperatures 21°C below the thermal phase transition temperature of DPL. As a comparison, no high resolution hydrocarbon chain resonances of DPL vesicles without cholesterol can be observed at 20°C.

4. CONCLUSIONS

We have provided experimental evidence for a differential mobility of the cholesterol nucleus and its isopropyl tail. The tail has a greater mobility than the nucleus. The molecule as a whole undergoes rapid rotation about its long axies. Below the phase transition temperature the isopropyl tail still has a considerable degree of motional freedom.

FIGURE 4

High resolution 220 MHz spectra of DPL (D) vesicles containing cholesterol, molar ratio 2:1, at 82°, 60° and 40°C.

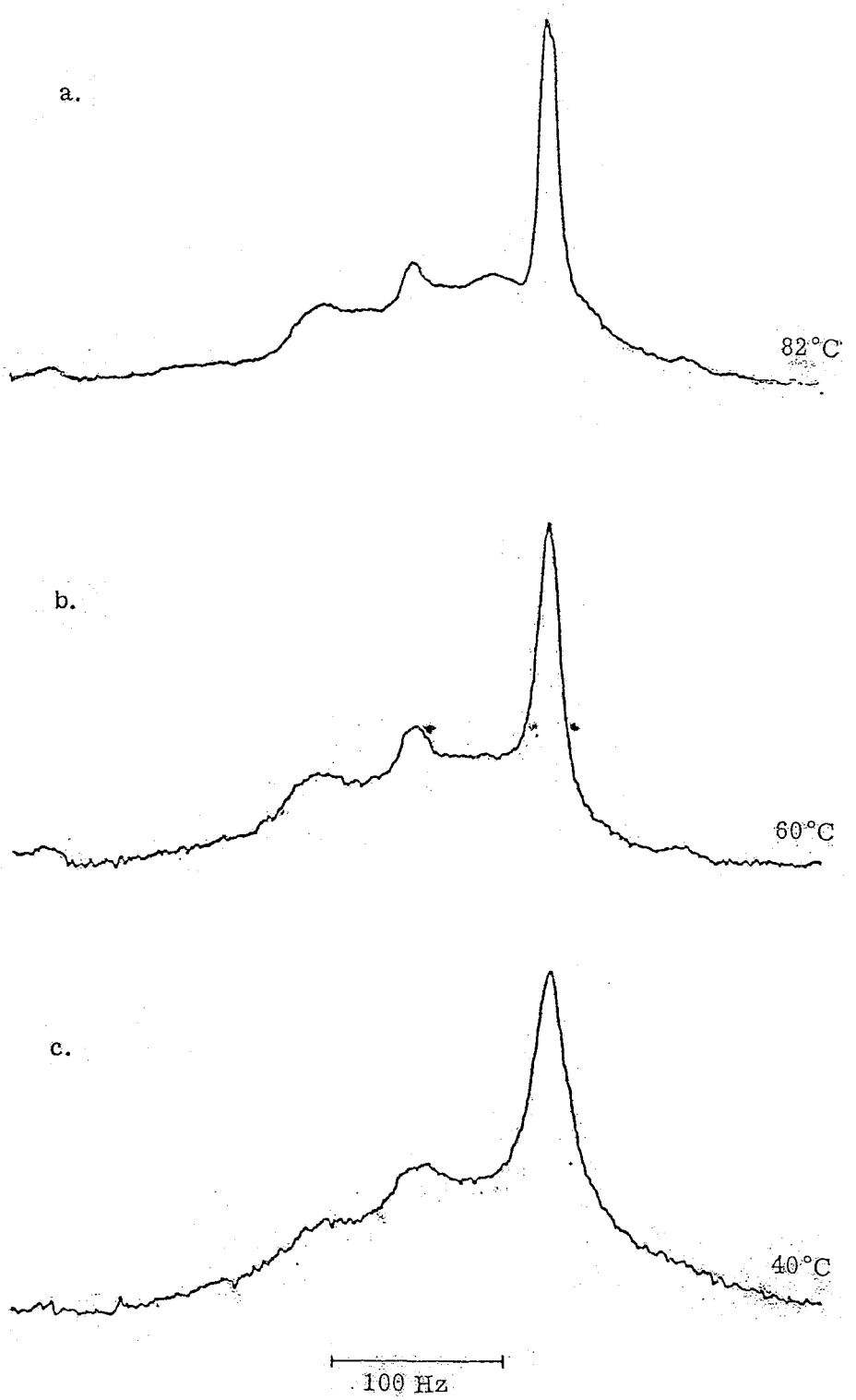
a.
82°C
b.
60°C
c.
40°C
100 Hz

TABLE II. Temperature Dependence of the Spin Lattice Relaxation Times (sec) for Cholesterol Protons and Residual DPL (D) Hydrocarbon Chain Protons

Protons	82 °C	40 °C
Methyl (26, 27)	0.7	0.5
"Background"	0.4	0.3
CHD	2.2	0.9

Our data provide support for the model proposed by Rothman and Engelman and cast serious doubt on the validity of a number of previous NMR studies.

References

1. D. Chapman, in Biological Membranes (edited by D. Chapman) (Academic Press, New York, 1968).
2. R. A. Demel, L. L. M. van Deenen and B. A. Pethica, Biochim. Biophys. Acta 135, 11 (1967).
3. P. Joos and R. A. Demel, Biochim. Biophys. Acta 183, 447 (1969).
4. B. de Kruyff, R. A. Demel and L. L. M. van Deenen, Biochim. Biophys. Acta 255, 331 (1972).
5. B. D. Ladbrooke and D. Chapman, Chem. Phys. Lipids 3, 304 (1969).
6. M. J. Hinz and J. M. Sturtevant, J. Biol. Chem. 247, 3697 (1972).
7. Y. K. Levine and M. H. F. Wilkins, Nature New Biol. 230, 69 (1971).
8. M. H. F. Wilkins, A. E. Blaurock and D. M. Engelman, Nature New Biol. 230, 72 (1971).
9. D. M. Engelman and J. E. Rothman, J. Biol. Chem. 247, 3694 (1972).
10. E. J. Shimshick and H. M. McConnell, Biochem. Biophys. Res. Commun. 53, 446 (1973).
11. D. Marsh and I. C. P. Smith, Biochim. Biophys. Acta 298, 133 (1973).
12. M. A. Hemminga and H. J. C. Berendsen, J. Magn. Resonance 8, 133 (1972).
13. D. Chapman and S. A. Penkett, Nature 211, 1304 (1966).
14. A. Darke, E. G. Finer, A. G. Flook and M. C. Phillips, FEBS

Lett. 18, 326 (1971).

15. A. Darke, E. G. Finer, A. G. Flook and M. C. Phillips, J. Mol. Biol. 63, 265 (1972).

16. M. C. Phillips and E. G. Finer, Biochim. Biophys. Acta 356, 199 (1974).

17. J. E. Rothman and D. M. Engelman, Nature New Biol. 237, 42 (1972).

18. A. Seelig and J. Seelig, Biochemistry 13, 4839 (1974).

19. G. Slomp and F. A. MacKellar, J. Amer. Chem. Soc., 84, 204 (1962).

IV. Synthesis of Deuterated Lecithins

1. INTRODUCTION

In this Chapter we shall describe the procedures used to synthesize several deuterated phospholipids, in particular 1, 2-dipalmitoyl (d_{62})-phosphatidylcholine, 1-palmitoyl-2-palmitoyl (d_{31})-phosphatidylcholine and 1, 2-distearoyl (d_{70})-phosphatidylcholine. First, however, we shall present a brief survey of the synthetic methods currently used for the synthesis of 3-sn-phosphatidylcholines, followed by a brief discussion of synthetic procedures used to deuterate fatty acids.

Synthesis of 3-sn-phosphatidylcholines

Two approaches can be taken in the synthesis of phosphoglycerides with well defined fatty acid compositions; the first involves a complete chemical synthesis [1, 2] and the second a partial synthesis, in which naturally occurring phosphoglycerides as well as lipolytic enzymes are used as a synthetic starting point. [3] Although the complete chemical synthesis is very versatile, it is a rather time consuming procedure involving a large number of steps. Thus in cases where labelled fatty acids or a labelled choline moiety are required, the procedure is not very attractive. Mono-acid lecithins (lecithin carrying two identical acyl chains) and mixed-acid lecithins are most conveniently prepared by partial synthetic procedures.

The partial synthetic procedures are outlined in scheme 1.

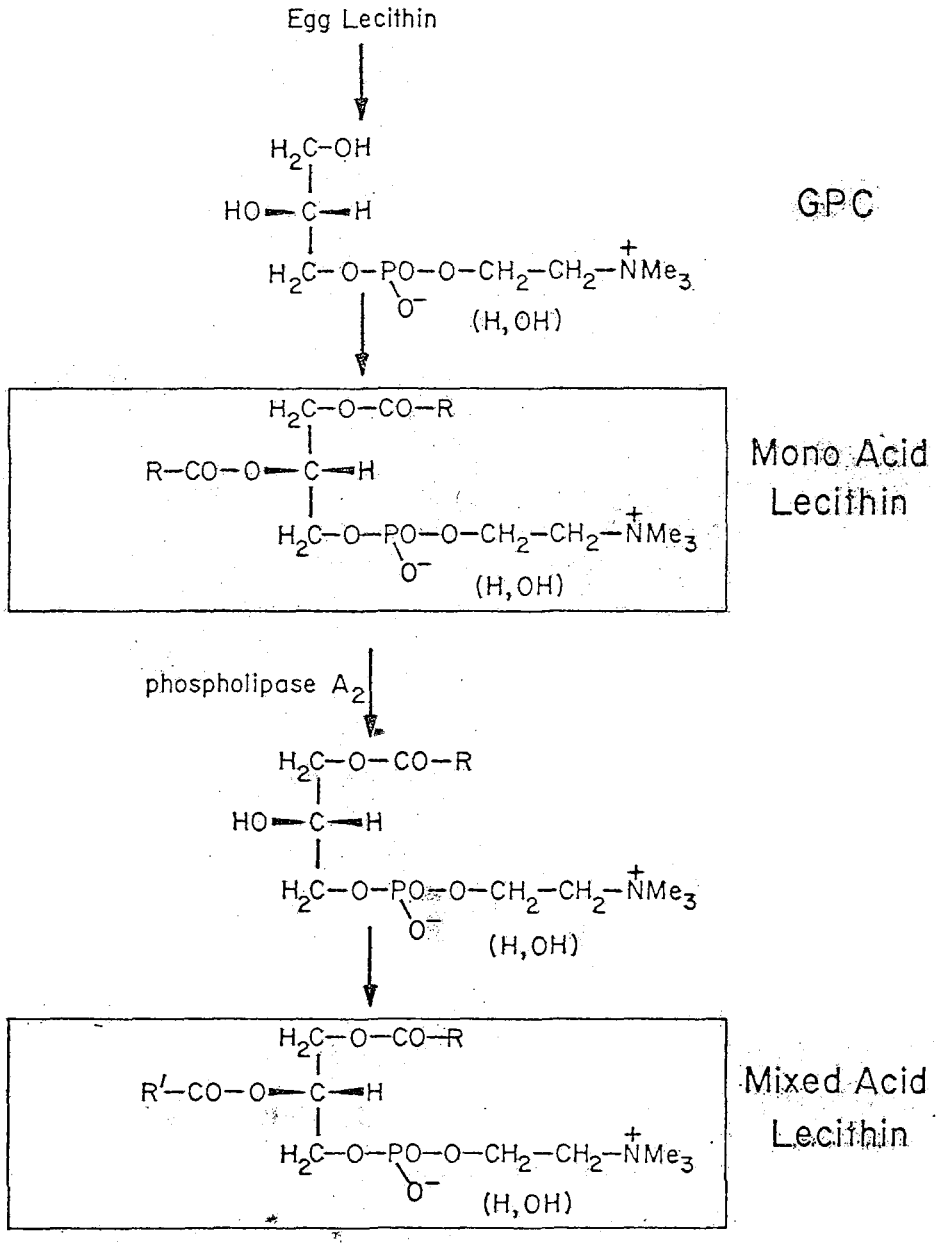
Egg Lecithin
GPC
(H, OH)
Mono Acid Lecithin
(H, OH)
phospholipase A2
(H, OH)
Mixed Acid Lecithin
(H, OH)

SCHEME 1

Acylation of sn-glycero-3-phosphorylcholine (GPC) furnishes mono-acid lecithins. GPC can be obtained by deacylation of purified egg yolk lecithin. Hydrolysis of the mono-acid lecithin by phospholipase A_2 (EC 3.1.1.4), and subsequent reacylation of the resulting 1-acyl-sn-glycero-3-phosphorylcholine (lysolecithin) with another fatty acid produces a mixed acid lecithin.

Mono-acid lecithin can be prepared by reacylation of free GPC or of its $CdCl_2$ adduct. This can be achieved using a 7-10 fold molar excess of fatty acid chloride in the presence of pyridine.[4] Yields are generally about 50%. The formation of by-products such as phosphatidic acid, isomeric lysolecithins, and choline chloride esters of the fatty acids complicates the purification. These problems have been largely overcome by Robles and Van den Berg,[5] who acylated GPC and its $CdCl_2$ adduct with fatty acid anhydrides in the presence of an easily dissociable salt of the same fatty acid. Much smaller amounts of by-products are formed, facilitating purification and increasing the yield (70-90% based on GPC and 7-9% based on the fatty acids). Of the two methods (i. e. acid chloride and anhydride) the anhydride method of Robles and Van den Berg is the most convenient for the preparation of mono-acid lecithins, especially those with saturated fatty acids. The fatty acid chloride method, however, is much milder than the anhydride method and appears to be preferable for lecithins containing polyunsaturated fatty acids.[3]

The anhydride method can be used to acylate either GPC or its $CdCl_2$ complex.[5] The GPC-$CdCl_2$ complex reaction is performed

in dry ethanol-free chloroform in the presence of the anhydride and the tetraethylammonium salt of the fatty acid (GPC-anhydride-salt molar ratio 1:6:6). Acylation of free GPC is effected by heating GPC, the anhydride, and the potassium salt of the fatty acid (molar ratio 1:2:4) in a sealed evacuated flask, at 80°C for 48 hours.

The latter procedure was chosen for the synthesis of deuterated phospholipids because of the smaller excess of anhydride and fatty acid salt needed.

Finally, the acylation of lysolecithin can also be performed using either the fatty acid chloride[4] or the fatty acid anhydride[5] (the yields are similar, ~70%). Since the anhydride method requires a smaller excess (GPC-anhydride molar ratio 1:4) this method was used for the synthesis of mixed-acid lecithins containing one perdeuterated fatty acid.

Synthesis of perdeuterated fatty acids

Perdeuterated fatty acids have been produced by biosynthetic methods[6] and by catalytic hydrogen-deuterium exchange of proton containing fatty acids.[7] Merck, Sharp and Dohme Ltd., for example, have produced a series of perdeuterated saturated and unsaturated fatty acids from algae (Scenedesmus obliquus) grown in 99.7% deuterium oxide.[6] The advantage of catalytic H-D exchange over biosynthetic methods, however, lies in the fact that well defined fatty acid preparations can be obtained.

Recently a convenient method for the synthesis of fatty acids

with a high deuterium content (up to 99%) has been described.[7] It consists of an H-D exchange performed by heating the fatty acid in D_2O in the presence of a homogeneous (alkali) catalyst, a heterogeneous catalyst (Pt) and a peroxide promoter. A convenient alkali catalyst and peroxide promoter solution can be prepared by hydrolysis of sodium peroxide with D_2O at low temperature:[8]

$$Na_2O_2 + 2\,D_2O \xrightarrow{< 10°C} 2\,NaOD + D_2O_2$$

At higher temperatures the reaction is:

$$Na_2O_2 + 2\,D_2O \longrightarrow 2\,NaOD + D_2O + \tfrac{1}{2}\,O_2$$

Finally, the platinum catalyst can be conveniently prepared by reducing a suspension of $PtO_2 \cdot H_2O$ in D_2O with deuterium gas. Neither reduced platinum oxide nor sodium hydroxide when used separately with D_2O_2 leads to any appreciable H-D exchange. These catalysts primarily influence the H-D exchange of the labile α-hydrogen atoms of the carboxylates.

A description of the experimental details is given in the following sections.

2. GENERAL METHODS

Nuclear magnetic resonance (NMR) spectra were recorded on a Varian HR-220 spectrometer equipped with a Fourier Transform accessory and interfaced with a 16 K Varian 620i computer. The probe temperature was ~20°C.

Infrared (IR) absorption spectra were recorded on a Perkin Elmer model 137 spectrophotometer. The lipid of interest was thoroughly mixed with potassium bromide and ground to a fine powder in an agate mortar. The powder was compressed into a pellet (1-2 mm thick by 10 mm in diameter) at 12000 psi under vacuum.

Optical rotations were measured with a Perkin Elmer 141 polarimeter. A 1 ml quartz cell, 1.001 dm long, was used for the measurements. Lecithin concentrations were approximately 1% (wt/volume) in chloroform-methanol (1:1 v/v). Because of the small rotation of lecithin (+6°), and the low concentrations used, the measurements were taken at 436 mμ and 365 mμ (Hg lines).

All solvents used were distilled less than two weeks before use.

3. SYNTHESIS OF PERDEUTERATED FATTY ACIDS

The steps involved in the synthesis of perdeuterated fatty acids are illustrated below.

$$PtO_2 \xrightarrow[D_2,\ D_2O]{} Pt$$

$$Na_2O_2 \xrightarrow[D_2O]{} NaOD + D_2O_2$$

$$CH_3(CH_2)_nCO_2H + Pt + NaOD + D_2O_2 \xrightarrow[\substack{D_2O \\ 240°C \\ 24\ hr}]{} CD_3(CD_2)_nCO_2Na$$

The exchange reaction was either performed on a small (< 2 g) or on a large scale (5-12 g). The small scale ("tube") reactions were performed in 1" thick walled pyrex tubes (Fig. 1a) sealed under vacuum. The tubes were heated in a "sealed tube" oven. The volume of D_2O used in these reactions (see Table I) was less than 40% of the total tube volume (35% was generally used). Larger volumes invariably result in an explosion. Figure 1b illustrates the containers used for the large scale ("bomb") reactions. The sealed pyrex containers were placed inside a one liter stainless steel Parr bomb which was flushed with N_2 and then heated in a "bomb oven".

The extent of deuteration was estimated from the integrated NMR signal of the methyl ester of the deuterated fatty acid. A single exchange reation resulted in 90-96% deuteration. After two exchanges, however, the deuterium content was 98.8% or better.

Reduction of $PtO_2 \cdot H_2O$

PtO_2 (10 g) was suspended in D_2O (100 ml) in a 250 ml erlenmeyer flask which was then attached to a standard reduction apparatus (see Fig. 2). While the suspension was stirred, the apparatus was alternately evacuated and flushed and N_2 (a total of three times) and finally evacuated. Deuterium gas was introduced slowly, filling the gas reservoir (500 ml). The suspension was stirred vigorously to effect reduction (the rate of the reduction was found to depend largely on the rate of stirring). As the reduction progressed the grey suspension turned black. The gas reservoir was filled several times

FIGURE 1

Reaction vessels used for fatty acid deuteration experiments: (a) for small scale experiments, constructed from heavy walled pyrex tubes, and (b) for large scale experiments made from regular pyrex tubes.

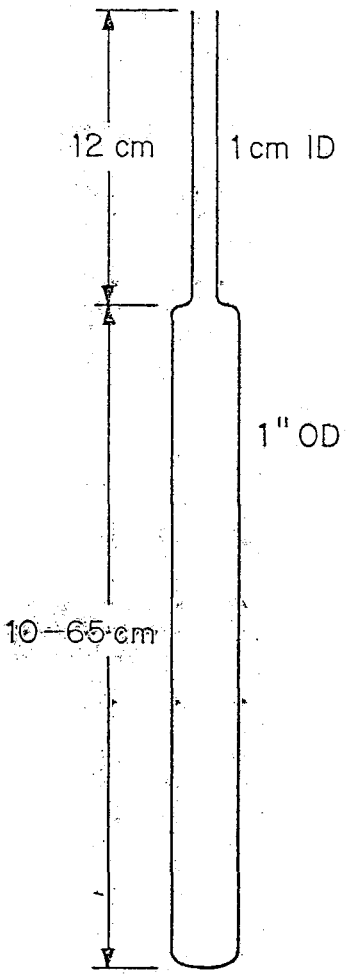

a

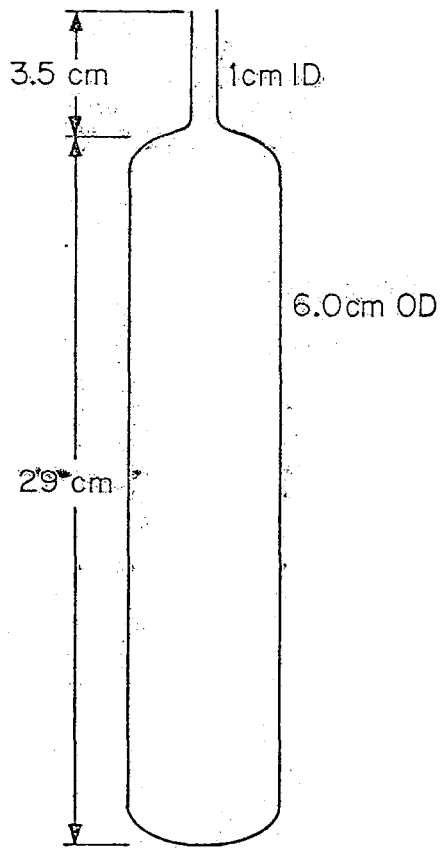

b

FIGURE 2

Hydrogenation apparatus used to reduce PtO_2.

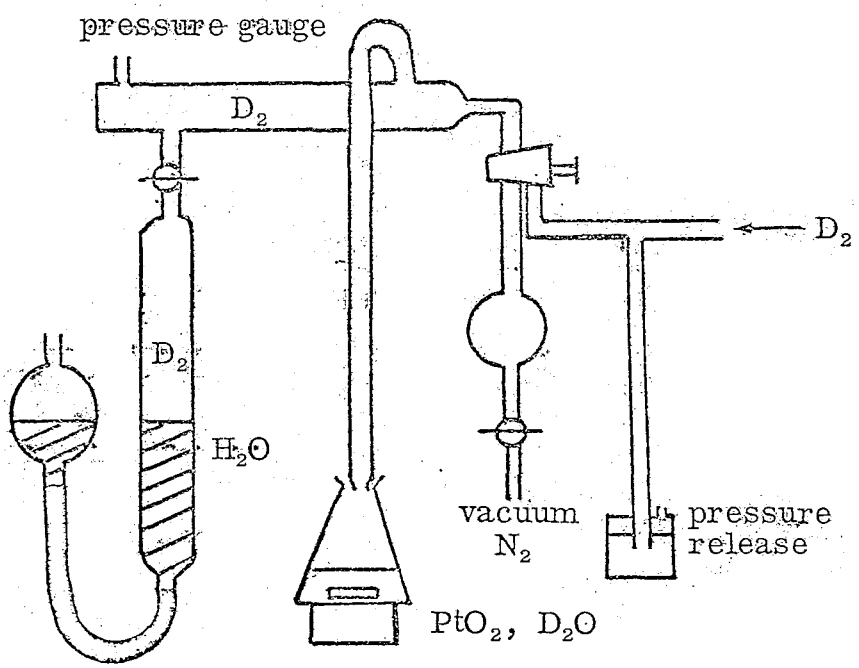
pressure gauge
D_2
D_2
H_2O
D_2
vacuum
N_2
pressure
release
PtO_2, D_2O

during the course of the reaction. Deuterium uptake ceased abruptly when the reduction was completed. A total of 1.5 to 2 ℓ of D_2 was used.

Upon complete reduction the apparatus was evacuated and filled with N_2 to remove excess D_2. The Pt suspension was transferred to a 250 ml round bottom flask with a side arm which was connected to a short piece of tygon tubing and a stopcock. The flask was flushed with N_2 and was closed.

Prior to removal of Pt, argon was introduced into the flask through the side arm. The suspension (6.5% Pt in D_2O, w/w) was stirred and an appropriate volume of the suspension pipetted out.

Preparation of alkaline catalyst and promoter ("bomb" scale)

D_2O (200 ml) in a 500 ml erlenmeyer flask was cooled by partially immersing the flask in an ice-water bath. Sodium peroxide (3.1 g) was added cautiously, in small portions, with stirring.

The resulting solution contains a 2:1 molar ratio of NaOD and D_2O_2.

The exchange reaction

(a) "Bomb" scale. The reaction vessel was partially immersed in an ice-water bath and was flushed with dry argon. Pt-D_2O (60 ml) was transferred to the reaction vessel, followed successively by 40 mmole of the fatty acid (stearic or palmitic), the alkaline catalyst and promoter solution and finally 100 ml of D_2O (Table I).

TABLE I. Summary of reactants needed for hydrogen-deuterium exchange

Compound	Molar Ratios	Parts by Weight
Fatty acid	2	
C_{16}		51
C_{18}		57
Na_2O_2	2	15.5
D_2O for Na_2O_2	500	1000
Pt	1	19.5
D_2O	250	500

The reaction vessel was sealed off and the position of the breather hole was marked (near the seal). The vessel was placed in the bomb (seal up) and a sheet of folded TEF teflon was inserted between the bomb wall and glass to keep the glass vessel from moving. Finally the bomb head was attached, with the safety outlet facing the same direction as the breathing hole. The bomb was placed in the bomb oven in a horizontal position. The gas inlet system was connected, after which the bomb was slowly filled with N_2 ($\sim$100 atm) and kept at this pressure, with the bomb head valve closed, for $\sim$5 min to check for leaks. The N_2 was removed slowly, and the process was repeated once to remove residual air. With the bomb head valve closed, the bomb was kept at 240°C for 24 hours. The pressure reached $\sim$60 atm during this time.

Two points are worthy of mention. Although initially the bomb was rocked during the reaction to ensure thorough mixing of the reactants, this was found to result in large losses, presumably through the breather hole. Secondly, it is not advisable to perform the reaction directly in a stainless steel bomb. At the temperature and concentration of NaOD used this can result in damage to the bomb surface.[9]

(b) "Tube" scale. The reactions were introduced into the tube as described for the "bomb" experiment, with the amounts scaled down appropriately (see Table I) and with the total volume of $D_2O \leq 35\%$ of the total tube volume. The contents were frozen (using dry ice-acetone), after which the tube was evacuated and

sealed off. The tube was kept at 240°C in a tube oven for 24 hours.

Extraction

After cooling, the reaction vessel (tube or bomb type) was opened and the contents, which exist in a soap-water gel phase, were stirred up. Most of the contents were transferred to a beaker. The remaining contents were scraped from the wall of the reaction vessel and were combined with the first fraction by rinsing the vessel with 5% HCl. Enough 5% HCl was then added to the combined fractions to convert the fatty acid salt to the acid (a total of ~200 ml for the bomb scale (40 mmole) reaction). The solution was transferred to a separatory flask, extracted three times with diethyl ether (with extensive shaking), washed with water and dried over Na_2SO_4. The solution was filtered and the solvent removed under reduced pressure.

No attempt was made to remove the hydrocarbon corresponding to the decarboxylated fatty acid which is formed as an impurity. Gas chromatographic measurements indicated that it was present only in very small amounts.

The yield for a "tube" reaction was approximately 87% and for a "bomb" reaction 70%.

Synthesis of methyl ester to estimate deuterium content

Perdeuterated fatty acid (20-50 mg) was dissolved in methanol (15 ml). Concentrated sulfuric acid (0.45 ml) was added to the solution, which was then refluxed for 2 hours. Most of the methanol was

evaporated under reduced pressure. Water (1 ml) was added to the solution, which was then extracted with diethyl ether, washed with sodium bicarbonate to remove residual sulfuric acid, and finally dried over sodium sulfate. The solution was filtered and the ether removed under reduced pressure. The methyl ester was dissolved in chloroform-d (~0.5 ml) for nmr measurements.

Characterization

(a) IR. The IR spectra of palmitic and deuterated palmitic acid are illustrated in Fig. 3. Both spectra exhibit features characteristic of carboxylic acids,[10] that is, an O-H stretch band between 3 and 4 μ, a C=O stretch band between 4.8 and 5.9 μ, C-O stretch vibrations between 7.5 and 8.5 μ, an O-H deformation band at 7.1 μ (hidden under CH_2 bands for the protio palmitic acid) and finally an O-H deformation band at ~10.5 μ. The most characteristic differences between the two fatty acids are the shifts observed for the methyl and methylene absorptions: the C-H stretch absorptions at 3.4-3.5 μ are replaced by C-D stretch absorptions at 4.54 and 4.78 μ, the C-H bending absorptions at ~6.8 μ are replaced by C-D absorptions at 9.18 and 9.47 μ and finally, the CH_2 rocking absorption at 13.8 μ is replaced by a CD_2 band which appears at $\lambda > 15$ μ (too high to be observed).

(b) NMR. Spectra of the methyl esters of deuterated fatty acids indicate that the extent of deuteration ranges from 90-96% after one exchange reaction. The figure is close to 96% for a "tube"

FIGURE 3

Infrared spectra of palmitic and deuterated palmitic acid, KBr pellets.

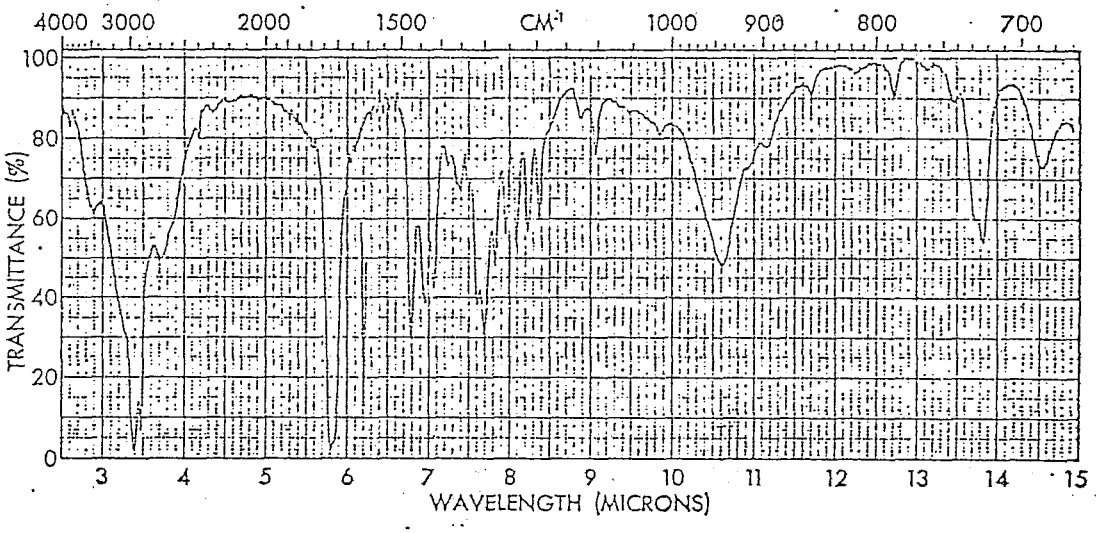

a. Palmitic Acid ($C_{16}H_{32}O_2$)

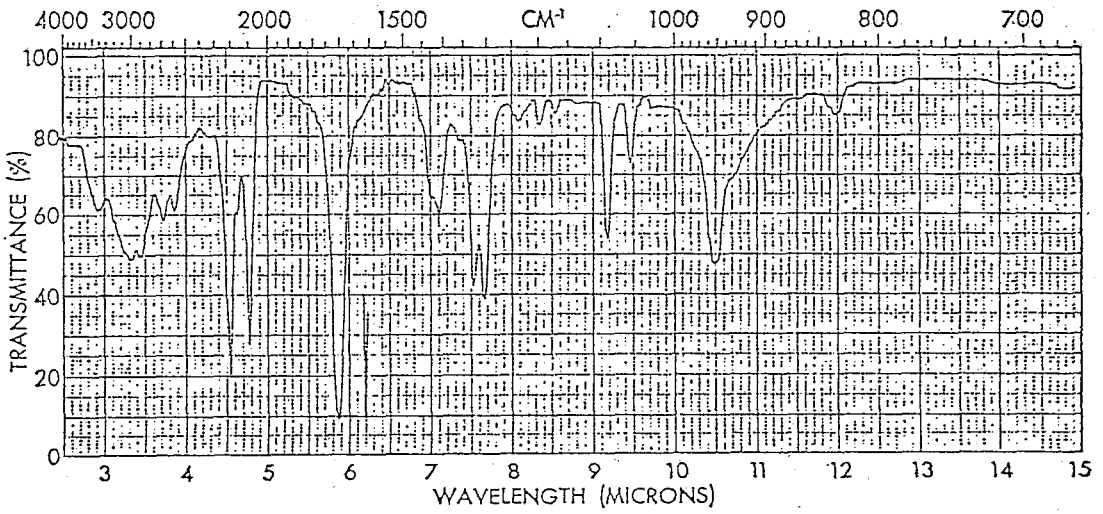

b. Deuterated Palmitic Acid ($C_{16}D_{31}HO_2$)

experiment and is generally somewhat larger than 90% for a "bomb" experiment. Deuterated stearic acid, which was used for the synthesis of distearoyl lecithin, was prepared on a "tube" scale and its deuterium content was 96.0%. Palmitic acid was exchanged twice (on a "bomb" scale). This gave a deuterium content of better than 98.8%.

It has been reported that during the reaction 15-20% of the fatty acid is converted to the corresponding hydrocarbon.[7] As we mentioned previously, the amount of hydrocarbon formed in the reactions reported here appeared to be very small. This has been further substantiated by the fact that the deuterium content measured for the fatty acids when they are esterified to GPC is the same as the values given above (see section 8). In the presence of an appreciable quantity of hydrocarbon in the fatty acid preparations, the deuterium content estimated from the methyl ester would have been lower than that estimated from the corresponding lecithin.

4. SYNTHESIS OF FATTY ACID ANHYDRIDES

The anhydrides of deuterated palmitic and stearic acid were synthesized from the fatty acids and dicyclohexyl carbodiimide (DCC).[11] DCC (I) reacts with long chain fatty acids to form the anhydride (II) and dicyclohexylurea (DCU, III). A small amount of dicyclohexylacylurea (IV) is also formed.

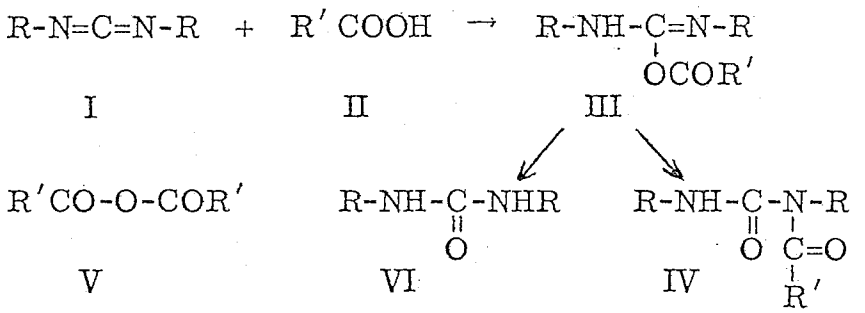

A solution of DCC (10 mmole) in dry CCl_4 (50 ml) was added to a solution of deuterated fatty acid (20 mmole) in dry CCl_4 (150 ml). The reaction mixture was stirred at room temperature for 5 hours. DCU precipitated soon after mixing the reactants. After 5 hours the precipitate was filtered off, and the solvent removed by evaporation under reduced pressure. The crude anhydride was recrystallized from acetone (125 ml). The yield was 8.1 mmole for palmitic anhydride (81% of the theoretical yield).

5. PURIFICATION OF EGG LECITHIN

Egg lecithin was extracted and purified following the basic procedure of Rhodes and Lea.[12] The procedure involves two steps: (1) the isolation of crude phospholipids, and (2) the separation of lecithin from this mixture.

Fresh egg yolks (24) were blended with cold (4°C) acetone (1 liter). The solution was filtered. This procedure was repeated with the residue. The acetone extract which contained triglycerides, steroids and pigments was discarded. The residue was extracted with 1:1 (v/v) methanol-chloroform (600 ml) at 4°C (with stirring)

for 30 minutes. The solution was filtered, and the residue was extracted once more in the same manner. The solvent was removed from the combined extracts by evaporation under reduced pressure. The lipids were dissolved in a minimal volume of chloroform and were precipitated twice with eight volumes of cold (4°C) acetone.

Acidic phospholipids were removed by passage through an alumina column. The column measured 4 cm ID by 100 cm in length, and was equipped with a teflon stopcock. Glass wool was placed at the bottom of the column to prevent elution of alumina. Alumina (625 g) was slurried with 1:1 (v/v) chloroform-methanol (700 ml) and was added to the column in one portion. Solvent flow was adjusted to 10 ml/min. The column was washed with 300 ml of solvent. Twenty-five g of the crude lipids were dissolved in 1:1 (v/v) chloroform-methanol (250 ml) and added to the column. The phospholipids were eluted with the same solvent. Progress of the fractionation was followed by TLC (solvent chloroform-methanol-water, 65:25:4). The ensuing preparation contained lecithin and smaller amounts of lysolecithin and sphingomyelin. The phospholipids were stored under argon at -20°C.

6. PREPARATION OF GPC FROM EGG YOLK LECITHIN

GPC was prepared by deacylation of egg yolk lecithin using the procedure of Brockerhoff and Yurkowski.[13]

Egg lecithin (15 g) was dissolved in diethyl ether (150 ml). An appreciable fraction of the lecithin fraction did not dissolve

(probably the lyso form) and was removed by centrifugation. With stirring, 15 ml of a 1.0 M methanolic tetrabutylammonium hydroxide solution was added. After one hour at room temperature, the solvent was decanted from the viscous precipitate of GPC, and the vessel rinsed with diethylether. The GPC was dried under vacuum for 48 hours. Because of the difficulty in handling the viscous liquid, it was dissolved in methanol to give a concentration of 92 mg/ml (1 mmole per 3 ml) and was stored at -20°C.

7. PREPARATION OF LYSOLECITHIN FROM DIPALMITOYL LECITHIN

1-palmitoyl-sn-glycero-3-phosphorylcholine (lysolecithin) was prepared by hydrolysis of the fatty acid ester bond at the 2-position using phospholipase A_2. Phospholipase A_2 (Crotalus terrificus terrificus) was obtained from Boehringer Mannheim as a 0.1% solution in 50% glycerol, with an activity of 200 units per mg (a unit of phospholipase activity is defined as that amount of protein which catalyzes the hydrolysis of 1 mmole of lecithin per minute).

Dipalmitoyl lecithin (DPL) (140 mg) was dissolved in ethanol (1 ml). This solution was diluted with diethyl ether (100 ml). $CaCl_2$ (0.5 ml of a 10 mM solution) was added to a 1 ml solution of venom (0.1% in 50% glycerol), which was then transferred to the rather cloudy DPL ether solution. After three hours, ethanol (30 ml) was added and the volume reduced to about 8 ml using a rotary evaporator. The solution was centrifuged to remove the precipitated enzyme.

The precipitate was washed once with 2:1 v/v chloroform-methanol. The extract was combined with the original supernatant. The volume of this solution was reduced to approximately 1 ml and the lysolecithin was precipitated with diethyl ether (20 ml). The precipitate was washed twice with diethyl ether and was dried under vacuum.

8. ACYLATION OF GPC

The synthesis of DPL will be described in some detail. Reaction conditions and yields were essentially the same for distearoyl lecithin. A solution containing GPC (2.5 mmole) and perdeuterated palmitic acid (5 mM) in 0.1 N methanolic KOH (50 ml) was evaporated to dryness under reduced pressure in a rotary evaporator at 60°C. The white powder was dried overnight under high vacuum and was transferred to a 50 ml flask (round bottomed, with an 11 cm long, 1 cm ID thickwalled neck). Following the addition of perdeuterated palmitic anhydride (10 mmole) the flask was sealed under vacuum and was heated in a glycerol bath at 80°C for 48 hours while it was rotated mechanically to ensure good contact between the contents. A homogeneous oil was obtained, which solidified at room temperature. The solid was broken up with a spatula and was ground to a powder in a mortar. The powder was stirred up with diethyl ether (70 ml), filtered, washed with the same solvent, and was finally dissolved in boiling chloroform (250 ml). After cooling in a refrigerator the solution was filtered and washed with chloroform.

Most of the palmitic acid, anhydride and salt was removed in this way.

The phospholipid was further purified by silicic acid column chromatography. Unisil (140 g) (Clarkson Chemicals) was activated by heating at 120°C for 12 hours. A slurry was prepared with chloroform (300 ml), which was poured into the chromatography column (4 cm ID by 100 cm long equipped with a teflon stopcock) which had a small plug of pyrex glass wool at the bottom. With the stopcock open the tube was tapped gently to dislodge air bubbles. The column was washed with 2% methanol in chloroform (~1 ℓ) until the silicic acid appeared uniform. With the solvent just covering the silicic acid, the phospholipid, dissolved in 25 ml of 2% MeOH in $CHCl_3$, was added. After the solution had settled into the column the glassware washings (~20 min) were added, followed by ~50 ml of solvent to rinse the sides of the column. Elution was carried out at a flow rate of 7 ml/min beginning with 200 ml of 2% $CHCl_3$ in MeOH, followed successively by 200 ml portions of 5% to 35% MeOH in $CHCl_3$, incremented in 5% steps. Elution was continued with 40% MeOH in $CHCl_3$. Fractions (~20 ml each) were tested by TLC (solvent $CHCl_3$-MeOH-H_2O, 65:25:4). Palmitic acid, salt and anhydride were collected in fractions 9-19, a small amount of unreacted GPC was collected in fractions 95-107 and DPL was collected beginning with fraction 169. Fractions 9-19 were combined, evaporated to dryness and kept for future reactions. The DPL fractions were also combined, evaporated to dryness in a

rotary evaporator and were finally dried under high vacuum.

The white powder was chromatographically pure and had the same R_f as commercially available DPL. The yield was 2.0 mmole (80% of the theoretical yield).

Phospholipase A_2 degradation of the synthetic phospholipids (DPL(D) or DSL(D)) yielded lysolecithin and fatty acid. Since phospholipase A_2 specifically removes the fatty acid from the 2 position of 3-sn-phosphatidylcholines, and not from 1-sn-phosphatidylcholines, the lipids are optically pure. This was further substantiated for DSL(D) by comparing the optical rotation of DSL(D) and DSL. For DSL(D) $[\alpha]_{436} = +12.2°$, and $[\alpha]_{365} = +19.8°$, while for DSL $[\alpha]_{436} = +12.5°$ and $[\alpha]_{365} = +20.1°$.

Characterization

(a) IR. Spectra of DPL and DPL(D) are illustrated in Fig. 4. Both spectra exhibit characteristic phospholipid absorptions,[14] P=O at ~8 μ, P-O-C at ~9.2 μ and P-OH at 10.25 μ, and are consistent with published spectra for synthetic phospholipids. The principal differences between the two spectra arise in the fatty acid methyl and methylene absorptions. These have been discussed previously (see section 3). Briefly, the C-H stretch bands at 3.4-3.5 μ are replaced by C-D bands at 4.54 and 4.78 μ, the 6.79 μ C-H bending absorptions are replaced by C-D absorptions (hidden under the P-O-C band), and finally the CD_2 band corresponding to the CH_2 rocking absorption at 13.8 μ is not seen (it presumably

FIGURE 4

Infrared spectra of DPL and DPL (D) , KBr pellets.

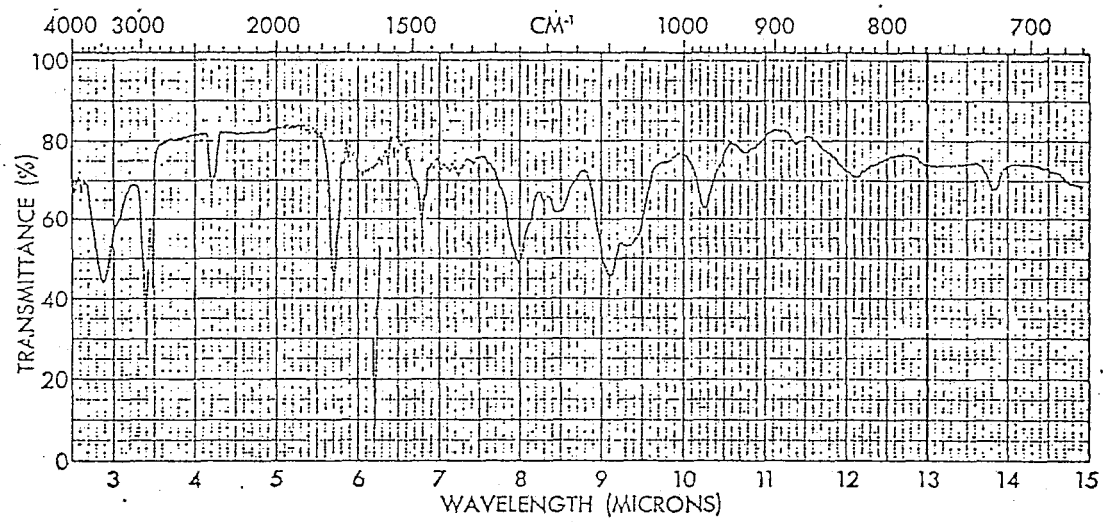
4000 3000 2000 1500 CM-1 1000 900 800 700
100
80
60
40
20
0
TRANSMITTANCE (%)
3 4 5 6 7 8 9 10 11 12 13 14 15
WAVELENGTH (MICRONS)

a. DPL

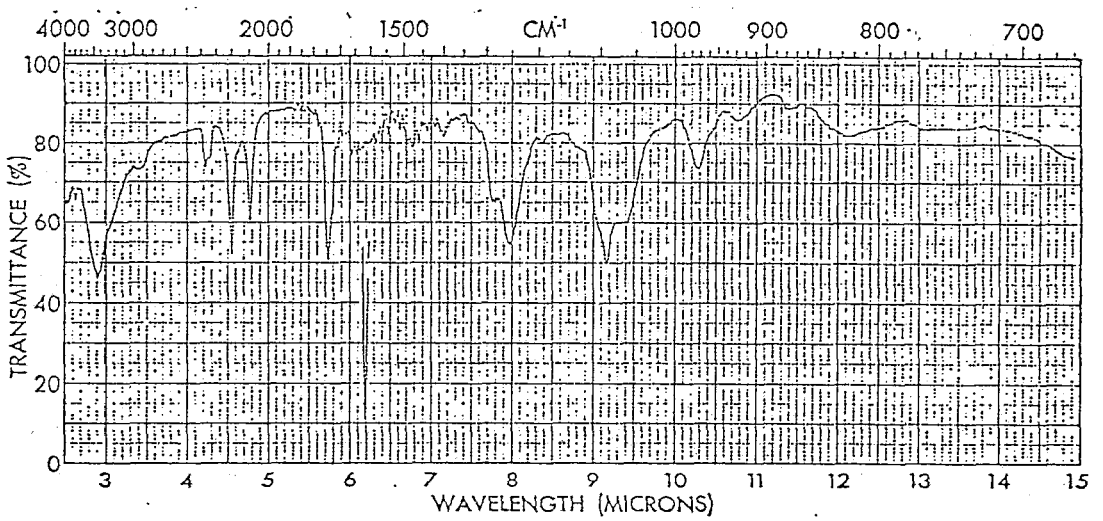
4000 3000 2000 1500 CM-1 1000 900 800 700
100
80
60
40
20
0
TRANSMITTANCE (%)
3 4 5 6 7 8 9 10 11 12 13 14 15
WAVELENGTH (MICRONS)

b. DPL (D)

occurs at $\lambda > 15\ \mu$).

(b) NMR. Spectra of DPL and DPL(D) are shown in Fig. 5. The most prominent features are the small fatty acid methyl and methylene resonances. A comparison of the choline methyl and the fatty acid methylene and methyl resonances shows that except for the α methylene the deuterium content is 98.8%. The deuterium content of the α methylenes is only 91.5%. Since the α methylenes are rather labile some H-D exchange may have occurred during the acylation.

9. ACYLATION OF LYSOLECITHIN

1-palmitoyl lysolecithin (0.1 mmole) dissolved in methanol was transferred to a 10 ml pear-shaped flask. The methanol was removed under vacuum. Following the addition of palmitic anhydride (0.4 mmole) the flask was heated at 80°C to melt the anhydride which was distributed evenly over the lysolecithin. Finely powdered sodium oxide (0.05 mmole) was quickly introduced into the flask, which was then closed under vacuum and rotated in a glycerol bath at 80° for 48 hours. The purification procedure was similar to that for 1, 2-dipalmitoyl (d_{62}) lecithin. The final product was chromatographically pure but was slightly yellow in appearance.

Characterization

(a) IR. The IR spectrum of 1-palmitoyl-2-palmitoyl (d_{31})-phosphatidylcholine (DPL(H, D)) is shown in Fig. 6. It is a composite of the DPL and DPL(D) spectra (see Fig.4) in that it exhibits C-H

FIGURE 5

Fourier Transform NMR spectra at 220 MHz of DPL (top) and DPL (D) (bottom) in $CDCl_3$. Temperature at 20°C.

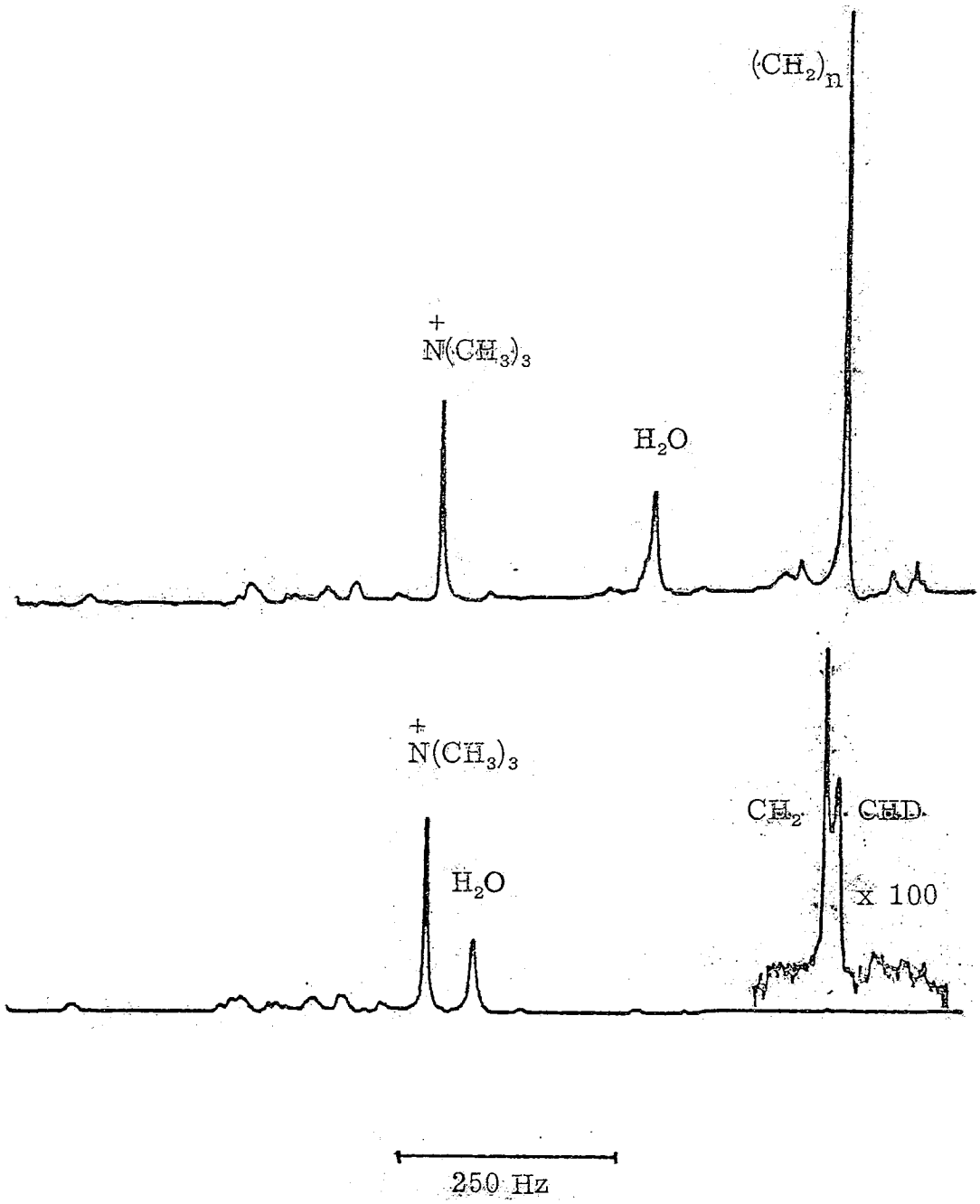
$(CH_2)_n$
$\overset{+}{N}(CH_3)_3$
H_2O
$\overset{+}{N}(CH_3)_3$
CH_2
CHD
x 100
H_2O
250 Hz

FIGURE 6

Infrared spectrum of DPL (H, D), KBr pellet.

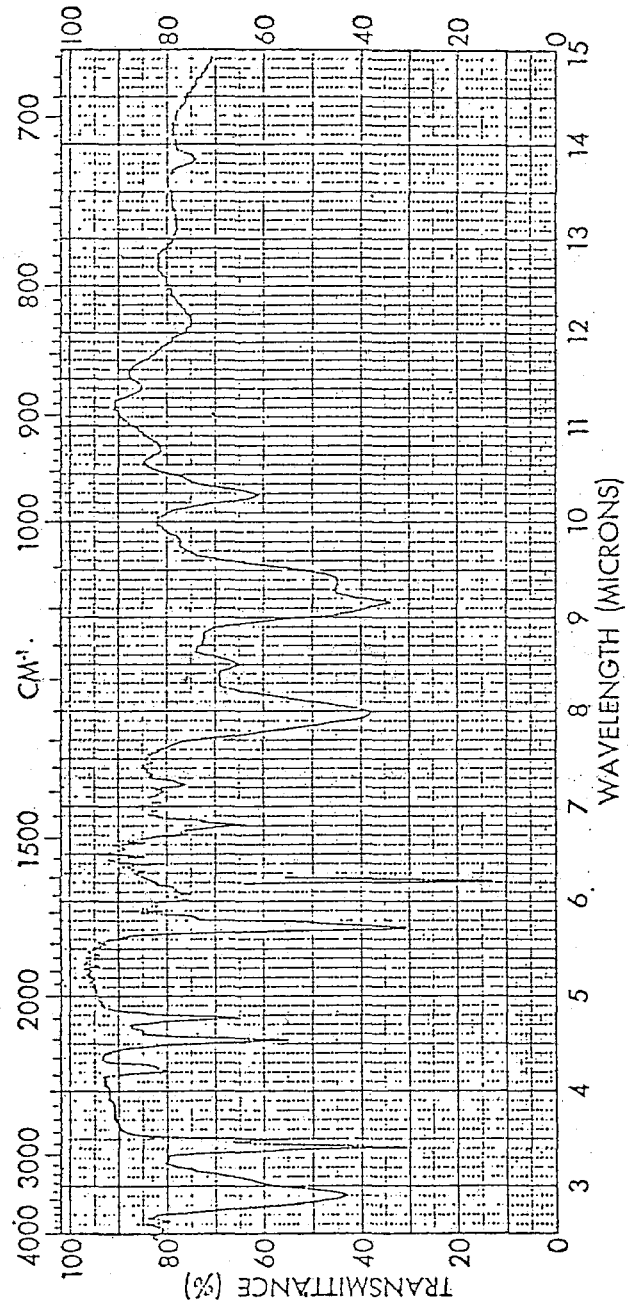
4000 3000 2000 1500 CM-1. 1000 900 800 700
100 80 60 40 20 0
TRANSMITTANCE (%)
3 4 5 6 7 8 9 10 11 12 13 14 15
WAVELENGTH (MICRONS)

DPL (H, D)

absorptions at 3.4-3.5 and 6.79 μ, C-D absorptions at 4.53 and 4.78 μ as well as the P=O, P-O-C and P-OH absorptions characteristic of phospholipids.

(b) NMR. The nmr spectrum of DPL(H, D) is similar to that of DPL with the exception that the DPL(H, D) methylene intensity is half of the DPL methylene intensity.

References

1. L. L. M. van Deenen and G. D. de Haas, in: Advances in Lipid Research, Vol. 2, ed. by R. Paoletti and D. Kritchevsky, Academic Press, New York, p. 164 (1964).
2. R. G. Jensen and D. T. Gordon, Lipids, 7, 611 (1972).
3. A. J. Slotboom, H. M. Verheij and G. H. de Haas, Chem. Phys. Lipids, 11, 295 (1973).
4. E. Baer and D. Buchnea, Can. J. Bioch. Physiol., 37, 953 (1959).
5. E. Cubero Robles and D. van den Berg, Biochim. Biophys. Acta, 187, 520 (1969).
6. Merck, Sharp and Dohme of Canada Ltd., catalogue issued September 1966.
7. Ng. Dinh-Nguyen, A. Raal and E. Stenhagen, Chem. Scripta, 2, 171 (1972).
8. G. D. Parkes, Mellor's Modern Inorganic Chemistry, John Wiley and Sons Inc., New York (1963).
9. F. L. LaQue and H. R. Copsen, ACS Monograph No. 158.
10. J. R. Dyer, Applications of Absorption Spectroscopy of Organic Compounds, Prentice Hall, New Jersey (1965).
11. Z. Selinger and Y. Lapidot, J. Lipid Res., 7, 174 (1966).
12. D. N. Rhodes and C. H. Lea, Biochemistry J, 65, 526 (1975).
13. H. Brockerhoff and M. Yurkowski, Can. J. Bioch., 43, 1777 (1965).

14. G. H. De Haas and L. L. M. van Deenen, Rec. Trav. Chim., 80, 951 (1961).

PART II

THE EFFECT OF CHAIN LENGTH ON THE SECONDARY STRUCTURE OF OLIGOADENYLATES

PART II

THE EFFECT OF CHAIN LENGTH ON THE SECONDARY STRUCTURE OF OLIGOADENYLATES

Abstract

The oligoadenylates $(Ap)_{2-4}A$ have been studied by proton magnetic resonance (pmr) spectroscopy. All the exterior base protons and a number of the interior base proton resonances have been assigned. The results of this work showed that the adenine bases in these oligoadenylates are intramolecularly stacked at 20 °C with their bases oriented preferentially in the anti conformation about their respective glycosidic bonds. The oligomers were found to associate extensively even at concentrations of 0.02 M, primarily via "end to end" stacking. With increasing temperature the oligomer bases destack, but it is argued that this unfolding process cannot be described in terms of a two-state stacked vs. unstacked model. Instead, the temperature dependences of the base proton chemical shifts support a base-oscillation model. The relationship between this model and the "two-state" model is discussed. Finally, on the basis of the chain-length dependence of the proton chemical shifts of the various adenine bases, it was concluded that subtle variations in the secondary structure of these oligomers exist with increasing chain length. Evidence is presented to show that the effects of distant base shielding are considerably smaller than what was previously estimated. The

observed departures from the "extended dimer" model are attributed to differences in the relative orientations of the bases with respect to their neighbors in the oligomer.

INTRODUCTION

A natural extension of the proton magnetic resonance studies of the conformational properties of dinucleoside monophosphates in aqueous solution is the study of similar conformational properties of oligonucleotides. Although the dinucleotides provide a convenient model for the conformation of the exterior bases along a polynucleotide chain, it is conceivable that the conformation of the interior bases of a polynucleotide is somewhat different from the conformation of the dinucleotide bases. The base stacking interactions in the oligonucleotides should be more representative of these interactions. The oligonucleotides therefore serve as useful models for both the exterior and interior bases of a polynucleotide. Accordingly our proton magnetic resonance studies of the dinucleoside monophosphates[1-3] have been extended to the study of base stacking and conformation of several oligonucleotides in aqueous solution.

We have chosen the adenine (3′→5′) oligoribonucleotides as the initial system for our nmr studies of the oligomers because the pmr spectral properties of adenylyl (3′→5′) adenosine (ApA) have been studied under a wide range of different experimental conditions,[2, 4-6] and sufficient data are available to make meaningful comparisons between the results of the experiments involving this

dinucleotide and the adenine oligonucleotides. In addition, the results of various optical studies of oligoadenylic acids of varying chain length are available for comparison.[7-9] These studies have demonstrated that the oligoadenylate molecules possess a considerable degree of ordered structure in a neutral aqueous solution at room temperature; this secondary structure is generally attributed to the formation of intramolecular adenine-adenine base stacks. The ordered structure of the adenine oligonucleotides is consistent with the strong intramolecular base stacking interaction observed for ApA. The optical studies of the oligomers, however, provide very little information about the specific conformations of these molecules in solution. In view of the successful application of pmr spectroscopy towards the investigations of the conformational properties of the dinucleoside monophosphates,[1-6] the pmr experiments would be expected to yield more detailed information concerning the conformation of the respective oligonucleotides than the optical experiments.

EXPERIMENTAL

The adenylate oligomers ApA, $(Ap)_2A$, $(Ap)_3A$, and $(Ap)_4A$ (lithium salts), were obtained from Miles Laboratories, Inc., Elkhart, Indiana, and were used without further purification. Solutions of each of the adenylates (0.05 M in base) were made up in a pD 7.6 sodium phosphate buffer (I = 0.1), containing 10^{-4} EDTA. More dilute samples were made up by successive dilution of these solutions with D_2O. The use of Fourier Transform techniques made

it possible for nmr measurements to be extended to concentrations as low as 5×10^{-4} M. The more concentrated samples were prepared by lyophilizing the dilute samples and dissolving the solid in D_2O. Purine, supplied by Calbiochem, San Diego, California, was recrystallized from toluene before use. Deuterium oxide (99.7%) was obtained from Columbia Organic Chemicals, Columbia, South Carolina.

Oligomer concentrations were determined by measuring the absorption of suitably diluted samples at 260 mμ using a Beckman DU spectrophotometer. The extinction coefficients reported by Brahms et al.[8] were used, after allowing for the number of adenine bases per oligomer.

The proton magnetic resonance spectra were recorded on a Varian HR-220 spectrometer modified for Fourier Transform operation. This system is interfaced with a 16 K 620/i computer. 5 mm nmr tubes were used, except for the more concentrated samples. For these, 2 mm O.D. capillaries were used. The capillaries were fitted into 5 mm nmr tubes using teflon spacers. Chemical shifts were measured from internal tetramethyl ammonium chloride ($(CH_3)_4NCl$). The $(CH_3)_4NCl$ resonance falls 3.20 ppm downfield from TSP. The probe temperature was regulated (± 1°C) by a Varian 4540 variable temperature unit, and was monitored by measuring the ethylene glycol splitting. Unless specified otherwise, measurements were made at 20°C.

RING CURRENT CALCULATIONS

Isoshielding curves were calculated using the general approach of Johnson and Bovey[10] extended for polycyclic systems by Giessner-Prettre and Pullman.[11] In this treatment, the electrons of each ring are assumed to circulate in two loops, one at a distance p above, and the other at a distance p below the plane of the molecule. The effect of a purine base on the chemical shift of a proton, located at the cylindrical coordinates z, ρ_{hex}, and ρ_{pent} (all expressed in ring radius units) with respect to the hexagonal and pentagonal purine rings, can then be expressed by:

$$\Delta\delta = \frac{e^2}{2\pi mc^2} \sum_R \frac{I_R}{a_R} \left[\frac{1}{[(1+\rho_R)^2 + z_-^2]^{\frac{1}{2}}} \left(K + \frac{1 - \rho_R^2 - z_-^2}{(1-\rho_R)^2 + z_-^2} E \right) + \right.$$

$$\left. \frac{1}{[(1+\rho_R)^2 + z_+^2]^{\frac{1}{2}}} \left(K + \frac{1 - \rho_R^2 - z_+^2}{(1-\rho_R)^2 + z_+^2} E \right) \right]$$

where the summation over R is to include contributions from both the hexagonal and pentagonal rings of the adenine base, $z_\pm = z \pm p$, and a_R denotes the radius of the appropriate ring. K and E are complete elliptic integrals of the first and second kind having as modulus $k = \left(\frac{4p}{(1+p)^2 + z_\pm^2}\right)^{\frac{1}{2}}$. Ring current intensities I_R are expressed as a fraction of the benzene ring current. These have been calculated by Giessner-Prettre and Pullman.[12]

We have followed the approach of Johnson and Bovey[10] by

using p as an adjustable parameter to obtain the 1.5 ppm shielding difference between benzene and cyclohexadiene. This differs from the calculations of Giessner-Prettre and Pullman[11] wherein they located the two loops at the theoretical average distance for $2p_z$ Slater orbitals, and then scaled the result calculated above to obtain 1.5 ppm for benzene.

Isoshielding curves for adenine, calculated in the above manner, are illustrated in Fig. 1 for distances (z) 3.4 and 6.8 Å from the molecular plane.

NOMENCLATURE

We shall refer to specific oligonucleotide bases and ribose moieties by the letters α, β, γ, etc. The terminal ribose with a free 5′ hydroxyl group will be referred to as the α ribose, and the terminal ribose with a free 3′ hydroxyl group will be referred to as the ω ribose. The corresponding bases will be referred to as the α and ω bases. The remaining ribose moieties and bases along the chain will be designated by β, γ, δ, ... in order, beginning with the ribose neighboring the α ribose. Thus the tetramer (ApApApA) ribose moieties (and bases) will be referred to (in order) as ribose (or base) α, β, γ, and ω. Base protons will be designated by $H_2(x)$ and $H_8(x)$, where x denotes the base to which the proton belongs.

FIGURE 1

Calculated isoshielding curves for adenine in planes (a) 3.4 Å and (b) 6.8 Å away from the molecular surface (in ppm).

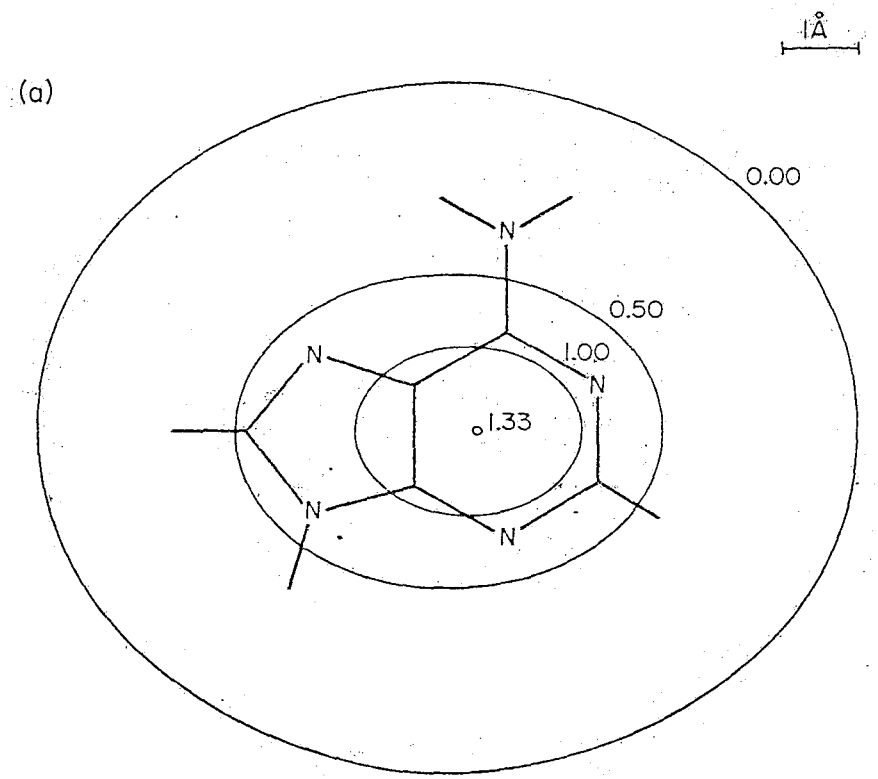
1Å
(a)
0.00
0.50
1.00
1.33
N
N
N
N
N

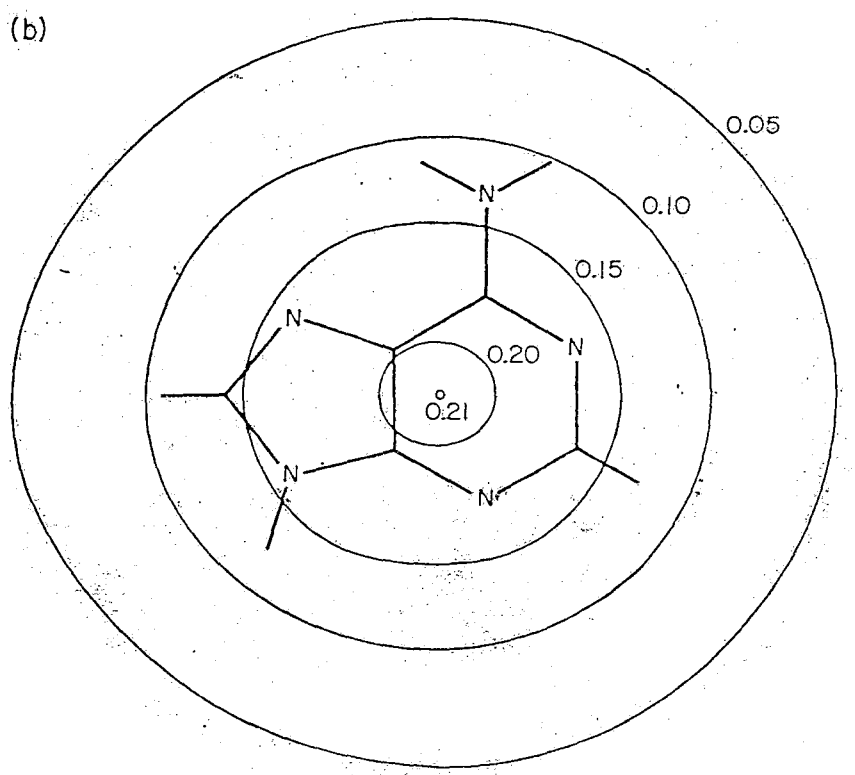
(b)
0.05
0.10
0.15
0.20
0.21
N
N
N
N
N

RESULTS AND DISCUSSION

Assignment of Adenine Base Conformation

The base proton resonances of the oligonucleotides studied occur in the region 4-5 ppm downfield from $(CH_3)_4NCl$. These resonances are generally well resolved, although some overlapping is observed at several temperatures and concentrations. Spectra of the tetramer and pentamer, in the region of the base protons, are illustrated in Figs. 2 and 3, respectively. The pentamer spectrum is given at two different oligomer concentrations in order to illustrate the effects of intermolecular association.

Table I lists a summary of the chemical shifts for the various oligomers. In order to avoid complications from intermolecular association, these results are reported at infinite dilution. Unless specified otherwise, any reference to chemical shifts will involve the infinite dilution values.

In an effort to assign the resonances and to determine details about intramolecular base stacking, we have investigated the effect of temperature, concentration, and purine binding on the oligoadenylates.

The H_8 resonances are readily distinguished from the H_2 resonances by deuterium exchange of the H_8 protons in D_2O at elevated temperatures.[13] In this manner it was found that for each of the oligomers, all but one of the H_2 resonances appear upfield from the H_8 resonances. All of these resonances are shifted from their spectral position in the component adenosine nucleoside. This is due in

FIGURE 2

220 MHz pmr spectrum of $(Ap)_3A$ in the region of the base protons at an oligomer concentration of $\sim 10^{-3}$ M. The chemical shift marker is 5.00 ppm downfield from TMACl. Temperature ~20° C. See text for discussion of assignments.

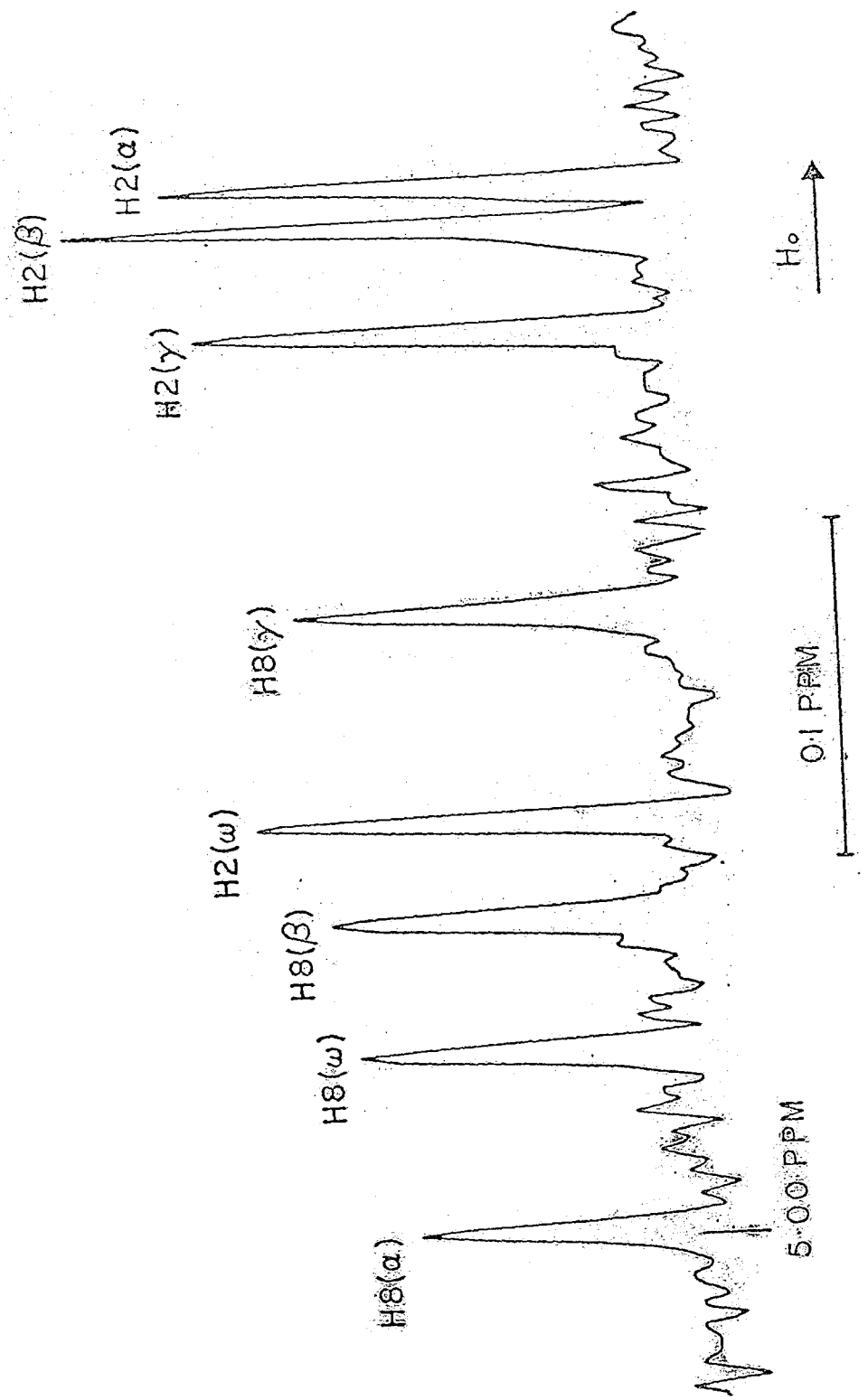
H2(β)
H2(α)
H2(γ)
H8(γ)
H2(ω)
H8(β)
H8(ω)
H8(α)
H₀
0·1 PPM
5·00 PPM

FIGURE 3

220 MHz spectra of $(Ap)_4A$ in the region of the base protons at two concentrations. (a) 6.4 mM; (b) 17.3 mM. Temperature: 20 °C. See text for discussion of assignments.

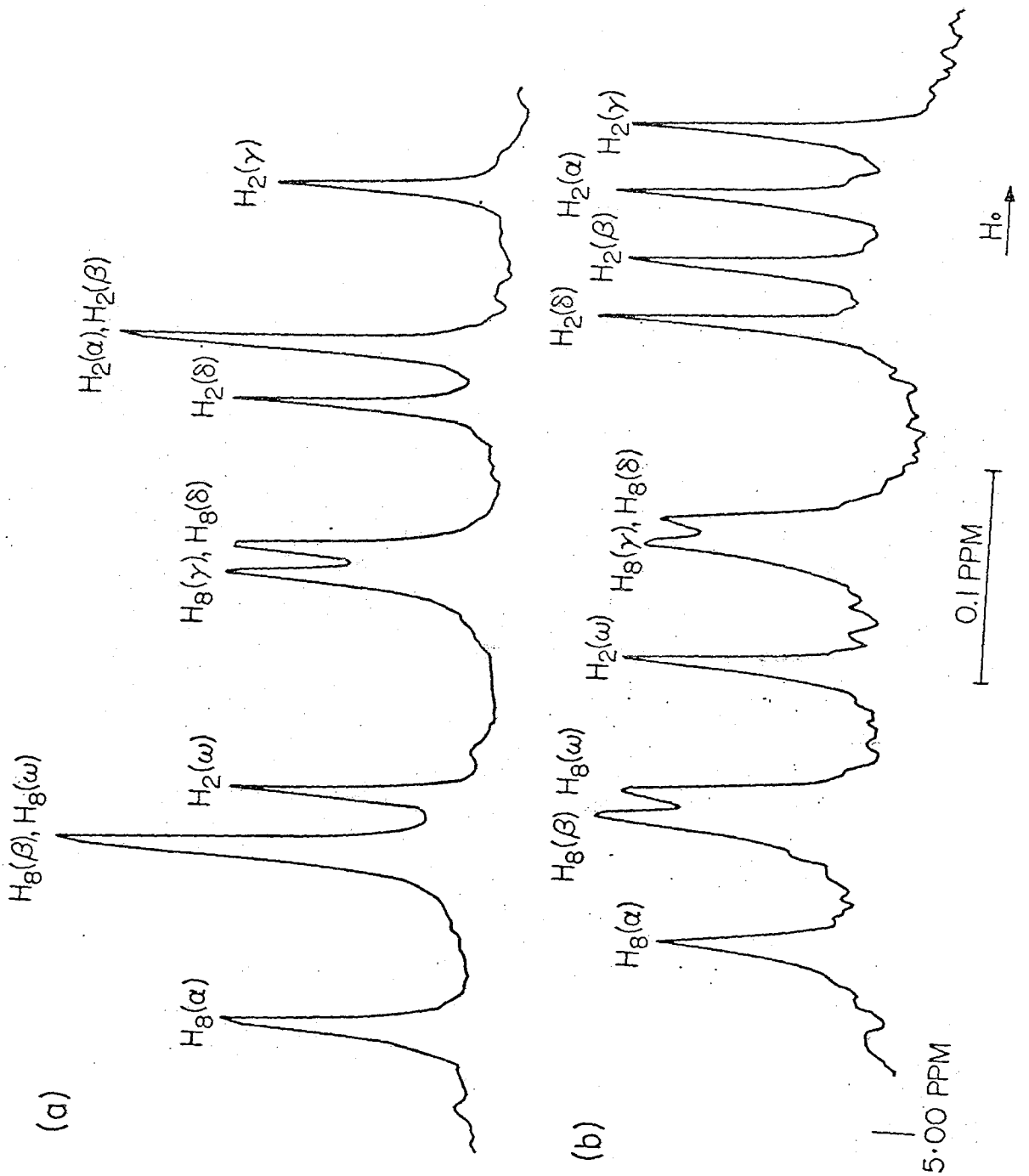
(a)
$H_8(\beta), H_8(\omega)$
$H_8(\alpha)$
$H_2(\omega)$
$H_8(\gamma), H_8(\delta)$
$H_2(\alpha), H_2(\beta)$
$H_2(\delta)$
$H_2(\gamma)$
(b)
$H_8(\alpha)$
$H_8(\beta)$ $H_8(\omega)$
$H_2(\omega)$
$H_8(\gamma), H_8(\delta)$
$H_2(\delta)$
$H_2(\beta)$
$H_2(\alpha)$
$H_2(\gamma)$
5·00 PPM
0.1 PPM
H_0

TABLE I

Infinite Dilution Chemical Shifts of the
Oligo A Base Protons at 20°C
(ppm downfield from internal TMACl)

	$(Ap)_2A$		$(Ap)_3A$		$(Ap)_4A$	
Base	H_8	H_2	H_8	H_2	H_8	H_2
α	5.05	4.72	5.03	4.71	4.99	4.69
β	4.93	4.80	4.92[a]	4.71[a]	4.91[a]	4.68[b]
γ			4.82[a]	4.75[a]	4.78[b]	4.60[b]
δ					4.79[b]	4.70[a]
ω	4.97	4.92	4.96	4.91	4.91	4.89

[a] Tentative assignment.

[b] No specific assignment.

part to the large ring current magnetic anisotropy of the adenine bases, which effectively shields protons close above or below the adenine bases. The singly charged phosphate groups also have an effect. Their influence is primarily a consequence of the negative charge and of the resulting electric field. Protons close to the phosphate group are deshielded. The magnetic nonequivalence of the H_8 protons and H_2 protons attached to different bases can thus be attributed primarily to the position of these protons relative to the neighboring base(s) and phosphate groups.

Mn^{+2} binding studies were used to determine the predominant conformation of the base about the glycosidic bond. At low concentrations ($[Mn^{+2}]/[\text{oligomer}] \sim 10^{-3}$-$10^{-2}$), Mn^{+2} ions have been shown to bind primarily to the phosphate group and thus broaden the resonances of nearby protons by electron spin-nuclear spin dipole-dipole interactions.[2] This effect is extremely distant dependent (proportional to r^{-6}), consequently only those protons close to the phosphate groups are affected.

Two of the three trimer H_8 resonances were broadened in the presence of Mn^{+2}, while none of the H_2 resonances were broadened. We may draw two conclusions from this observation. First, the H_8 resonance which was not broadened (at 5.05 ppm) may be assigned to $H_8(\alpha)$ since the α ribose is the one without an esterified phosphate group at the 5′ position. Secondly, since the β and ω H_8 resonances were broadened and there was no evidence for broadening of the H_2 resonances, the β and ω bases must exist predominantly in the anti

conformation (about the glycosidic bond). In this conformation only the H_8 protons are close to the phosphate groups. Of the four tetramer H_8 resonances three were broadened. Using the same arguments as those used for the trimer, we assign the resonance which was not broadened (at 5.03 ppm) to $H_8(\alpha)$. The broadening of the β, γ, and ω H_8 resonances indicates that the β, γ, and ω bases exist predominantly in the anti conformation.

There is no a priori reason not to expect a similar preferential anti conformation for the α base, since all indications are that the conformation of a base is primarily dependent upon the rotational barriers about the glycosidic bond. This question can be further resolved by a consideration of the magnitude of the temperature dependence of the $H_8(\alpha)$ chemical shift. An examination of a CPK molecular model (with the bases overlapping) indicates that if the α base is in a syn conformation (with the β and ω bases anti), $H_8(\alpha)$ will be shielded strongly by its neighboring base, whereas if the α base is in the anti conformation the shielding of $H_8(\alpha)$ will be significantly less. The same conclusion is reached whether the oligomer helix axis is right- or left-handed. As the intramolecular base stacking is disrupted at high temperatures, we expect this ring current shielding to become less important. Thus, if the α base is in the syn conformation we should observe a large downfield shift with increasing temperature. On the other hand, with the α base in the anti conformation, only a small shift would be observed. Experimentally, the trimer $H_8(\alpha)$ resonance was found to exhibit a small (0.02 ppm) upfield shift (see

Fig. 4) when the temperature was increased from 20° to 60°C! The trimer α base thus must also exist preferentially in the anti conformation. The small shift of the tetramer $H_8(\alpha)$ resonance between 20° and 89°C (see Fig. 5) also clearly indicates the preferential anti conformation for this base.

The above considerations strongly suggest that both the trimer and tetramer exist preferentially in the all-anti conformation. Similar conclusions have been drawn for the dimer and polymer.[2, 4, 14] Although no Mn^{+2} binding studies were performed for the pentamer, the above observations, in conjunction with the overall similarity of the pentamer base proton chemical shifts and their temperature dependence when compared with those of the trimer and tetramer, strongly indicate that the pentamer also exists preferentially in the all-anti conformation. Here again, the most downfield pentamer H_8 resonance was found to exhibit a very small temperature dependence. On the basis of an all-anti conformation we assign this resonance to $H_8(\alpha)$.

Concentration Dependence

The concentration dependence of the oligo A base proton chemical shifts at 20°C is summarized in Table II. All resonances are shifted to higher fields with increasing oligonucleotide concentration. It is interesting to note the differences between the concentration shifts observed for different protons. For example, over the concentration range of 0.02 M to infinite dilution, one of the trimer

TABLE II

Concentration Induced Shifts of Oligo A Base Protons at 0.02 M and 20°C (ppm)

	$(Ap)_2A$		$(Ap)_3A$		$(Ap)_4A$	
Base	H_8	H_2	H_8	H_2	H_8	H_2
α	0.10	0.12	0.09	0.13	0.09	0.13
β	0.04	0.08	0.07	0.09	0.06	0.09[a]
γ			0.04	0.09	0.06[a]	0.06[a]
δ					0.06[a]	0.08
ω	0.03	0.12	0.05	0.12	0.06	0.12

[a] No specific assignment.

H_8 resonance shifts by 0.1 ppm whereas the other two shift a mere 0.03-0.04 ppm. Differences between the H_2 shifts are also appreciable. In the pentamer, for example, these concentration shifts range from 0.06 to 0.13 ppm.

These shifts cannot be attributed to the (linear) increase in ionic strength with increasing oligomer concentration since the ionic strengths used were low to begin with (a maximum of 0.2 for a 0.02 M pentamer solution), and besides the effect of ionic strength is expected to be small.[15] We attribute the upfield shifts observed to intermolecular association of the oligomers. A number of modes of intermolecular interaction are possible: (a) self-intercalation of the oligomers -- in this mode the bases of one oligomer are inserted between the bases of another; (b) "end to end" stacking of intramolecularly stacked molecules; and (c) interactions between two partially (or possibly completely) stacked oligomers in some fashion other than the "end to end" mode.

If the intramolecular stacking of the adenine bases is weak, the formation of self-intercalated complexes is possible. However, if the intramolecular stacking of the adenine bases is strong, self-intercalation becomes unimportant.[2,3] This is the case for the dimer ApA, where self-intercalation has been ruled out as a major mode of intermolecular association.[2] On the basis of the chain length dependence of stacked chain to random coil transition temperatures, it is apparent that the extent of intramolecular base stacking increases somewhat with increasing chain length.[8] Thus it appears that the

extent of intramolecular base stacking for the longer chain oligomers is at least as strong as that for ApA, and hence we surmise that self-intercalation is unlikely to be important for any of the oligomers. Previous studies on ApA have shown that this dinucleotide self-associates principally by intermolecular stacking of the intramolecularly stacked molecules.[2, 4] We believe "end to end" stacking to be the primary mode of association for the longer chain length oligomers.

Because the H_2 protons are relatively far removed from the ribose phosphate backbone, H_2 protons of the exterior adenine bases (α and ω) should be affected to a similar extent by "end to end" stacking. The H_2 resonances from the interior bases, however, should be affected to a smaller extent by "end to end" stacking. An examination of the results (Table II) reveals that for each of the oligomers, two of the H_2 concentration induced shifts are indeed larger than the remaining ones. Furthermore they are equal within experimental error ($\pm$ 0.01 ppm). We assign these resonances to the α and ω base H_2 protons. A comparison of these concentration shifts with those for the dimer indicates that the concentration shifts do not differ much from oligomer to oligomer over the same concentration range.[2, 4] This indicates that the self-association tendency as well as the nature and degree of external stacking is very similar among the various adenylates. These results are in contrast to those of Jaskunas et al.[16] who reported no self-association of the tetramer, on the basis of optical rotatory dispersion measurements. The concentration range employed in these latter studies, however, was an order of

magnitude smaller than that used in the present work.

A specific assignment of the external H_2 protons can now be made in light of the above considerations. In the stacked all-anti conformation, the H_2 protons are strongly shielded by their leading adenine bases (progressing from the α to the ω end), whereas shielding by their lagging adenine bases is small. For example, in the trimer, $H_2(\alpha)$ is shielded strongly by the leading β base, and $H_2(\beta)$ by the leading ω base. However the shielding contribution of $H_2(\beta)$ by the lagging α base and of $H_2(\omega)$ by the lagging β base is small. Of the three trimer H_2 protons, $H_2(\alpha)$ and $H_2(\beta)$ are therefore shielded strongly by a neighboring base, whereas $H_2(\omega)$ is only shielded to a small extent by its neighboring base. The $H_2(\omega)$ resonance should therefore appear downfield from the other H_2 resonances. An examination of the infinite dilution chemical shifts in Table I reveals that one of the trimer H_2 resonances does in fact appear far downfield from the others. The same is true for the tetramer and pentamer. On the basis of these considerations, we assign these downfield H_2 resonances to the $H_2(\omega)$ protons. For each oligomer this H_2 resonance is one of the two assigned to the exterior base H_2 protons on the basis of the concentration induced shifts. The remaining exterior H_2 resonance for each of the oligomers can then be assigned to $H_2(\alpha)$ by elimination.

Althpugh the interior H_2 shifts are smaller (46-75%) than the exterior H_2 shifts, they are still appreciable, and indicate that "end to end" stacking is not the only form of association. Since an

appreciable fraction of each oligomer exists in the "destacked" form even at 20°C, [8] interactions are possible between partially stacked and fully stacked oligomers. Another example of such interactions is the stacking of the exposed or partially exposed bases of two incompletely stacked oligomers. There is also the possibility that intermolecular "end to end" association could enhance intramolecular base stacking, and give rise to upfield shifts for the H_2(interior) resonances. Such an effect should affect $H_2(\alpha)$ more than $H_2(\omega)$, since $H_2(\alpha)$ is closer to the strongly shielding region of its neighboring base than $H_2(\omega)$ is. In light of the fact that the $H_2(\alpha)$ and $H_2(\omega)$ resonances undergo approximately equal shifts with increasing concentration, this effect appears to be unimportant. Finally, there is the possibility that "end to end" association of the oligomers results in long range intermolecular shielding. If this contribution is important, it should manifest itself in the dimer concentration induced shifts. If, for example, two dimers associate in an "α-end to α-end" manner, the ω base protons should be shielded by intermolecular long range shielding. For longer chain oligomers this effect should be of decreasing importance because of the inverse cube distance dependence of ring current shielding. In the case of two "α-end to α-end" associated pentamers there can thus be no long range intermolecular shielding contribution for the ω base protons. Since we noted previously that the concentration induced shifts of the α and ω base protons are almost independent of chain length (at least up to the pentamer), this long range intermolecular shielding is clearly unimportant.

We now turn to the concentration dependence of the H_8 (α and ω) resonances. The situation here is not quite as simple as that for the H_2 protons because of the proximity of the $H_8(\alpha)$ and $H_8(\omega)$ protons to the ribose phosphate backbone, which (because of steric factors) reduces the accessibility of these protons to the strongly shielding region of the "end to end" stacked oligomers. An examination of molecular models shows that the $H_8(\omega)$ accessibility is affected more than the $H_8(\alpha)$ accessibility. The difference between the dimer $H_8(\omega)$ and $H_8(\alpha)$ concentration shifts has been attributed to this effect.[2, 4] Our results show a similar differentiation.

The difference between the H_8(interior) and $H_8(\omega)$ concentration shifts is so small that a definite assignment for $H_8(\omega)$ cannot be made on the basis of the concentration shifts. The H_8(interior) shifts are presumably caused by the same mode of interaction that gives rise to the H_2(interior) shifts. That they are smaller is probably also a result of steric interactions caused by the ribose phosphate backbone.

Purine Interactions

Purine has been used very successfully as an nmr probe to study the nature of base stacking interactions in oligonucleotides.[1, 2, 14, 17] In particular its interaction with dinucleotides has been studied in great detail. Two modes of interaction were shown to exist: intercalation between the dimer bases, and external stacking on the folded dimer. Similar interactions can take place with

the longer-chain oligomers. The effects of purine on the trimer, tetramer, and pentamer base proton chemical shifts are described here.

Chemical shift changes of the various adenine protons upon the addition of purine are illustrated in Table III. A number of factors contribute to these observed purine induced shifts. First, the α and ω base protons are shielded by externally stacked purine molecules in a manner similar to "end to end" stacking of the adenine oligomers. The observed shifts also arise in part from the disruptive effects of purine when it intercalates between two contiguous adenine bases. Purine intercalation results in an increased separation between neighboring bases and hence leads to a reduction in intramolecular adenine shielding. This effect, however, is replaced by the intermolecular shielding of the inserted purine itself. Thus, the purine induced shifts reflect compensating effects of intermolecular and intramolecular ring current shielding.

A comparison of the purine induced shifts shows that for each oligomer the $H_2(\omega)$ shift is larger than the $H_2(\alpha)$ shift while the induced shifts for both of these exterior protons are larger than those for the interior H_2 protons. This observation is readily understood in terms of the contributions discussed above. Both $H_2(\alpha)$ and $H_2(\omega)$ are shielded to a similar extent by an externally stacked and/or by an intercalated purine molecule. However, moving the bases apart to accommodate an inserted purine molecule affects $H_2(\alpha)$ and $H_2(\omega)$ quite differently. Since $H_2(\alpha)$ experiences a greater intramolecular

TABLE III

Purine Induced Chemical Shifts (ppm)[a]

	$(Ap)_2A$[b] (30°C)		$(Ap)_3A$[c] (20°C)		$(Ap)_4A$[d] (20°C)	
Base	H_8	H_2	H_8	H_2	H_8	H_2
α	0.29	0.40	0.27	0.24	0.21	0.21
β	0.08	0.37	0.03	0.20	0.04	0.17[e]
γ			0.00	0.23	-0.01[e]	0.14[e]
δ					0.01[e]	0.19
ω	0.16	0.48	0.08	0.35	0.07	0.29

[a] Corrected for the effect of purine on the reference standard (TMACl).

[b] $(Ap)_2A$ concentration 7×10^{-3} M, $[\text{Purine}]/[(Ap)_2A] = 114$.

[c] $(Ap)_3A$ concentration 2.5×10^{-3} M, $[\text{Purine}]/[(Ap)_3A] = 97$.

[d] $(Ap)_4A$ concentration 4.1×10^{-3} M, $[\text{Purine}]/[(Ap)_4A] = 48$.

[e] No assignment made.

ring current from its neighboring adenine base than $H_2(\omega)$, the increased adenine-adenine base separation concomitant with the purine intercalation reduces the $H_2(\alpha)$ shielding more than it does the $H_2(\omega)$ shielding. Thus, the purine interactions should result in a larger net upfield shift for $H_2(\omega)$ than for $H_2(\alpha)$. The observed differences in the effects of purine on the interior and exterior H_2 base protons can be attributed to the fact that the interior base protons are only affected by purine intercalation. Thus, although the interior base protons can experience intermolecular ring current shielding from two inserted purine molecules, these purine induced shifts are necessarily smaller as a result of the aforementioned compensating intermolecular and intramolecular ring current effects. Furthermore for a strongly stacked oligomer there are reasons to expect external stacking to be more favorable than purine insertion.

Similar considerations apply to the H_8 protons. Accordingly, the exterior H_8 protons, namely $H_8(\alpha)$ and $H_8(\omega)$, are expected to exhibit greater purine induced shifts than the interior base H_8 protons. Arguments analogous to those presented for the $H_2(\alpha)$ and $H_2(\omega)$ protons also lead to the expectation that $H_8(\alpha)$ exhibits a larger purine induced shift than $H_8(\omega)$. All these expectations are in fact borne out. However it should be noted that the difference between the induced shifts for $H_8(\omega)$ and the interior H_8 protons is rather small. This we feel reflects the limited accessibility of the intercalated purine molecule to the region bearing these protons because of steric interactions with the ribose phosphate backbone. The observation

that the purine induced shifts for the H_8 protons are significantly smaller than the H_2 protons is consistent with this view. Similar differential effects between the H_2 and H_8 protons have been discussed earlier with respect to the intermolecular "end to end" stacking of the oligonucleotides.

Temperature Studies

Several times we have alluded to the destacking of bases with increasing temperature. Some questions regarding the details of the destacking process can be answered from the temperature dependence of the base proton chemical shifts. We have measured this dependence over the temperature range of 20° to 50°C for the trimer and pentamer, and over the range 20° to 90°C for the tetramer. The results are summarized in Figs. 4-6. Low oligomer concentrations ($\sim 10^{-3}$ M) were used to minimize the effects of intermolecular association.

With the exception of the H_8 (α) resonances, all resonances undergo large downfield shifts with increasing temperature. These downfield shifts can be attributed to a decrease in the ring current shielding as the bases destack with increasing temperature. It is interesting to note that at 50°C, for each oligomer, the different H_2 and H_8 protons are still magnetically nonequivalent. Even at 90°C we find that neither the tetramer H_2 protons nor the tetramer H_8 protons are equivalent. Hence even at 90°C the bases are not completely destacked.

FIGURE 4

Temperature dependence of the $(Ap)_2A$ H_8 (o) and H_2 (x) chemical shifts. Chemical shifts are referred downfield from TMACl.

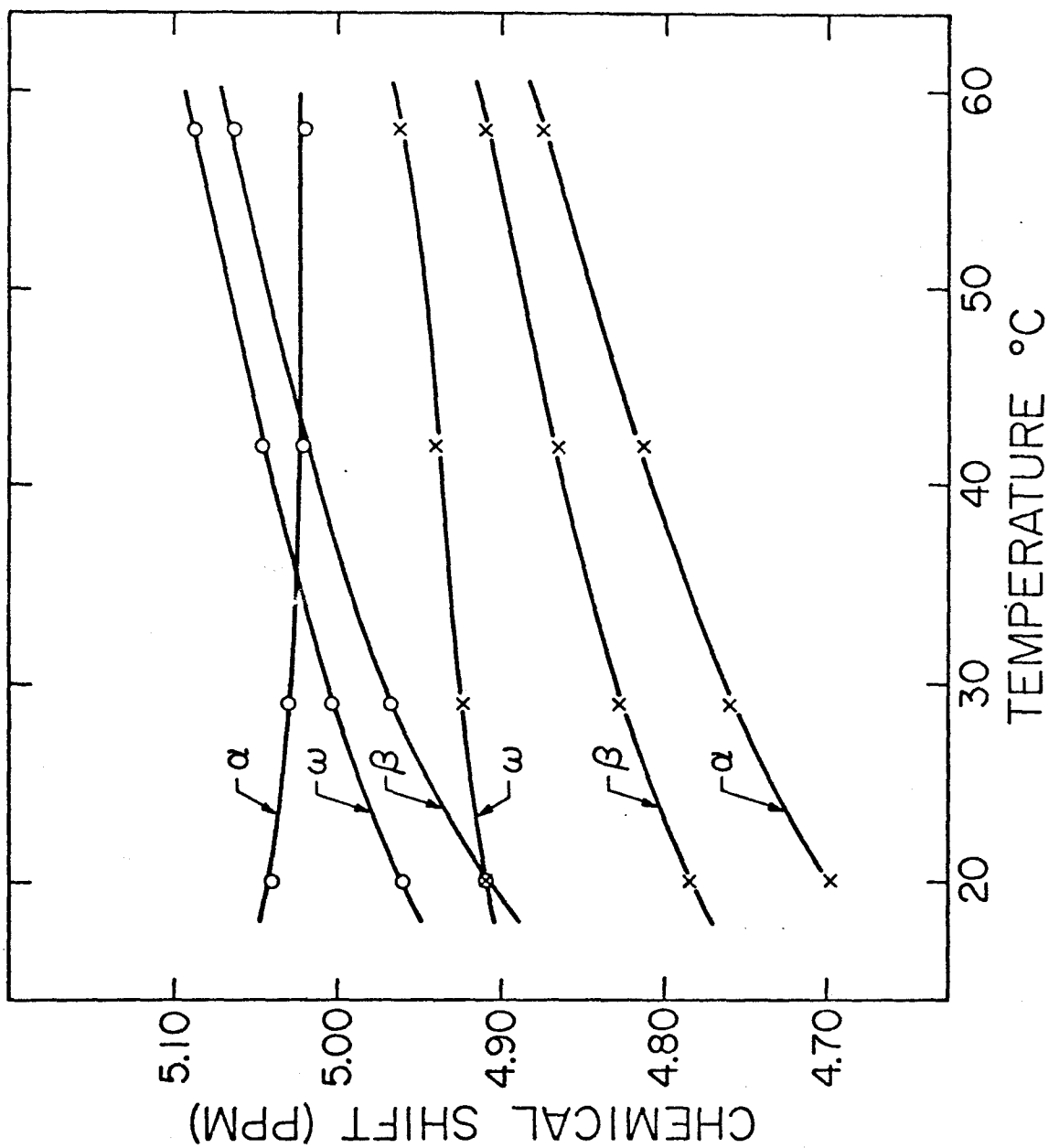
CHEMICAL SHIFT (PPM)
5.10
5.00
4.90
4.80
4.70
TEMPERATURE °C
20
30
40
50
60
α
ω
β
ω
β
α

FIGURE 5

Temperature dependence of the $(Ap)_3A$ H_8 (o) and H_2 (x) chemical shifts. Chemical shifts are referred downfield from TMACl.

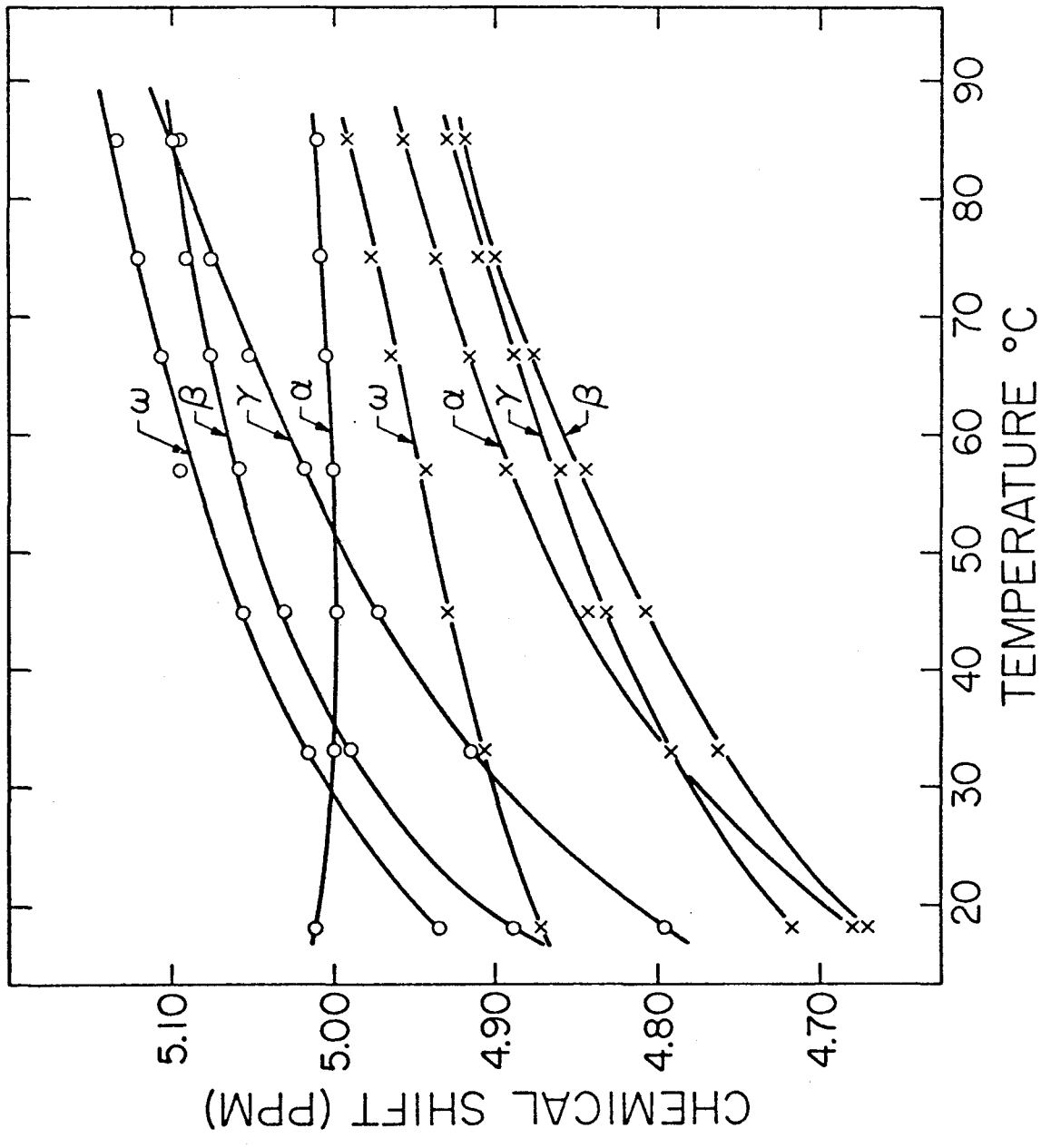
CHEMICAL SHIFT (PPM)
5.10
5.00
4.90
4.80
4.70
TEMPERATURE °C
20
30
40
50
60
70
80
90
ω
β
γ
α
ω
α
γ
β

FIGURE 6

Temperature dependence of the $(Ap)_4A$ H_8 (o) and H_2 (x) chemical shifts. Chemical shifts are referred downfield from TMACl.

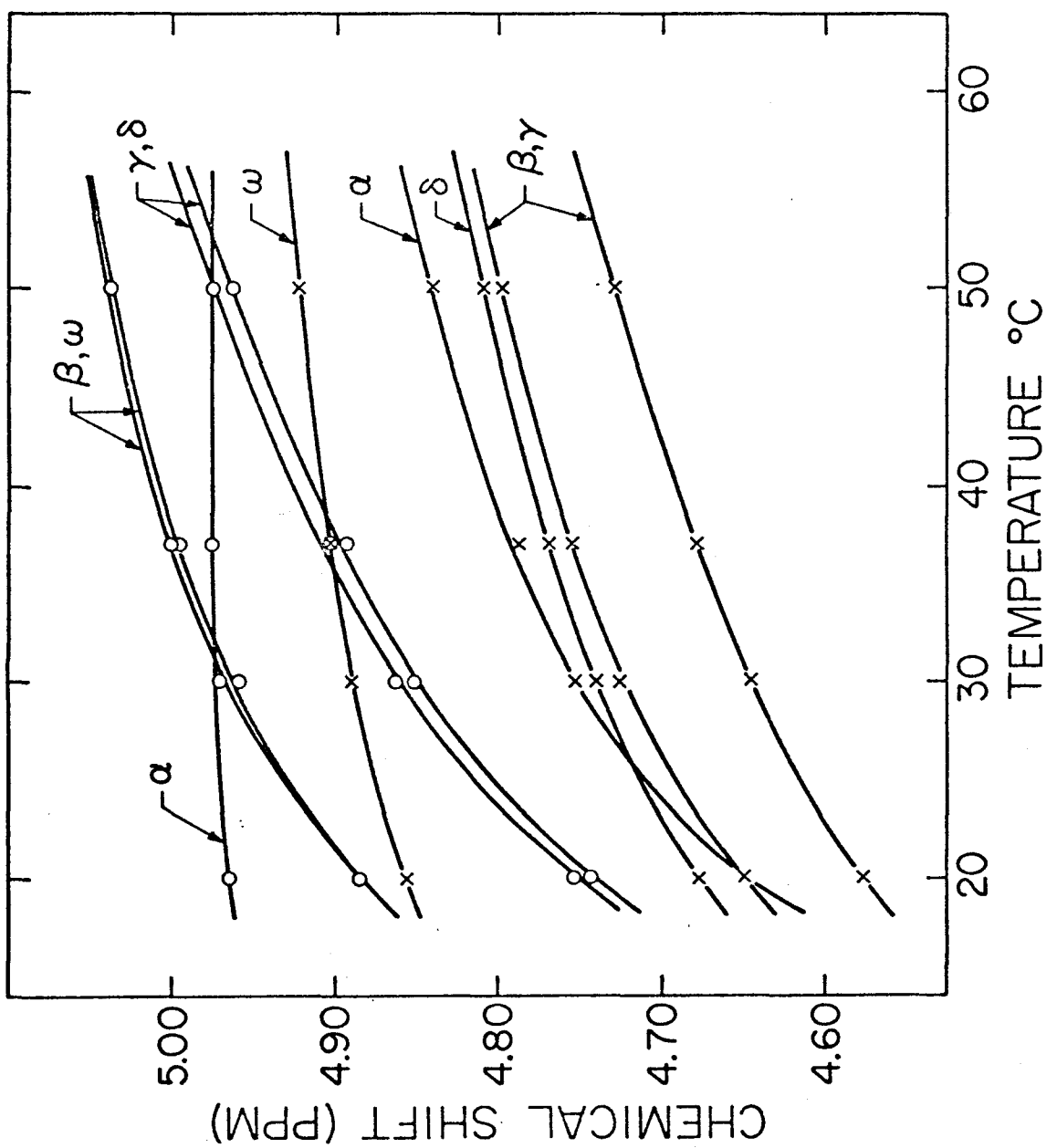
CHEMICAL SHIFT (PPM)
5.00
4.90
4.80
4.70
4.60
TEMPERATURE °C
20
30
40
50
60
β,ω
γ,δ
ω
α
δ
β,γ
α

The temperature behavior of the $H_8(\alpha)$ resonances is different from that of the other resonances. In the first place, their shifts are small. In the second place, between 20° and 50°C the trimer and tetramer $H_8(\alpha)$ resonances shift upfield. On the other hand, the pentamer $H_8(\alpha)$ resonance shifts slightly downfield over this same temperature range. A comparison of these shifts with each other and with the $H_2(\alpha)$ shifts can best be made through a comparison of changes in their polymerization shifts with temperature.

The polymerization shift (δ_p) of a particular base proton is defined as its chemical shift relative to that of adenosine at infinite dilution. It gives a measure of the ring current effect of neighboring bases and of the electric field effect of nearby phosphate groups on the base proton in question. The percent changes in δ_p for the $H_2(\alpha)$ and $H_8(\alpha)$ protons between 20° and 50°C, namely $((\delta_p^{50°} - \delta_p^{20°})/\delta_p^{20°})$, are summarized in Table IV. It is apparent from these data that the temperature behavior of the α base protons cannot be described by a two state model (stacked vs. unstacked), since this model predicts an equal percentage change for both the $H_8(\alpha)$ and $H_2(\alpha)$ protons with temperature. Similar conclusions have previously been drawn for the dimer.[18] The relative temperature dependence of these H_8 and H_2 resonances therefore suggests an alternative model for the destacking process. As an alternative to the two state model, others have proposed models based on the concept of oscillatory motions, wherein the bases slide over each other while remaining parallel.[18-20] At low temperatures the conformation can then be

TABLE IV

Variation[a] in the $H_8(\alpha)$ and $H_2(\alpha)$ Polymerization Shifts Between 20°C and 50°C

	H_8	H_2
$(Ap)_2A$	30 (+)	43 (-)
$(Ap)_3A$	15 (+)	46 (-)
$(Ap)_4A$	4 (-)	47 (-)

[a] Expressed as a percentage change, or $100\% \times (\delta_p^{50°} - \delta_p^{20°})/\delta_p^{20°}$.

characterized by a narrow distribution of the bases relative to each other about some equilibrium position. As the temperature increases the bases begin to oscillate with increasing amplitude.

The temperature behavior of the α base protons can be understood in terms of such a model. An examination of a CPK molecular model shows that as the oscillations become larger $H_8(\alpha)$ spends an increasing amount of time close to the five-membered ring of the β base. In this position $H_8(\alpha)$ is shielded to a greater extent than it is in the low temperature state. During part of the time, however, $H_8(\alpha)$ is further removed from the shielding region of the β base than it is in the low temperature state. The resultant temperature behavior expected on the basis of this model is thus a compromise between these two effects. It will depend on the position of $H_8(\alpha)$ in the low temperature state, and on the relative amount of time spent in the strongly and poorly shielding regions as amplitude of the oscillation increases with increasing temperature. Thus the observation that the trimer and tetramer $H_8(\alpha)$ resonances shift upfield between 20° and 50°C indicates that with increasing temperature the time spent in the strongly shielding region gives a somewhat larger contribution to the net shifts than the time spent in the poorly shielding region. It is interesting to note that between 50° and 90°C the tetramer $H_8(\alpha)$ resonance actually shifts downfield. This is not unexpected in terms of this model, since as the amplitude of the oscillations become larger, there is a point at which $H_8(\alpha)$ passes the region of maximum shielding into a region of decreased shielding. From that point on,

the resonance should shift downfield with increasing temperature.

A comparison of the trimer, tetramer and pentamer $H_8(\alpha)$ resonances shows that there is a small upfield shift for this resonance with increasing chain length (see Fig. 8). We attribute this shift to small changes in conformation (or more accurately, to small changes in the equilibrium conformation about which the bases oscillate). We shall discuss this point in greater detail in the following section of this paper. The conclusion which we shall draw is that the $H_8(\alpha)$ proton (at 20°C) is positioned (on the average) closer to the strongly shielding region of the β base with increasing chain length. The somewhat greater upfield ($\delta_p^{50°} - \delta_p^{20°}$) observed for $H_8(\alpha)$ of the trimer vs. the tetramer is consistent with this picture, as is the observed downfield ($\delta_p^{50°} - \delta_p^{20°}$) observed for $H_8(\alpha)$ in the pentamer. In the latter case, $H_8(\alpha)$ must be at, or must have passed the point of maximum shielding at 20°C.

The situation for the $H_2(\alpha)$ protons is quite different. To begin with, at 20°C these protons oscillate about a position close to the strongly shielding region of the β base. Increasing temperature, and consequently increasing oscillations, thus merely expose these protons to regions of decreased shielding. The same situation is true for $H_8(\alpha)$. On the other hand $H_2(\alpha)$, like $H_8(\alpha)$, is located in the weakly shielding region of its neighboring base (at 20°C). Unlike $H_8(\alpha)$, however, $H_2(\alpha)$ is not exposed to the strongly shielding region of its neighboring base with increasing oscillations. Consequently, the $H_2(\alpha)$ resonance is expected to undergo a considerable downfield

shift with increasing temperature, as observed.

The above model predicts a different behavior for each of the exterior base proton resonances with increasing temperature. This behavior is complex in that the temperature shifts depend on the position of the protons relative to the shielding region of their neighboring base at low temperatures as well as on the details of the oscillatory motions. The temperature behavior of the interior base proton resonances seems even less amenable to unambiguous interpretation since the temperature shifts observed for these protons should depend on the motion of the base protons in question relative to both of their neighboring bases. These considerations would seem to argue against using the temperature behavior of interior base protons to obtain information regarding the nature of the destacking process.

In contrast to nmr data, optical data for the oligoadenylates have been analyzed in terms of a two-state model.[7-9] The nmr and optical results are compatible, however, if the optical "stacked" state can be assumed to consist of a number of substates, corresponding to different oscillation amplitudes, whose optical properties are similar but whose nmr properties are different. The unfolding of an oligonucleotide can then be described in terms of the increased accessibility of the higher energy substates of the "stacked" states as well as the substates of the "unstacked" state with increasing temperature. The chemical shifts observed at any temperature thus represent an ensemble average over all these accessible states.

Chain Length Dependence of Chemical Shifts

The simplest model for the oligonucleotides is an "extended dimer" model, in which each oligomer is constructed as an exact extension of the dimer, both with regard to geometry and stacking forces (i.e., a right-handed helix with the bases in the anti conformation[2, 4]), and in which the shielding effect of bases does not extend beyond nearest neighbors. We shall discuss the oligomer polymerization shifts in terms of this model. Several questions arise in such a discussion: (1) What are the predicted base proton polymerization shifts based on this model? (2) Do the experimental and predicted polymerization shifts differ? and (3) If they differ, what can we attribute these differences to?

The predictions are rather simple. The exterior base proton polymerization shifts should be independent of chain length and should be equal to those for the dimer. Similarly the interior base proton polymerization shifts should be independent of chain length. Interior base protons, however, are shielded by two neighboring bases. Thus there are two contributions to each of their polymerization shifts, which are equal to the polymerization shifts of the corresponding α and ω protons. Based on the "extended dimer" model, the oligomer spectra should therefore consist of four exterior base proton resonances, $H_2(\alpha)$, $H_8(\alpha)$, $H_2(\omega)$ and $H_8(\omega)$, and of two interior base proton resonances consisting of the interior H_2 and H_8 resonances. The relative intensities of the interior and exterior resonances will of course depend on the number of interior bases.

The chain length dependence of the oligoadenylate polymerization shifts is summarized in Figs. 7 and 8. An examination of these data shows that the experimental polymerization shifts bear little resemblance to those predicted above. The exterior base proton polymerization shifts are different for each of the oligomers. The interior base polymerization shifts are also different for each of the oligomers, and even for a particular oligomer they are not all the same. Lastly, the polymerization shifts for the interior base protons are not equal to the sum of the corresponding polymerization shifts of the exterior base protons.

We can classify the differences between the expected spectral properties on the basis of the admittedly simple model and the experimental spectral properties into two distinct considerations. The first of these concerns a problem related to the actual measurement, specifically to the possible contribution of distant (or third) base shielding to the polymerization shifts.[15, 21] The second concerns the influence of chain length on the extent of base stacking and on the geometric relationship between adenylyl residues. Our first concern is to determine to what extent distant base shielding can account for the difference between the observed polymerization shifts and those expected on the basis of the "extended dimer" model. We shall focus our attention on the trimer α and ω base protons. Each of these protons can in principle be shielded by one distant base: the α base protons can be shielded by the ω base, and the ω base protons by the α base. This shielding contribution will only be significant if <u>both</u>

FIGURE 7

Chain length dependence of the H_2 polymerization shifts.

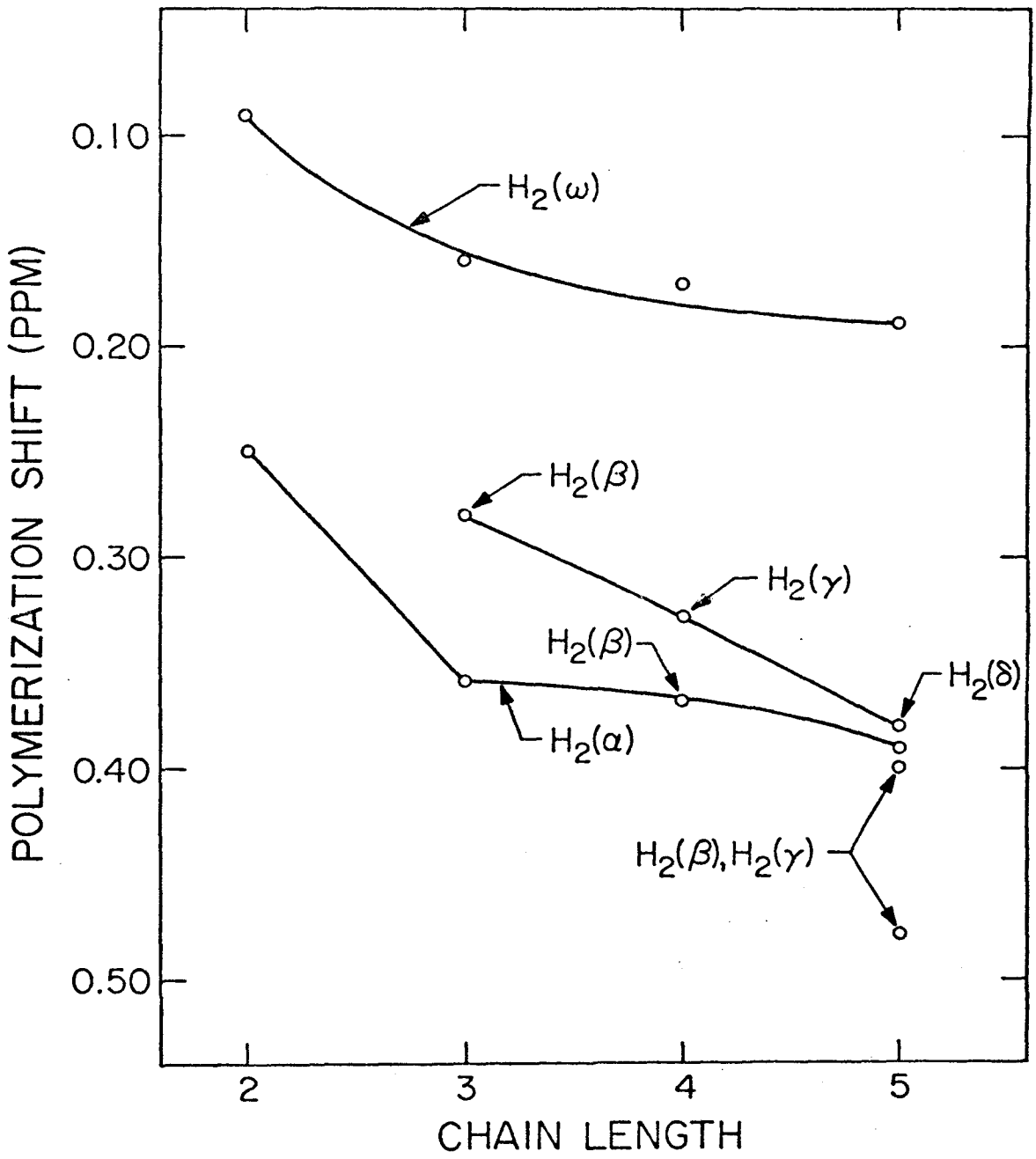
POLYMERIZATION SHIFT (PPM)
0.10
0.20
0.30
0.40
0.50
2
3
4
5
CHAIN LENGTH
H2(ω)
H2(β)
H2(γ)
H2(β)
H2(δ)
H2(α)
H2(β),H2(γ)

FIGURE 8

Chain length dependence of the H_8 polymerization shifts.

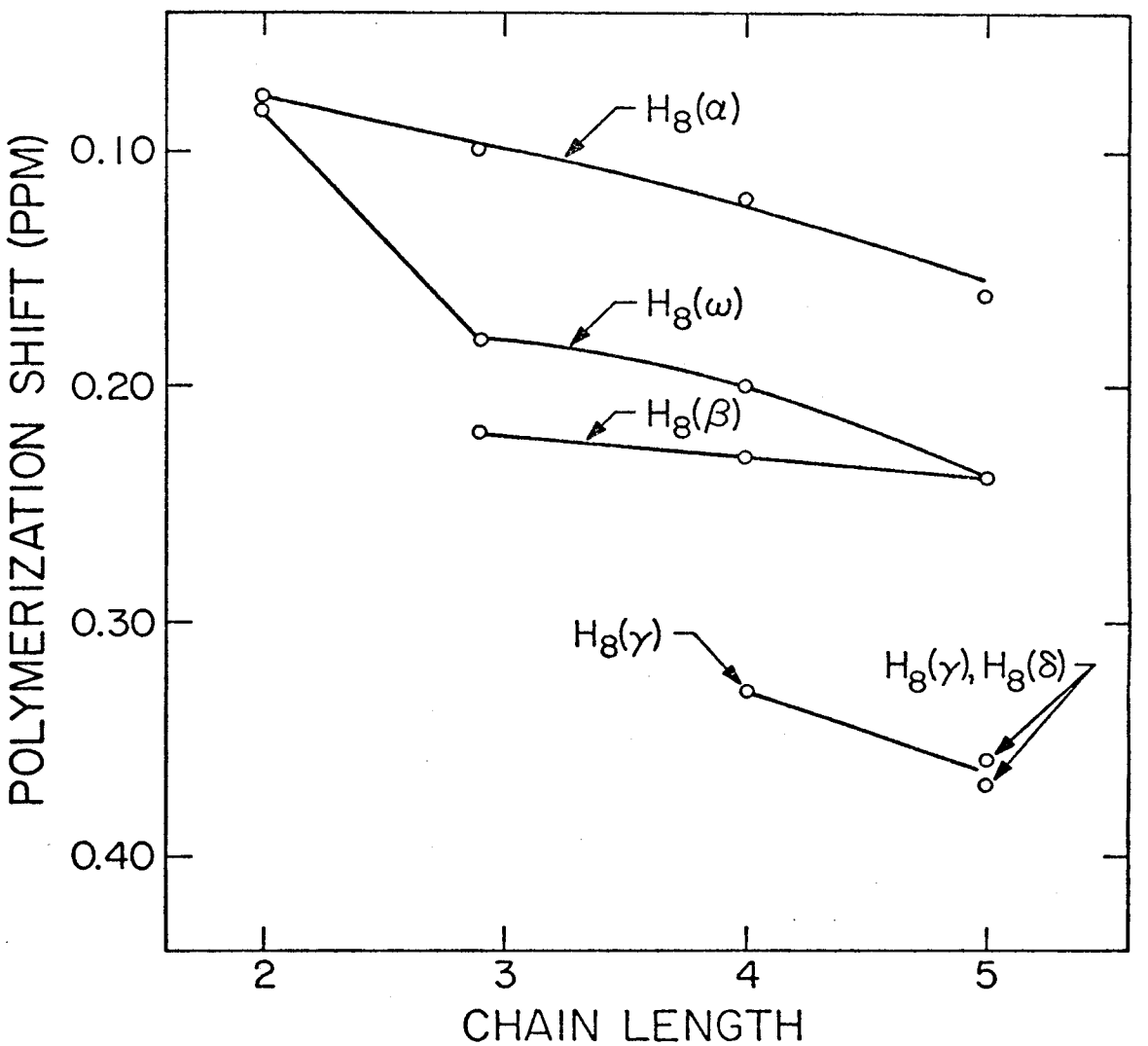
POLYMERIZATION SHIFT (PPM)
0.10
0.20
0.30
0.40
2
3
4
5
CHAIN LENGTH
$H_8(\alpha)$
$H_8(\omega)$
$H_8(\beta)$
$H_8(\gamma)$
$H_8(\gamma), H_8(\delta)$

the α, β and the β, α base pairs are in the stacked state.

A qualitative estimate of this distant base shielding effect can be made if we reall that the ring current magnetic anisotropy effect has essentially an r^{-3} dependence. Since in the stacked state the distance between the α and α bases in the trimer is approximately double that between two contiguous bases, the ring current contribution from the distant base should amount to no more than 13% of the nearest-neighbor shift. The magnitude of this nearest-neighbor effect may be estimated from the polymerization shift observed for the base protons in the dimer. Using this, we obtain an upper limit of 0.03 ppm for the shielding effect of the distant base.

The above estimation assumes that the geometrical distribution between the α and α bases is correlated to the same extent as between two contiguous bases. This of course is not true. Moreover, a precise estimate is only possible when we include the angular dependence of the ring current effect. In order to do this we have carried out ring current calculations for the adenine base similar to those previously reported by Giessner-Prettre and Pullman.[11] These calculations have been described earlier in this paper, and we will now use these results in conjunction with thermodynamic stacking parameters deduced from optical data to obtain a more realistic estimate of the magnitude of this distant base shielding.

The thermodynamics of the stacking and destacking processes of the oligoadenylates have been studied by a number of investigators. It has been shown that optical data for the dimer can be analyzed in

terms of a simple two state (i. e., stacked versus unstacked) model. Optical data for the trimer have also been analyzed in terms of this model (there appears to be little cooperativity for the destacking process). The results show that the extent of base stacking is similar for the dimer and trimer. Using the thermodynamic parameters determined by Brahms et al.,[8] we find that at 20°C approximately 41% of the dimers are stacked. More recent studies[22] indicate that the percentage is somewhat higher (up to 57%). Since the extent of base stacking is similar for the trimer, a reasonable estimate for the percentage of trimer base pairs (α, β and β, ω) stacked at 20°C is 50%. Thus, at 20°C, 25% of the trimer molecules exist with all bases stacked, 25% with all bases destacked, and 50% with either the α, β or β, ω bases stacked. The effect of distant base shielding in the stacked molecules can be estimated from shielding zones calculated at a distance of 6.8 Å from the adenine base (see Fig. 1b). For a completely stacked trimer, the maximum effect is 0.21 ppm. Thus at 20°C, with 25% of the trimers completely stacked, the maximum possible distant base shielding effect is 0.05 ppm. From a CPK molecular model it is apparent that $H_8(\alpha)$ will be least affected by distant base shielding (less than 0.01 ppm at 20°C). Similarly the effect for $H_2(\omega)$ should be small (less than 0.02 ppm). However both $H_2(\alpha)$ and $H_8(\omega)$ can be placed quite close to the point of maximum distant base shielding, although not simultaneously. If $H_2(\alpha)$ is placed near the point of maximum shielding of the ω base, the shielding of $H_8(\omega)$ by the α base will only be of the order of 0.01 ppm, and

vice versa. Actually, since it appears that the bases can oscillate with respect to each other, the distant base shielding contribution for a particular proton will be an ensemble average over different base orientations. The net result of this is to reduce the estimated maximum distant base shielding effect for the $H_2(\alpha)$ and $H_8(\omega)$ protons further.

The above considerations indicate that the differences between the trimer α and ω base proton chemical shifts and those expected on the basis of an "extended dimer" model cannot be attributed to distant base shielding alone. In particular the differences between the dimer and trimer $H_2(\alpha)$ chemical shifts (0.11 ppm) and $H_8(\omega)$ chemical shifts (0.10 ppm) are much larger than the estimated upper limit for distant base shielding. This conclusion is at odds with the results of a recent pmr study of a number of trinucleotides,[21] wherein chemical shift differences of up to 0.1 ppm have been observed between the terminal thymine resonances of TpTpdA, dApTpT and those of TpT and have been attributed totally to through-space shielding effects of the added adenine base. Since the dTpdA (and dApT) sequences are supposedly less strongly stacked than ApA sequences, and since all indications are that two contiguous thymine bases are only weakly stacked, any distant base shielding effect arising from the adenine base in these trimers would be expected to be much smaller than that observed in the case of ApApA. The fact that the magnitude of the shifts observed for the terminal thymine protons of TpTpdA and dApTpT are the same as those observed for ApApA would seem to suggest an alternate

interpretation for these observations. In the case of TpTpdA and dApTpT, we note that because of the relatively weaker vertical interactions between the bases in these trimers, particularly between the two thymine bases, there is a strong possibility for looping out of the center nucleoside followed by close range face-to-face stacking of the α and ω bases, and the so-called distant base shielding shifts may well have origin in these gross conformational effects. We believe that one must reserve judgment on the importance of the proposed through-space effects until these conformational factors are clarified. Similar gross conformational effects are not, however, expected to occur in the oligoadenylates because of the relatively stronger vertical interactions in these oligonucleotides. We are therefore compelled to attribute the discrepancies between the observed chemical shifts and those expected on the basis of the simple extended dimer model primarily to the influence of increasing chain length on the extent of base stacking and on the geometric relationship between neighboring adenylyl residues.

The effect of chain length on the extent of base stacking has been studied by several authors.[7, 8] In each case the stacking enthalpy is found to be independent of chain length. On the other hand, the stacking entropy depends on the number of adjacent nucleotide residues. With increasing chain length the entropy change decreases, leading to an increase in the extent of base stacking at a particular temperature and a shift to higher temperatures of the stacked chain to random coil transition point. It should be noted that these

observations are based on a two state analysis of optical spectroscopic results. As mentioned previously, the nmr data suggest that at least one of these "optical" states consists of a number of substates which can be distinguished by nmr. Thus an increase in the "extent" of base stacking (measured by nmr) may involve a change both in the equilibrium population of the gross states (stacked and unstacked) and of the substates (e.g., those with different oscillation amplitudes in the stacked state). An estimate of the chemical shift differences expected as a result of the increased base stacking can be obtained from the temperature dependence of the chemical shifts and the values of the transition temperatures. From the thermodynamic data of Brahms et al.[8] we can estimate the T_M values to be 13°C for both the dimer and trimer and 17°C for the pentamer. The increases are therefore rather small. From the temperature dependence of the trimer base protons we can roughly estimate an expected shift of 0.01 ppm per °C change in T_M. This estimate is based on the assumption that a change in T_M, (ΔT_M), affects the "gross" states and the substates as if the temperature is changed by ΔT_M. As a first order estimate this does not seem unreasonable. The contribution to the polymerization shifts from increased base stacking is thus expected to be rather small.

It seems therefore that the deviations from the "extended dimer" model must be explained in terms of conformational differences between the dimer units (consisting of two neighboring nucleosidyl units) of the oligomers. The largest change in the exterior base proton δ_p's occurs between the dimer and trimer. Thus the major

conformational changes of the external bases takes place upon the incorporation of a third nucleotide. We conjecture that the presence of a third ribose moiety can lead to a change in the conformation of the exterior ribose moieties (compared to those of the dimer) to accommodate three stacked bases. This in turn may lead to a change in the relative position of the bases with respect to each other, with the net result that the base protons are placed in different parts of their neighboring base's shielding region. The fact that the trimer $H_2(\beta)$ polymerization shift is 0.06 ppm smaller and the $H_8(\beta)$ polymerization shift is 0.08 ppm larger than expected on the basis of the "extended dimer" conformation, provides additional evidence for such conformational changes. The somewhat unexpected result is that the interior $H_2(\beta)$ proton is less shielded than the exterior $H_2(\alpha)$ proton!

An examination of a CPK molecular model suggests that we can at least qualitatively account for the observed chemical shift changes. If we begin with the trinucleotide in an "extended dimer" conformation, and move the α base, by rotations about the P-O bonds, to bring $H_2(\alpha)$ closer to the strongly shielding region of the central base, while keeping $H_8(\alpha)$ in an area of approximately constant shielding, and move the ω base to place $H_8(\omega)$, and to a somewhat lesser extent $H_2(\omega)$, closer to the strongly shielding region of the central base, we obtain the net result that $H_2(\beta)$ is shielded to a smaller extent and $H_8(\beta)$ is shielded to a larger extent from that expected on the basis of the "extended dimer" model. These are all rather qualitative notions. One thing is clear, however, and that is that there are

significant differences between the relative orientation of the α, β and β, α base pairs in the trimer, both of which are in turn oriented differently as compared with the dimer α, ω pair.

Further evidence for conformational differences between the various adenine bases of an oligomer is provided by a comparison of the $H_2(\alpha)$ chemical shifts with those of the interior bases in the case of the tetramer and the pentamer. In the tetramer, we note that both $H_2(\alpha)$ and $H_2(\beta)$ can be shielded by distant adenine bases (the γ and ω bases respectively). However, $H_2(\alpha)$ experiences a ring current shift from one neighboring base only (the β base) whereas $H_2(\beta)$, which is sandwiched between the α and γ bases, is shielded by two neighboring bases. In the absence of conformational differences between the α, β, and γ nucleosidyl moieties, we expect the $H_2(\alpha)$ resonance to appear approximately 0.09 ppm downfield from the $H_2(\beta)$ resonance, if ring current field contributions from nearest neighbors as well as distant bases are included. In fact, $H_2(\alpha)$ has the same chemical shift as the interior base H_2 resonance which appears to highest field in the spectrum. An analogous situation occurs in the case of the pentamer, except that here two interior base H_2 protons, namely $H_2(\beta)$ and $H_2(\gamma)$, are shielded by a distant as well as contiguous adenine bases. However only one of these (which we have tentatively assigned to $H_2(\gamma)$) appears to be much higher field than $H_2(\alpha)$, while the other appears only 0.01 ppm to higher field than $H_2(\alpha)$. Once again these observations suggest subtle differences in the relative orientation of the contiguous bases in each of the oligomers.

CONCLUSIONS

The oligoadenylates $(Ap)_{2-4}A$ have been examined by pmr spectroscopy. All the external base H_2 and H_8 resonances and a number of the internal base proton resonances have been assigned, and their spectral behavior has been studied as a function of concentration, solution temperature and concentration of added purine. On the basis of this extensive work, it is shown that, although the oligoadenylates bear many similar structural features, including relatively strong adenine-adenine interactions and preferentially anti conformation for the various adenine bases about their respective glycosidic bonds, significant albeit subtle conformational differences exist among them. These structural differences are reflected in deviations of the oligomer spectral parameters from those expected on the basis of the "extended dimer" model. We have attributed these departures to subtle differences in the geometrical relationship between neighboring bases in these molecules.

This work suggests that care must be exercised before structural information from dinucleotides can be extrapolated to infer the conformational properties of oligo- and polynucleotides. Although pair-wise addition of the interactions deduced from studies of dimers probably serves as a reasonable starting point for such studies, meaningful interpretation of precise spectroscopic results on the oligomers is, however, only possible after the effects of chain length on the secondary structure of these molecules are also taken into consideration.

References

1. S. I. Chan, B. W. Bangerter and H. H. Peter, Proc. Nat. Acad. Sci. U. S., 55, 720 (1966).
2. S. I. Chan and J. H. Nelson, J. Amer. Chem. Soc., 91, 168 (1969).
3. B. W. Bangerter and S. I. Chan, J. Amer. Chem. Soc., 91, 3910 (1969).
4. P. O. P. Ts'o, N. S. Kondo, M. P. Schweizer and D. P. Hollis, Biochemistry, 8, 997 (1969).
5. N. S. Kondo, H. M. Holmes, L. M. Stempel and P. O. P. Ts'o, Biochemistry, 9, 3479 (1970).
6. N. S. Kondo, K. N. Fang, P. S. Miller and P. O. P. Ts'o, Biochemistry, 11, 1991 (1972).
7. M. Leng and G. Felsenfeld, J. Mol. Biol., 15, 455 (1966).
8. J. Brahms, A. M. Michelson and K. E. Van Holde, J. Mol. Biol., 15, 467 (1966).
9. D. Poland, J. N. Vournakis and H. A. Scheraga, Biopolymers, 4, 223 (1966).
10. C. E. Johnson, Jr. and F. A. Bovey, J. Chem. Phys., 29, 1012 (1958).
11. C. Giessner-Prettre and B. Pullman, J. Theor. Biol., 27, 87 (1970).
12. C. Giessner-Prettre and B. Pullman, C. R. Acad. Sci., Ser. D, 268, 1115 (1969).
13. M. P. Schweizer, S. I. Chan, G. K. Helmkamp and P. O. P.

Ts'o, J. Amer. Chem. Soc., 86, 696 (1964).

14. J. E. Crawford, Ph. D. Thesis, California Institute of Technology, 1971.

15. S. Tazawa, I. Tazawa, J. L. Alderfer and P. O. P. Ts'o, Biochemistry, 11, 3544 (1972).

16. S. R. Jaskunas, C. R. Cantor and I. Tinoco, Jr., Biochemistry, 7, 3164 (1968).

17. B. W. Bangerter and S. I. Chan, Biopolymers, 6, 983 (1968).

18. L. S. Kan, J. C. Barrett, P. S. Miller and P. O. P. Ts'o, Biopolymers, 12, 2225 (1973).

19. R. C. Davis and I. Tinoco, Jr., Biopolymers, 6, 223 (1968).

20. D. Glaubiger, D. A. Lloyd and I. Tinoco, Jr., Biopolymers, 6, 409 (1968).

21. L. S. Kan, J. C. Barrett and P. O. P. Ts'o, Biopolymers, 12, 2409 (1973).

22. J. T. Powell, E. G. Richards and W. B. Gratzer, Biopolymers, 11, 235 (1972).

PROPOSITION I

The concept of fluidity is important in current membrane theories. Singer,[1] for example, views a membrane as a two-dimensional phospholipid fluid. Fluidity in this sense entails notions regarding molecular mobility as well as order. The mobility of membrane components in this fluid bilayer is considered to be important in a large number of cellular processes, such as transport, antibody-antigen interaction and cell surface organization.[1, 2]

On a molecular basis, membrane fluidity is determined to a large extent by the lipid fatty acid composition, for example unsaturated fatty acids give rise to a more fluid environment than saturated ones. In most organisms, including bacteria and higher forms, the fatty acid composition, and hence the fluidity, is carefully controlled. The fatty acid composition of mycoplasma laidlawii cells, on the other hand, can be drastically altered when these cells are grown with specific fatty acid supplements.[3] When the organism is grown on pentadecanoic acid (an odd-chain fatty acid!) for example, 83% of the total fatty acid content consists of pentadecanoic acid.[3] The fatty acid composition can therefore be carefully controlled. The importance of membrane fluidity becomes apparent when cells are grown on long chain fatty acids, such as stearic acid. These cells swell and eventually lyse. In the presence of short chain acids however the cells grow as long filaments and show no evidence of swelling.[3] This phenomenon has been attributed to the crystallization of the long chain fatty acids at the growth temperature of 37°C.

Active transport processes are also affected by the membrane fluidity. The rate of 2-deoxyglucose transport across the membrane, for example, decreases rapidly at the temperature corresponding to the beginning of the broad lipid melt observed by differential scanning calorimetry.[4]

The fluidity of the membrane is clearly important. However there is no clear understanding of what the notion of fluidity entails on a molecular level in whole cells. NMR can yield such information. It is proposed therefore that the mobility and order of the fatty acid chains be measured by NMR, with a view to relating these quantities to cell growth and active transport phenomena.

The study envisaged involves the synthesis of fatty acids deuterated at specific points along the chain. This is described in the appendix. By including these fatty acids in the growth medium, they will be incorporated into the membrane lipids (primarily glycolipids). Deuterium NMR spectra of the whole cells can then be taken. From the observed deuteron quadrupole splitting one can estimate the order of the chain at the C-D site.[5] Furthermore, from the spin-lattice and spin-spin relaxation times, one can determine the mobility of the chain at the C-D site.[6]

These experiments should be performed at different temperatures and with different fatty acid chain lengths labelled in various positions. It would be interesting to use a mixture of fatty acids with different chain lengths with only one of them labelled. This would show whether any phase separation occurs over the

temperature range studied, and could be related to cell growth and transport phenomena.

In summary, this study would put the qualitative notions of membrane fluidity in terms of a quantitative description on a molecular basis of order and mobility.

Appendix

Specifically deuterated fatty acids are conveniently prepared from the corresponding long chain keto esters of the general formula

$$CH_3(CH_2)_m\overset{\overset{O}{\|}}{C}(CH_2)_nCOOCH_3$$

by forming the tosylhydrazone followed by reduction with $LiAlD_4$.[7]

The long chain keto esters can be prepared by the reaction of alkylcadmium compounds with ω-carbalkoxyacyl chlorides.[8] The latter can be prepared by the reaction of thionylchloride with the corresponding acidic esters.[9]

References

1. S. J. Singer and G. L. Nicholson, Science 175, 720 (1972).
2. M. Edidin, Ann. Rev. Biophys. Bioengineering 8, 179 (1974).
3. R. McElhaney and M. E. Tourtellotte, Science 164, 434 (1969).
4. J. M. Steim, M. E. Tourtellotte, J. Reinert, R. McElhaney and R. Rader, Proc. Nat. Acad. Sci. 63, 104 (1969).
5. A. Seelig and J. Seelig, Biochemistry 13, 4839 (1974).
6. H. Saito, S. Schreier-Muccillo and I. C. P. Smith, FEBS Lett. 33, 281 (1973).
7. L. Tökés and L. J. Throop, Organic Reactions in Steroid Chemistry, Vol. 1, J. Fried and J. A. Edwards, Eds., Van Nostrand Reinhold, New York, 1972.
8. J. Cason, Chem. Rev. 40, 15 (1947).
9. J. Cason, Organic Synthesis, Coll. Vol. III, E. C. Horning, Ed., Wiley, New York, 1955.

PROPOSITION II

Cytochrome c is an important constituent of the electron transport chain in mitochondria.[1] Its function is to shuttle electrons from cytochrome bc_1 to cytochrome oxidase. In contrast to other cytochromes of the respiratory chain, cytochrome c is readily extractable from mitochondria and is water soluble. It is therefore a peripheral protein.

At physiological pH, cytochrome c contains a net positive change of 8.[2] Its interaction with mitochondrial phospholipids is believed to be mainly ionic in character. Cardiolipin, a negatively charged phospholipid which is present in mitochondria, is believed to be intimately involved in cytochrome c membrane binding.[3] Few details are known about the interaction of cytochrome c with the membrane phospholipids. It is proposed therefore that NMR be used to study the nature of this association on a molecular basis.

Cytochrome c is particularly amenable to NMR studies, since well resolved spectra covering a large chemical shift range are observed for both the reduced and oxidized forms of this protein.[4,5] The oxidized form, ferricytochrome c, has an NMR spectrum which ranges from the porphyrin ring methyl resonance at -35 ppm to the axial methionine methyl resonance at +24 ppm (referenced to internal DSS).

The experiments envisaged involve a study of the interaction of cytochrome c with sonicated phospholipid vesicles. Interfering phospholipid hydrocarbon chain protons and choline methyl protons

should be replaced by their deuterated counterparts.[6,7] By observing the cytochrome c spectrum as a function of phospholipid vesicle concentration it should be possible to detect changes in the NMR spectrum which can be related to conformational changes or to the site of binding. Such factors can be related to the known X-ray structure of cytochrome c.[8] The effect of varying the phospholipid content should also be investigated. Increasing amounts of the negatively charged phospholipid cardiolipin results in stronger binding, which should be reflected in the NMR spectrum.

Finally, it should be possible to study the interaction of cytochrome c with reconstituted cytochrome oxidase vesicles.[9] The presence of the cytochrome oxidase may alter the details of the cytochrome c vesicle interactions, which should be reflected in the NMR spectrum. Of course any observable cytochrome oxidase resonances would be interesting in their own right, and might reveal some details of its interaction with the phospholipids or with added cytochrome c.

References

1. A. L. Lehninger, The Mitochondrion, Benjamin, New York, 1964.
2. E. Margoliash, J. R. Kimmel, R. L. Hill and W. R. Schmidt, J. Biol. Chem. 237, 2148 (1962).
3. D. E. Green and S. Fleisher, Biochim. Biophys. Acta 70, 554 (1963).
4. C. C. McDonald, W. D. Phillips and S. N. Vinogradov, Biochem. Biophys. Res. Commun. 36, 442 (1969).
5. R. K. Gupta and S. H. Koenig, Biochem. Biophys. Res. Commun. 45, 1134 (1971).
6. Part I of this thesis.
7. A. J. Slotboom, H. M. Verheij and G. H. de Haas, Chem. Phys. Lipids 11, 295 (1973).
8. R. E. Dickerson, T. Takano, D. Eisenberg, O. B. Kallai, L. Samson, A. Cooper and E. Margoliash, J. Biol. Chem. 246, 1511 (1971).
9. E. Racker and A. Kandrach, J. Biol. Chem. 248, 5841 (1973).

PROPOSITION III

It is proposed that the kinetics of aggregation of hemoglobin mixtures associated with various sickling disorders be measured as a function of temperature, concentration and pH. The purpose of this study is to clarify the relationship between the clinical severity of various sickling disorders and the rate of hemoglobin aggregation.

Many of the clinical aspects of sickle cell disorders have been attributed to the sickling of erythrocytes upon deoxygenation, which results in an increase in blood viscosity, and in a decrease in blood flow.[1] The tendency of cells containing hemoglobin S (Hb S) to rigidify and to take on a sickled shape upon deoxygenation has been attributed to the aggregation of deoxy Hb S to form a highly viscous gel.[1] This gel consists of long bundles of straight fibers of aggregated hemoglobin molecules.[2] Whether or not a solution of Hb S gels depends on the hemoglobin concentration, temperature, pH and oxygen concentration.[3] These factors can be important for in vivo sickling of Hb S containing erythrocytes. The kinetic aspects associated with gelation may be even more important than the thermodynamic ones however. In particular, there is a delay time which precedes gel formation, which is strongly temperature and concentration dependent.[4, 5] As an illustration, the delay time changes from 540 minutes at 16°C to 0.5 minutes at 30°C (for a 23% Hb S solution).[5] It is conceivable therefore that a small change in body temperature or other physiological condition of a patient with sickle cell anemia, may shorten the gelation delay time sufficiently to cause

sickling within the microcirculation or venous return to precipitate the painful vaso-occlusive episode known as sickle cell crisis.

In addition to the homozygous (S-S) sickle cell anemia, there are a number of heterozygous sickling disorders. These include sickle cell trait (A-S), sickle cell thalassemia (S-Thal), S-D, S-C and S-F diseases.[1] Red cells from persons with sickle cell trait require a much lower oxygen content to produce sickling than red cells from persons with sickle cell anemia. In fact, under normal physiological conditions the blood oxygen content is usually too high to cause intravascular sickling of A-S erythrocytes, unless the person is exposed to conditions of considerable anoxia. Red cells from persons heterozygous for Hb S and another mutant hemoglobin, generally sickle at an intermediate oxygen content. However, nothing is known about the delay times which precede sickling of these cells, nor is anything known about the delay times which precede gelation of their hemoglobin.

The research proposed concerns itself with the measurement of the kinetics of gelation of hemoglobin mixtures containing Hb S and a non-S hemoglobin (i. e. corresponding to the hemoglobin of persons with heterozygous sickling disorders). The kinetics can be followed conveniently by monitoring the linear birefringence, which accompanies gel formation.[5] Gelation can be induced by raising the temperature of an already deoxygenated hemoglobin mixture, from 0°C (where no gelation occurs), to the temperature of interest.

An understanding of the kinetics of gelation under various

conditions is important for a number of reasons. In the first place it should clarify the relationship between the gelation delay time and the clinical status of people with various sickle cell disorders. The clinical details of such people, as well as their hemoglobin composition and concentration, are well documented.[1] Measurements should be performed as a function of hemoglobin concentration and composition, since there is a considerable variation in these quantities. If the delay time is found to be a significant factor in determining the clinical status of persons with sickling disorders, it may be possible to predict the clinical consequence of a change in physiological conditions which are known to affect the delay time. The effect of pH and temperature should be investigated in this regard. Finally it should be pointed out that the gelation of hemoglobin is not the only manifestation of sickling disorders.[1] However a detailed understanding of the conditions which do affect gelation may also clarify some of the other factors involved.

References

1. J. Song, Pathology of Sickle Cell Disease, Thomas, Illinois, 1971.
2. J. T. Finch, M. F. Perutz, J. F. Bertles and J. Dobler, Proc. Nat. Acad. Sci., 70, 718 (1973).
3. A. C. Allison, Biochem. J., 65, 212 (1957).
4. R. Malfa and J. Steinhardt, Biochem. Biophys. Res. Commun., 59, 887 (1974).
5. J. Hofrichter, P. D. Ross and W. A. Eaton, Proc. Nat. Acad. Sci., 17, 4864 (1974).

PROPOSITION IV

Although Ca^{+2} has key regulating functions for numerous membrane processes, such as electrical excitability, the underlying physicochemical basis of these functions is not clear. One important facet, however, appears to be the binding of Ca^{+2} to negative changes on the membrane surface.[1] It is important therefore to determine the nature and physical consequences of this interaction on a molecular basis in simple phospholipid Ca^{+2} systems. NMR studies can provide such information. It is proposed therefore than an NMR study be made of bilayer vesicles containing both a negatively charged phospholipid, phosphatidyl serine (PS), and a neutral phospholipid, phosphatidyl choline (PC), in the presence and absence of Ca^{+2}, with a view to determining changes in molecular motion and phospholipid distribution.

The mobility and order of the phospholipid molecules can be estimated from the relaxation times of the chain methylene protons. These can be obtained selectively for one of the phospholipids by deuterating the hydrocarbon chains of the other. The synthesis of PC with deuterated chains PC (D) has been described in Part I of this thesis. PS with deuterated chains PS (D) is most conveniently prepared from the corresponding PC using the alcohol transferase activity of phospholipase D to replace the choline by a serine moiety.[2]

It has been suggested that Ca^{+2} binds to PS to form clusters of PC molecules and rigid PS-Ca^{+2} aggregates.[3,4] This should be easy to detect. If rigid patches of PS molecules are formed, the

PS methylene linewidths will be considerably broadened. Using recently developed methods, [5, 6] both the degree of order and the time scale of motion could be determined. Of course the motional state of the PC hydrocarbon chains are of interest also. It is possible, for example, that the formation of rigid PS aggregates loosens the rest of the phospholipid structure. Such effects have recently been observed by Hsu and Chan[6] in response to the addition of small amounts of valinomycin to PC bilayers. It would be of interest to perform these experiments using different PC to PS ratios. This would indicate whether a minimum amount of PS is needed to form rigid aggregates. It would be useful to compare the results obtained from this study with permeability studies, since the permeability of the PS aggregates and PC regions would presumably be quite different. The results of these experiments will give some insight into the effects of Ca^{+2} may have on biological membranes.

References

1. D. J. Triggle, Progr. Surface Membrane Sci. 5, 267 (1972).
2. A. J. Slotboom, H. M. Verheij and G. H. de Haas, Chem. Phys. Lipids 11, 295 (1973).
3. D. Papahadjopoulos, Biochim. Biophys. Acta 163, 240 (1968).
4. S. Ohnishi and T. Ito, Biochem. Biophys. Res. Commun. 51, 132 (1973).
5. C. H. A. Seiter and S. I. Chan, J. Amer. Chem. Soc. 95, 7541 (1973).
6. M. -C. Hsu and S. I. Chan, Biochemistry 12, 3872 (1973).

PROPOSITION V

It is proposed that the formation of concanavalin A (Con A) saccharide binding sites be investigated by spectrophotometric techniques.

Con A is a saccharide binding protein isolated from jack beans (canavalia ensiformis).[1] Although its function in the jack bean is not well understood, it exhibits some unusual properties associated with its ability to bind saccharides. It agglutinates erythrocytes, starch granules and some bacteria and yeasts.[1] Upon binding it often causes a change in the physiological functioning of a cell. For example if a virally transformed cell is treated with trypsinized Con A, normal growth can be restored. As a result of these properties, Con A is widely used in the study of cell surface structure and dynamics.

Con A exists mostly as a dimer below pH 6, and as a tetramer above pH 7.[3, 4] It contains two metal ion sites per subunit, S1 and S2, which in the native state are occupied by Mn^{2+} and Ca^{2+} respectively.[5] While the presence of Mn^{2+} is essential for saccharide binding activity there appears to be no absolute requirement for Ca^{2+}.[6] Recent studies have shown that as long as the correct conformation about the Mn^{2+} ion is attained, Ca^{2+} is not needed for saccharide binding.[6, 7] It has been speculated that the function of Ca^{2+} may be simply to accelerate the correct folding of the protein about the Mn^{2+} site.[6, 7]

If Mn^{2+} is added to a metal free solution of Con A, a Con A-Mn^{2+} complex is formed rapidly.[7] This complex does not possess

any saccharide binding activity.[6] Complex formation is followed by a structural rearrangement of the protein about the Mn^{2+} site. The rate at which the rearrangement takes place is pH dependent; it is much slower (one hour) at pH 5.67 than at pH 4.50 (within ten minutes).[7] If Ca^{2+} is added at any time, the rearrangement proceeds rapidly, and is complete within five minutes (which corresponds to the time resolution of the measurements).[7] This is accompanied by the formation of a saccharide binding site, which is retained even if Ca^{2+} is removed at this stage.[6] Although these observations indicate that the only function of Ca^{2+} is to accelerate the protein folding process, the picture is far from clear. In particular, it has been tacitly assumed that the structural rearrangement in the absence of Ca^{2+} is the same as that in the presence of Ca^{2+}. Equilibrium dialysis measurements however have given no evidence for saccharide binding to Con A in the absence of Ca^{2+}.[8] It is possible of course that under the experimental conditions used, folding about the Mn^{2+} ion took place very slowly. On the other hand, the structural rearrangements in the presence and absence of Ca^{2+} could be different, so that a saccharide binding site is only formed in the presence of Ca^{2+}. In view of these apparent contradictions it is important to determine the conditions under which saccharide binding sites are formed and what determines the rate of this process.

The formation of a saccharide binding site can be followed by measuring the amount of saccharide bound to the protein as a function of time. p-Nitrophenyl α-D-mannopyranoside (NPM) binds

tightly to Con A saccharide binding sites.[9] Upon binding there is a pronounced change in its UV spectrum, which can be related to the amount of NPM bound. Binding site formation can therefore by monitored by measuring the UV absorbance of NPM, following rapid mixing of all components (e.g. in a stopped flow apparatus). The limiting factor in these measurements is the rate at which NPM binds to Con A. This is not a serious limitation however, since NMR studies have shown that the exchange rate between bound and free saccharide is very fast.[10]

The proposed research involves a measurement of Con A binding site formation in the presence of Mn^{2+}, Ca^{2+} and other metal ions, and as a function of temperature and pH, in order to determine the requirements for saccharide binding site formation. These studies should resolve the question of whether or not, or under what conditions, Ca^{2+} is needed for binding site formation. Furthermore they should give some insight into the process of binding site formation, and into the process of protein folding about the Mn^{2+} site. The pH dependence of the kinetics of this process, in the presence and absence of Ca^{2+}, could identify some of the amino acids involved. Furthermore, the effect of other metal ions on the kinetics should shed some light on the role of the ionic radius, charge density and electronic structure in the folding process.

In summary, this study will clarify the role of Ca^{2+} in the formation of saccharide binding sites and will shed some light on the nature of the rearrangement about the Mn^{2+} ion which is necessary for binding site formation.

References

1. J. B. Sumner and S. F. Howell, J. Bacteriol. 32, 227 (1936).
2. M. M. Burger and K. D. Noonan, Nature 228, 512 (1970).
3. A. J. Kalb and A. Lustig, Biochim. Biophys. Acta 168, 366 (1968).
4. G. H. McKenzie, W. H. Sawyer and L. W. Nichol, Biochim. Biophys. Acta 263, 283 (1972).
5. J. Yariv, A. J. Kalb and A. Levitzki, Biochim. Biophys. Acta 165, 303 (1968).
6. C. F. Brewer, D. M. Marcus and A. P. Grallman, J. Biol. Chem. 249, 4614 (1974).
7. B. H. Barker and J. P. Carver, J. Biol. Chem. 248, 3353 (1973).
8. M. Shoham, J. Kalb and I. Pecht, Biochemistry 12, 1914 (1973).
9. W. Bessler, J. A. Shafer and I. J. Goldstein, J. Biol. Chem. 249, 2819 (1974).
10. G. M. Alter and J. A. Magnuson, Biochemistry 13, 4038 (1974).